https://doi.org/10.35662/unine-thesis-2884

UNIVERSITÉ DE NEUCHÂTEL

INVESTIGATION OF NOVEL ACTUATOR AND FREQUENCY NOISE IN QUANTUM CASCADE LASERS AND QCL COMBS

Thèse présentée à la Faculté des Sciences de l'Université de Neuchâtel pour l'obtention du grade de

Docteur ès Science

Atif Shehzad

M.Sc. in Photonics, University of Eastern Finland, Joensuu (Fin)

Acceptée le 28 janvier 2021 sur proposition du jury:

Prof. Thomas Südmeyer	Directeur
Prof. Marco Marangoni	Examinateur
Dr. Richard Maulini	Examinateur
Dr. Stéphane Schilt	Examinateur

Neuchâtel, 2021

UNIVERSITÉ DE NEUCHÂTEL

Faculté des Sciences
Secrétariat-décanat de Faculté
Rue Emile-Argand 11
2000 Neuchâtel – Suisse
Tél : + 41 (0)32 718 21 00
E-mail : secretariat.sciences@unine.ch

IMPRIMATUR POUR THESE DE DOCTORAT

La Faculté des sciences de l'Université de Neuchâtel autorise l'impression de la présente thèse soutenue par

Monsieur Atif SHEHZAD

Titre:

"Investigation of Novel Actuator and Frequency Noise in Quantum Cascade Lasers and QCL combs"

sur le rapport des membres du jury composé comme suit:

- Prof. Thomas Südmeyer, directeur de thèse, Université de Neuchâtel, Suisse
- Prof. Marco Marangoni, Politecnico di Milano, Italie
- Dr Richard Maulini, Alpes Lasers, Saint-Blaise, Suisse
- Dr Stéphane Schilt, Université de Neuchâtel, Suisse

Neuchâtel, le 5 mars 2021

Le Doyen, Prof. A. Bangerter

Keywords – Mots-clés

Keywords

Quantum cascade lasers, quantum cascade laser frequency combs, integrated heater, mid-infrared, frequency modulation, amplitude modulation, time and frequency metrology, frequency noise, phase noise, linewidth, narrow-linewidth laser, carrier-envelope offset frequency, voltage noise, frequency stabilization, stabilization loop, delay line, radio-frequency extraction, molecular spectroscopy

Mots-clés

Lasers à cascade quantique, peigne de fréquence à laser à cascade quantique, résistance intégrée, infrarouge moyen, modulation de fréquence, modulation d'amplitude, métrologie temps-fréquence, bruit de fréquence, bruit de phase, largeur de raie, laser à faible largeur de raie, décalage de fréquence entre porteuse et enveloppe, bruit de tension, stabilisation en fréquence, boucle de stabilisation, ligne à retard, extraction radio-fréquence, spectroscopie moléculaire

Abstract

Quantum cascade lasers (QCLs) have numerous applications especially in trace gas sensing and high-resolution spectroscopy. One of the key requirements for high-resolution spectroscopy is the laser spectral purity which is often represented in terms of the laser linewidth, i.e., the full width at half maximum of the emission spectrum. Another requirement is the ability to modulate the laser wavelength/frequency, which is routinely used in spectroscopic methods like wavelength modulation spectroscopy, frequency modulation spectroscopy, etc and is generally obtained through a modulation of the laser injection current. However, such modulation leads to a simultaneous modulation of the optical power which in many cases is undesired.

In this thesis, new approaches to address these needs are addressed. On one hand, a new actuator in QCLs in the form of a resistive element is investigated for its potential use in frequency noise reduction, hence, linewidth narrowing of a MIR QCL and encountered problems are discussed. The generation of pure amplitude or frequency modulation in a QCL using the resistive element is also presented. The proposed approach is attractive for enhanced performance in trace gas sensing applications in which the residual modulation harms the system performance and either pure amplitude or frequency modulation is required. A comprehensive analysis of residual modulation, presented at two modulation frequencies of 1 and 10 kHz, showed a reduction of the residual amplitude modulation by almost 20 dB in the case of pure frequency modulation and of the residual frequency modulation by more than 20 dB in the case of pure amplitude modulation as compared to the modulation applied to the QCL current. The proposed approach is simple and easy to implement as compared to some other methods previously reported that require external near-infrared lasers shining on the front facet of the QCL or a

specially designed three-section QCL for pure amplitude and frequency generation.

In the near-infrared, frequency stabilization to a long fiber delay line was demonstrated as an alternative scheme for ultra-narrow linewidth lasers. For the first time, the implementation of a delay line for frequency noise reduction in the MIR is presented in the thesis. Compared to former demonstrations in the near-infrared, several adaptations were required due to the poorer availability of key optical components such as low-loss singlemode optical fibers and acousto-optic modulators. In the proof-of-principle demonstration, a short free-space delay of only 1 m in a self-homodyne configuration avoiding the use of an acousto-optic modulator is implemented. A 40-dB reduction of the laser frequency noise power spectral density resulting in a sub-10-kHz linewidth for 1-s integration time has been achieved. By creating longer delays either in free space or using MIR optical fibers, this approach has the potential to achieve Hz-level linewidth in QCLs.

QCL comb is an emerging technology in the field of dual-comb spectroscopy. The direct observation of the offset frequency in a QCL comb has not yet been possible using standard *f*-to-2*f* interferometry as the laser does not emit short pulses. For the first time, the indirect characterization of the offset frequency in a MIR QCL comb is presented in terms of its frequency noise and modulation response, using a method based on the transfer oscillator concept.

Résumé

Les lasers à cascade quantique (QCL) ont de nombreuses applications, notamment dans la détection de traces de gaz et la spectroscopie à haute résolution. L'une des principales exigences de la spectroscopie à haute résolution est la pureté spectrale du laser qui est souvent représentée en termes de sa largeur de raie, c'est-à-dire la largeur totale à mi-hauteur du spectre d'émission. Une autre exigence est la capacité de moduler la longueur d'onde ou la fréquence du laser, qui est couramment utilisée dans les méthodes spectroscopiques comme la spectroscopie par modulation de longueur d'onde (Wavelength Modulation Spectroscopy – WMS), la spectroscopie par modulation de fréquence (Frequency Modulation Spectroscopy – FMS), etc, et qui est généralement obtenue par une modulation du courant d'injection du laser. Toutefois, cette modulation entraîne une modulation simultanée de la puissance optique qui, dans de nombreux cas, n'est pas souhaitée.

Cette thèse présente de nouvelles approches pour répondre à ces besoins avec des QCLs. D'une part, un nouvel actuateur sous la forme d'un élément résistif intégré est étudié pour son utilisation potentielle pour réduire le bruit de fréquence d'un QCL et, par conséquent, pour rétrécir sa largeur de raie. Les problèmes rencontrés sont discutés. La génération d'une modulation d'amplitude ou de fréquence pure dans un QCL en utilisant cet élément résistif est également présentée. L'approche proposée est prometteuse pour améliorer les performances dans des applications de détection de traces de gaz dans lesquelles la modulation résiduelle nuit aux performances du système et où une modulation pure d'amplitude ou de fréquence est souhaitée. Une analyse complète de la modulation résiduelle, présentée à deux fréquences de modulation de 1 et 10 kHz, a montré une réduction de la modulation d'amplitude résiduelle de près de 20 dB dans le cas de la modulation de fréquence pure et de plus

de 20 dB de la modulation de fréquence résiduelle dans le cas de la modulation d'amplitude pure par rapport à une modulation appliquée sur le courant d'injection du QCL. L'approche proposée est simple et facile à mettre en œuvre par rapport à d'autres méthodes précédemment présentées qui nécessitent soit l'utilisation de lasers externes dans le proche infrarouge éclairant la face avant du QCL ou un QCL à trois sections spécialement conçu pour obtenir des modulations d'amplitude ou de fréquence pure.

Dans le proche infrarouge, la stabilisation de la fréquence d'un laser sur une longue ligne à retard à fibre optique a été démontrée comme une méthode alternative pour atteindre des largeurs de raie ultra-étroites. Pour la première fois, la mise en œuvre d'une ligne à retard pour la réduction du bruit de fréquence d'un laser dans l'infrarouge moyen est présentée dans cette thèse. Par rapport aux démonstrations précédentes dans le proche infrarouge, plusieurs adaptations ont été nécessaires en raison de la disponibilité moindre des composants optiques clés tels que les fibres optiques monomodes à faibles pertes et les modulateurs acousto-optiques. Dans une démonstration de principe, un court délai en espace libre d'une longueur de 1 m seulement a été mis en œuvre dans une configuration self-homodyne évitant l'utilisation d'un modulateur acousto-optique. Une réduction de 40 dB de la densité spectrale de bruit de fréquence du laser a été obtenue, ce qui se traduit par une largeur de raie inférieure à 10 kHz pour un temps d'intégration de 1 s. En créant des délais plus longs, soit en espace libre, soit en utilisant des fibres optiques dans l'infrarouge moyen, cette approche devrait permettre d'obtenir une largeur de raie au niveau du hertz dans des QCLs.

Les peignes de fréquence produits par des QCL constituent une technologie émergente dans le domaine de la spectroscopie à deux peignes. L'observation directe de la fréquence d'offset dans un peigne QCL n'a pas été possible jusqu'à présent en utilisant la méthode standard par interférométrie *f*-to-2*f* car ces lasers n'émettent pas de courtes impulsions nécessaires pour élargir le spectre émis jusqu'à une octave de

fréquence. Pour la première fois, la caractérisation indirecte de la fréquence d'offset dans un peigne QCL dans l'infrarouge moyen est présentée dans cette thèse en termes de bruit de fréquence et de réponse de modulation, en utilisant une méthode basée sur le concept d'un oscillateur de transfert.

List of symbols and acronyms

Symbols

Δ, δ	Fluctuations
D	Slope coefficient
f_{CEO}, f_0	Optical comb offset frequency (Hz)
f_{rep}, f_{FSR}	Optical comb repetition frequency or intermode frequency (Hz)
L	Length (m)
P	Power (W)
S	Power spectral density
V	Voltage signal (V)
Γ_Δ	Coherence factor
$E(t)$	Electrical signal (V)
R	Resistance
T, H	Transfer function
ν, f	Frequency (Hz)
t	Time (s)
τ	Time delay (s)
ϕ, φ	Phase (rad, °)

Acronyms

AG	Anode ground
AM	Amplitude modulation
AOM	Acousto-optic modulator
AR	Active region
BS	Beamsplitter
CEO	Carrier-envelope offset
CG	Cathode ground
CW	Continuous-wave
DBM	Double-balanced mixer
DC	Direct current
DCS	Dual comb spectroscopy
DDS	Direct digital synthesizer
DFB	Distributed feedback
DFG	Difference frequency generation
DPSSL	Diode-pumped solid-state laser
ESA	Electrical spectrum analyzer/ European Space Agency
FFT	Fast Fourier transform
FM	Frequency modulation
FMS	Frequency modulation spectroscopy
FN	Frequency noise
FPGA	Field-programmable gate array

FSR	Free spectral range
FWHM	Full width at half maximum
ICL	Interband cascade laser
IH	Integrated heater
LLH	Laser laboratory housing
LNA	Low noise voltage amplifier
MCT	Mercury-Cadmium-Telluride
MIR	Mid-infrared
MLL	Mode-locked laser
MZI	Mach-Zehnder interferometer
NTC	Negative temperature coefficient
NIR	Near infrared
OFC	Optical frequency comb
OPO	Optical parametric oscillator
PAS	Photoacoustic spectroscopy
PCF	Photonic crystal fiber
PD	Photodiode, Photodetector
PDH	Pound-Drever-Hall
PID	Proportional-integral-derivative
PLL	Phase-locked loop
PM	Phase modulation
PN	Phase noise
PNA	Phase noise analyzer

PPLN	Periodically-poled lithium niobate
PSD	Power spectral density
PZT	Piezo-electric transducer
QCL	Quantum cascade laser
RAM	Residual amplitude modulation
RF	Radio-frequency
SC	Supercontinuum
SNR	Signal-to-noise ratio
SNSF	Swiss National Science Foundation
SSB	Single-side band
TBM	Triple-balanced mixer
TEC	Thermo-electrical cooler
ULE	Ultra-low expansion
VECSEL	Vertical external-cavity surface-emitting laser
WMS	Wavelength modulation spectroscopy

Publications

Parts of this thesis are published or submitted in the following journal papers. The text and figures are printed as published, only the format of the text, the numbering and the size of figures were adapted to the thesis style. The copyright of the original publications is held by the respective copyright holders.

Journal publications

1. **A. Shehzad**, P. Brochard, R. Matthey, S. Blaser, T. Gresch, R. Maulini, A. Muller, T. Südmeyer, and S. Schilt, *Electrically-driven pure amplitude and frequency modulation in a quantum cascade laser*, Optics Express 26(9), 12306-12317 (2018)

2. **A. Shehzad**, P. Brochard, R. Matthey, T. Südmeyer, and S. Schilt, *Sub-10-kHz-Linewidth Mid-Infrared Quantum Cascade Laser by Stabilization to an Optical Delay Line*, Optics Letters 44(14), 3470-3473 (2019)

3. **A. Shehzad**, P. Brochard, R. Matthey, F. Kapsalidis, M. Shahmohammadi, M. Beck, A. Hugi, P. Jouy, J. Faist, T. Südmeyer, and S. Schilt, *Frequency noise correlation between the offset frequency and the mode spacing in a mid-infrared quantum cascade laser frequency comb*, Optics Express 28(6), 8200-8210 (2020)

4. K. Komagata, **A. Shehzad**, G. Terrasanta, P. Brochard, R. Matthey, M. Gianella, P. Jouy, F. Kapsalidis, M. Shahmohammadi, M. Beck, V. J. Wittwer, J. Faist, L. Emmenegger, T. Südmeyer, A. Hugi, and S. Schilt, *Coherently-averaged dual comb spectrometer at 7.7 μm with master and follower quantum cascade lasers,* Optics Express (submitted)

Conference presentations

1. P. Brochard, S. Bilicki, **A. Shehzad**, S. Schilt, T. Südmeyer, *Laser Linewidth Optimization in a Feedback Loop*, oral #CH-4.3, CLEO Europe 2017, Munich, Germany, June 25-29, 2017

2. **A. Shehzad**, P. Brochard, R. Matthey, A. Bismuto, S. Blaser, T. Gresch, R. Maulini, A. Muller, T. Südmeyer, S. Schilt, *Pure Amplitude or Frequency Modulation of a Quantum Cascade Laser by Use of an Integrated Heater*, oral SF2G.7, CLEO US 2018, San Jose, USA, May 13-18, 2018

3. **A. Shehzad**, P. Brochard, R. Matthey, S. Blaser, T. Gresch, R. Maulini, A. Muller, T. Südmeyer, S. Schilt, *Generation of pure amplitude and frequency modulation in a quantum cascade laser using an integrated heater*, oral #413, Annual Meeting of the Swiss Physical Society, Lausanne, Switzerland, August 28-31, 2018

4. **A. Shehzad**, P. Brochard, R. Matthey, T. Südmeyer, S. Schilt, *Frequency Noise Reduction in a Quantum Cascade Laser Using a Short Free-Space Delay Line*, oral SW4N.5, CLEO US 2019, San Jose, USA, May 13-18, 2019

5. S. Schilt, P. Brochard, **A. Shehzad**, R. Matthey, A. Hugi, P. Jouy, F. Kapsalidis, M. Shahmohammadi, M Gianella, J. Faist, L. Emmenegger, T. Südmeyer, *Strategies for frequency stabilization and noise reduction in dual-QCL-comb spectroscopy*, invited, PIERS-2019, Roma, Italy; June 17-20, 2019

6. **A. Shehzad**, P. Brochard, R. Matthey, T. Südmeyer, S. Schilt, *Sub-10-kHz Linewidth Quantum Cascade Laser achieved by Stabilization to a Short Free-Space Delay Line*, oral CB-7.2, CLEO-Europe 2019, Munich, Germany; June 23-27, 2019

7. **A. Shehzad**, P. Brochard, R. Matthey, F. Kapsalidis, M. hahmohammadi, M. Beck, A. Hugi, P. Jouy, Faist, T. Südmeyer, S. Schilt, *Investigation of the Noise Properties of the Offset Frequency in a Quantum Cascade Laser Frequency Comb*, poster, Ultrafast Optics XII, Bol, Croatia; October 6-11, 2019

8. **A. Shehzad**, P. Brochard, K. Komagata, R. Matthey, F. Kapsalidis, M. Shahmohammadi, M. Beck, A. Hugi, P. Jouy, J. Faist, T. Südmeyer, S. Schilt, *Noise Correlation Between the Two Degrees of Freedom of a Mid-Infrared Quantum Cascade Laser Frequency Comb*, oral SF2G.2, CLEO US 2020, San Jose, USA, May 11-15, 2020

Table of content

Chapter 1

Introduction

Many molecular species (H_2O, CH_4, CO, CO_2, N_2O, NO, etc.) that are of great importance for environmental monitoring as well as for life sciences have intense fundamental vibrational bands in the mid-infrared (MIR) spectral region ($\lambda = 2–30$ μm), which is also most often referred to as the molecular fingerprint region. These vibrational resonances provide a non-intrusive way to analyze and identify the chemical composition of a sample. The strength of these resonances is more than 1000 times stronger in the MIR than in the near-infrared (NIR), which enhances the detection sensitivity by a similar proportion. The MIR also contains two important windows (3-5 μm and 8-12 μm) in which the atmosphere is relatively transparent. Small traces of environmental and toxic gases can be detected in these windows with sensitivities at the part-per-billion (ppb) level.

MIR laser sources are of great importance due to their applications in trace gas sensing[1], high-resolution spectroscopy, and precision frequency metrology[2]. In the past, several laser fabrication technologies have been developed and investigated to reach the important MIR spectral region. For instance, the first CO_2 gas laser operating at 10 μm was demonstrated

in 1964[3]. Lead-salt (PbS, PbTe, and PbSe) based laser diodes emitting in the 3−30 µm were readily available since the 1960s[4]. The drawback of these kinds of MIR laser sources is the limited output power and most importantly their operation at cryogenic temperatures which makes them not suitable for field-based applications. It took scientists more than 40 years to produce high-power and room temperature antimonide based laser diodes (In(Al)GaAsSb / GaSb) emitting at 2.8 µm[5,6]. Later on, interband cascade lasers (ICL) operating up to 5.6 µm were also demonstrated[7]. Other techniques involve converting the light from the NIR or visible region to the MIR using nonlinear frequency conversion processes such as difference-frequency generation (DFG)[8] or optical parametric oscillation (OPO)[9]. Each of these systems has its advantages and disadvantages, for instance, DFG systems are compact but provide low output power while OPO systems provide higher output power but are fairly bulky.

Nevertheless, fabricating compact and efficient laser sources in the MIR had remained quite challenging and it is only with the advent of the quantum cascade laser (QCL), first demonstrated in 1994 at Bell Laboratories[10], that the field of MIR spectroscopy, portable chemical sensors, trace gas sensing, etc. has become quite prominent. The intrinsic linewidth of a QCL can be as low as a few 100 Hz[11] but different noise sources result in the broadening of the linewidth to a few MHz. Narrow-linewidth and low-frequency noise QCLs have numerous applications for instance in the determination of fundamental physical constants[12] (proton to electron mass ratio = m_p/m_e and its possible variation over time), precision spectroscopy, etc.

Different modulation schemes such as wavelength and frequency modulation spectroscopy[13,14] have many applications, for instance, in optical communication, trace gas sensing, etc. These techniques, when combined in modulation and demodulation schemes, for example, lock-in detection, result in detection sensitivity improvements in trace gas

sensing. They consist in modulating the wavelength or frequency of a laser while obtaining a derivative-like signal of the absorption profile when the laser is slowly scanned through an absorption line. The wavelength/frequency tuning of a QCL with its injection current simultaneously leads to significant modulation of the output optical power that results in degradation of the system performance in many cases. Alpes Lasers incorporated a resistive element in the close vicinity of the QCL active region for fast spectral tuning properties[15]. In this thesis, this resistive element has been investigated for its potential use for linewidth reduction in a MIR QCL and the generation of pure amplitude or frequency modulation based on this device is demonstrated

Narrow-linewidth and frequency-stable lasers are often based on frequency stabilization onto a high-finesse ultralow thermal expansion Fabry-Pérot cavity, which leads to complex systems. An alternative approach based on a delay line that works on the principle of comparing the laser frequency to a delayed copy of itself to measure its frequency noise has previously been demonstrated in the NIR spectral region, where strong linewidth reductions were achieved owing to the use of long delays (km-scale) that is straightforwardly possible using optical fibers[16]. In this thesis, such a method has been implemented for the first time in the MIR, using a much shorter free-space delay in the meter scale, enabling the linewidth of a QCL to be reduced to the sub-10-kHz level.

In the last years, it was demonstrated that broadband QCLs can emit a comb spectrum that is characterized by equally-spaced modes in the frequency domain[17]. These very compact sources of MIR combs have a huge potential to combine broadband and high-resolution spectroscopy in the MIR, e.g., for sensitive multi-species detection[18–20]. The comb generation process in these lasers completely differs from the usual NIR mode-locked lasers and is based on a four-wave mixing process occurring in the semiconductor gain medium, which locks all modes together leading to a comb spectrum. Like in any other type of frequency comb, the

emitted optical spectrum is entirely defined by only two radio-frequencies, the mode spacing and the offset frequency. However, as a result of their different operation process, QCL combs do not emit short pulses but rather light with a small amplitude modulation. Therefore, the standard method used with mode-locked lasers to detect the offset frequency, which is based on non-linear interferometry (such as *f*-to-2*f*)[21], is not yet applicable with QCL combs. In this thesis, a detailed noise investigation of a QCL comb is presented, which is important for a better understanding of this novel comb technology. Using a method based on the transfer oscillator concept[22], a scheme enabling the offset frequency of a QCL comb to be characterized by circumventing its direct detection by standard *f*-to-2*f* interferometry has been implemented for the first time.

Organization of the thesis

This thesis is organized into the following chapters:

Chapter 2 is related to the investigation of a new actuator in a QCL in the form of an integrated heater used for fast wavelength/frequency tuning. Its use for the generation of pure amplitude and frequency modulation in a QCL is presented, and its potential for an all-electrical frequency noise reduction loop is also investigated and discussed.

Chapter 3 presents a new scheme to reduce the frequency noise in a QCL based on a free-space optical delay line in a Mach-Zehnder interferometer configuration resulting in a significant linewidth reduction by a factor of 60, to the sub-10-kHz level.

Chapter 4 reports the investigation of frequency noise and modulation bandwidth of the offset frequency in a MIR QCL comb that makes use of an indirect scheme to characterize the offset frequency without directly detecting it, which is applied for the first time in the MIR. A strong correlation between the frequency noise of the offset frequency and of the comb mode spacing is observed, which results in a degradation of the

offset frequency noise when the comb mode spacing is locked to a reference oscillator.

Finally, Chapter 5 concludes the thesis with an overview of this 4-year doctoral work.

Chapter 2

QCL with integrated heater as a new frequency actuator

2.1 **Basics of QCLs**

Conventional semiconductor laser operation is based upon the radiative recombination of electrons from the conduction band and holes in the valence band in a hetero-junction (diode) structure. The emitted wavelength or photon energy depends upon the bandgap of the semiconductor material. This energy bandgap can be engineered by combining different materials and thus, the emission wavelength can be tailored according to the requirements within the reachable range for a given ternary or quaternary material such as AlGaAs (600 nm – 1000 nm) or InGaAs (1000 nm – 2.2 μm).

Quantum cascade lasers (QCLs) are semiconductor lasers that emit in the mid to far-infrared spectral region as well as in the THz range. The operation principle of QCLs was first proposed by R.F. Kazarinov and R.A. Suris in 1971[23], but was demonstrated for the first time at Bell

Laboratories in 1994[10]. The working principle of QCLs strongly differs from conventional semiconductor laser diodes. Unlike electron-hole pair recombination in an inter-band transition, their operation relies on an electronic transition between discrete sub-levels within the conduction band (Figure 2.1). These energy states arise from the presence of alternating layers of semiconductor materials that results in quantified energy levels in the quantum wells.

An electron in a quantum well can jump from one state to the other in discrete steps, resulting in the emission of a photon of a given energy. The quantum well structure quantifies the energy (wavelength) of the emitted photons, which is determined by the geometry (depth and width) of the quantum well and not by the material used to fabricate the laser. Therefore, technologically-mature materials such as InGaAsP or AlGaAs with a large bandgap can be used to fabricate lasers that emit in the mid-infrared spectral range.

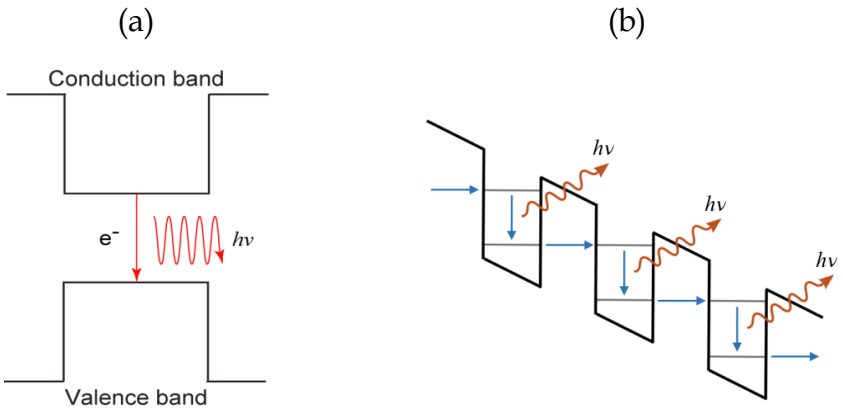

Figure 2.1: (a) Simple structure of a semiconductor laser where a photon is emitted through the recombination of an electron from the conduction band and a hole in the valence band, (b) Quantum well structure of a QCL. Blue lines represent the transmission path of an electron as it cascades through the quantum well structure resulting in the emission of a photon in each quantum well.

In a QCL, several active areas are combined in series that are separated by injection regions. As there is no electron-hole recombination involved, the same electron remains in the conduction band after emitting

a photon and can be recycled to emit multiple photons while passing through the cascaded sequences of quantum wells. This increases the efficiency and output power but at the same time results in higher operation voltage as compared to semiconductor laser diodes. Hence, the wavelength in a QCL can be tailored by engineering the quantum well structure that makes possible the laser to emit at wavelengths that are very challenging to achieve by inter-band transitions. QCLs wavelength emission ranges from 2.7 μm to 250 μm using III-V semiconductor materials such as InGaAs, InP, GaAs, AlGaAs, etc[24,25].

Because of the broad gain curve of the active medium, a QCL can operate in a multimode regime. A major advancement in the field of QCLs was the development of tunable single-frequency devices, that are required in applications like molecular spectroscopy, free-space communication, etc. Single-mode operation in QCLs is achieved by creating a periodic structure acting as a distributed-feedback grating (DFB) as shown in Figure 2.2 directly on top of the QCL active region[26,27] and the emission wavelength depends upon the grating period.

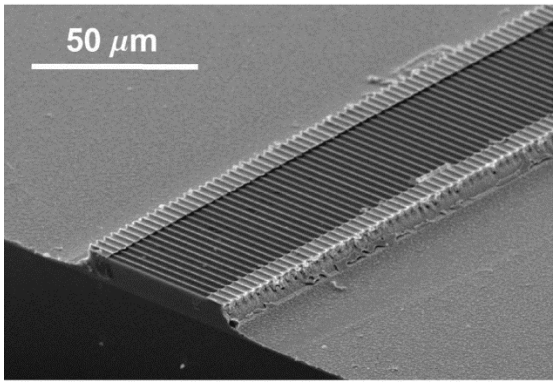

Figure 2.2: SEM image of a distributed-feedback grating fabricated on top of the QCL. The figure is taken from[27].

2.2 QCL with integrated heater

QCLs have a wide range of applications spanning from medical, industrial, and high-resolution spectroscopy to military applications in the MIR spectral region due to their spectral tuning properties. Wavelength tuning of QCLs is achieved either through their injection current or with their temperature. Generally, the QCL temperature is controlled with a thermo-electrical cooler (TEC), which results in a slow wavelength tuning. A typical value for the temperature-tuning coefficient of QCLs is around -3 GHz/K. However, the temperature change results in a slight change of the QCL output optical power. As the speed of temperature tuning depends upon the TEC size and the copper sub-mount that dissipates the heat in the surroundings, the temperature tuning is mainly used for large, but slow wavelength scans. In contrast, the QCL wavelength can be rapidly changed with the injection current, at frequencies as high as a few 100 kHz[28]. The downside of QCL wavelength tuning with its injection current is a limited tuning range and a significant change of the emitted optical power which is undesired in many applications.

A couple of years ago, Alpes Lasers (Neuchatel, Switzerland) introduced a new actuator for fast wavelength tuning in QCLs[15]. It consists of an integrated heater (IH) element placed in the close vicinity of the laser active region (AR) as shown in Figure 2.3. The IH is essentially a resistor in nature that is driven by a separate current source from the laser AR current source and dissipates heat via Joule-Thomson effect.

The IH in QCLs was developed not only for fast wavelength/frequency tuning but also to provide a large tuning range as compared to the tuning achieved with the laser current. The integrated heater has some interesting properties and applications. Before addressing some of them, a thorough characterization of the IH in terms of laser static tuning coefficient and its effect on the laser frequency noise was

performed. The experimental setup required for the characterization of the IH in a QCL is first introduced.

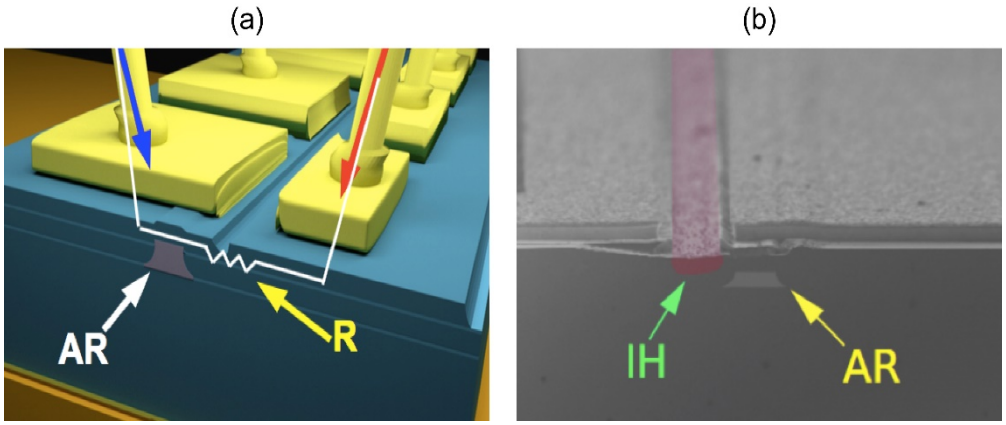

Figure 2.3: (a) Sketch of a QCL equipped with integrated heater positioned in the close proximity of the active region, (b) SEM image of one of the devices fabricated by Alpes Lasers. (AR; active region, R; resistor, IH; integrated heater). The figure is taken from[15].

2.2.1 Experimental setup

The laser used in this work is a DFB-QCL manufactured by Alpes Lasers, emitting at a center wavelength of 7.8 µm and equipped with an IH located at a few microns from the AR. It is similar to the one reported by Bismuto et al.[15] and later on extensively characterized in terms of tuning speed and modulation transfer functions by Gürel et al.[29]. The QCL covers a spectral range from 1275 cm^{-1} to 1277 cm^{-1} obtained at a constant sub-mount temperature of 20 °C by varying the AR current in the range of 280 mA to 410 mA and delivers up to 50 mW of output optical power. The laser chip was soldered on a copper sub-mount housed in a laser laboratory housing (LLH) provided by Alpes Lasers. The laser temperature is controlled through a thermoelectric cooler (TEC). The electrical connection scheme inside the LLH is made in such a way that both the QCL active region and the IH are independently driven by home-made low-noise current sources, as shown in Figure 2.4(a). These drivers can deliver a current of up to 1 A with a noise spectral density of less than

1 nA/√Hz at Fourier frequencies higher than 1 kHz measured on a 30-Ω test load [see Figure 2.4(b)].

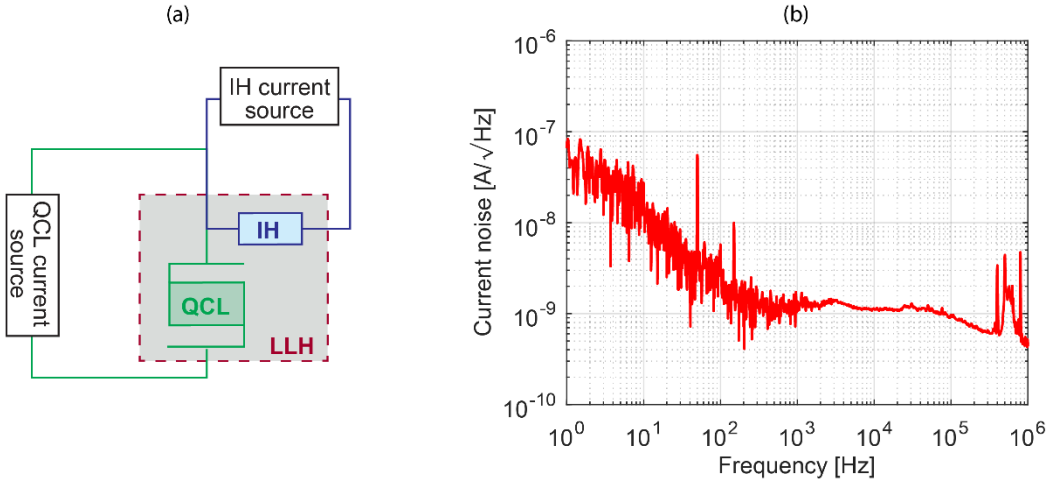

Figure 2.4: (a) Electrical connection scheme for the integrated heater (IH) and QCL placed inside laser laboratory housing (LLH), (b) current noise of the driver used to drive the QCL.

A single-stage TEC, along with a negative thermal coefficient (NTC) resistor as a temperature sensor, was used to control the QCL temperature with uncertainty at the mK level. As the IH is resistive in nature, its resistance value was assessed from its V-I curve measured for the QCL used in this experiment and is shown in Figure 2.5.

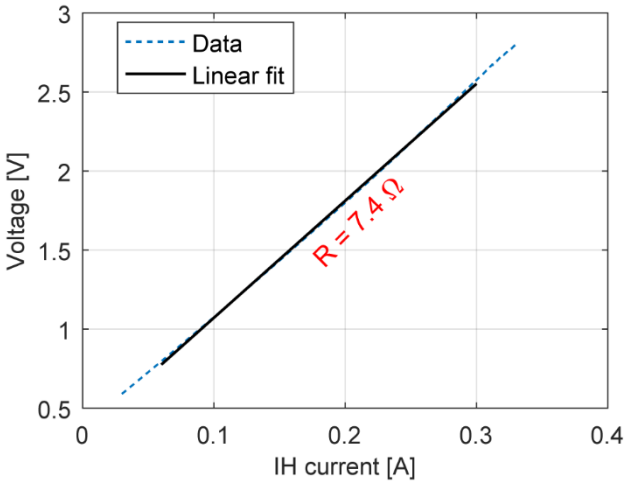

Figure 2.5: IH resistance value determined from the slope of its V-I curve.

2.2.2 Frequency tuning coefficients

The frequency tuning coefficients of the QCL were measured using a simple spectroscopic setup (see Figure 2.6) consisting of a low-pressure (2-mbar, 10-cm long) N_2O gas cell as a frequency reference. The position of several N_2O absorption lines was used to calibrate the frequency axis of large frequency scans performed as a function of the laser active region current (I_{AR}), sub-mount temperature (T), or IH current (I_{IH}), by comparing the position of the transitions listed in the HITRAN database[30].

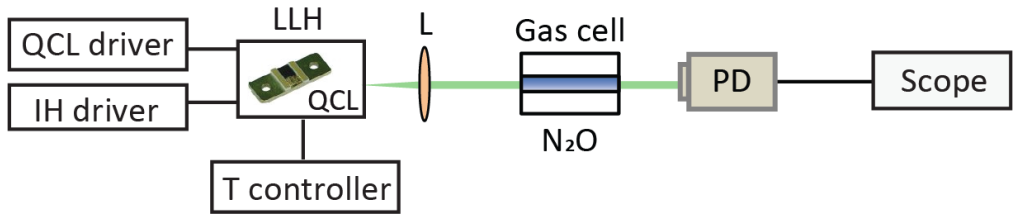

Figure 2.6: Schematic of the experimental setup used to measure the laser static tuning coefficients as a function of injection current, integrated heater current, and laser sub-mount temperature. LLH: laser laboratory housing; L: collimation lens; PD: photodetector; FFT: fast Fourier transform spectral analyzer.

The scan performed with the current of the QCL active region for a sub-mount temperature of 25 °C and no current in the IH section is displayed in Figure 2.7.

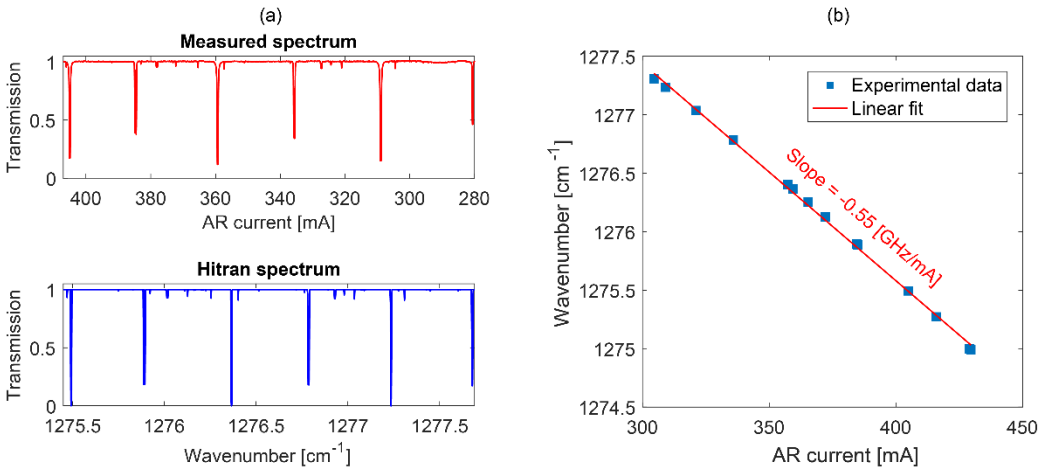

Figure 2.7: (a) Absorption spectrum of N_2O obtained by scanning the QCL active

region current (I_{AR}) (top spectrum obtained at a sub-mount temperature T = 25 °C and integrated heater current I_{IH} = 0 mA) and corresponding N_2O absorption spectrum from HITRAN database[30] (bottom spectrum). (b) Static tuning curve as a function of the AR current (blue markers: experimental data; solid red line: linear fit). The experimental points were extracted from the measured spectrum as the center of the different N_2O absorption lines and were compared to the corresponding wavenumbers from the HITRAN database.

The QCL frequency scales linearly with the AR current [Figure 2.7(b)] resulting in a current tuning coefficient of -0.55 GHz/mA or -40.47 GHz/W with the power dissipated in the AR (not shown in the figure).

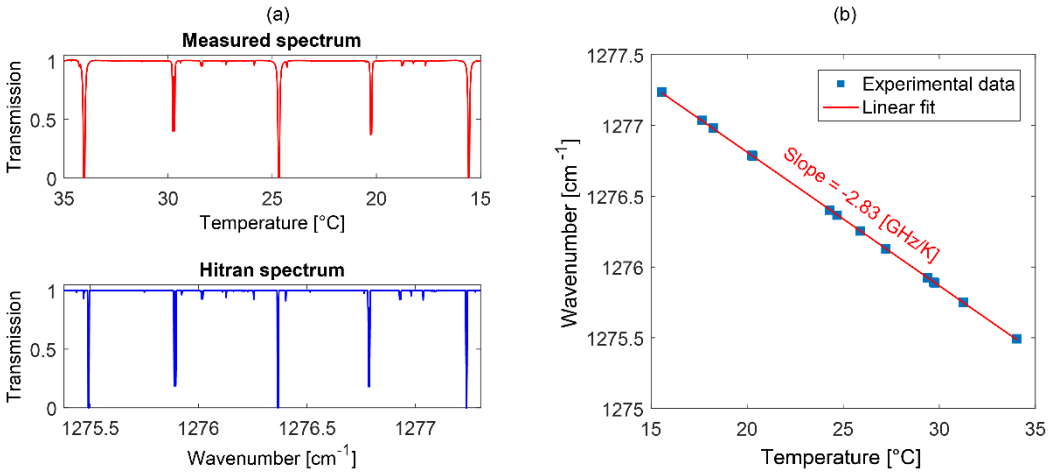

Figure 2.8: (a) Absorption spectrum of N_2O obtained by scanning the QCL sub-mount temperature (T) (top spectrum obtained at active region current I_{AR} = 400 mA and integrated heater current I_{IH} = 0 mA) and corresponding N_2O absorption spectrum from HITRAN database[30] (bottom spectrum). (b) Static tuning curve as a function of the sub-mount temperature (blue markers: experimental data; solid red line: linear fit). The experimental points were extracted from the measured spectrum as the center of the different N_2O absorption lines and were compared to the corresponding wavenumbers from the HITRAN database.

The QCL frequency also scales linearly with the sub-mount temperature [Figure 2.8(b)] resulting in a temperature tuning coefficient of -2.83 GHz/K.

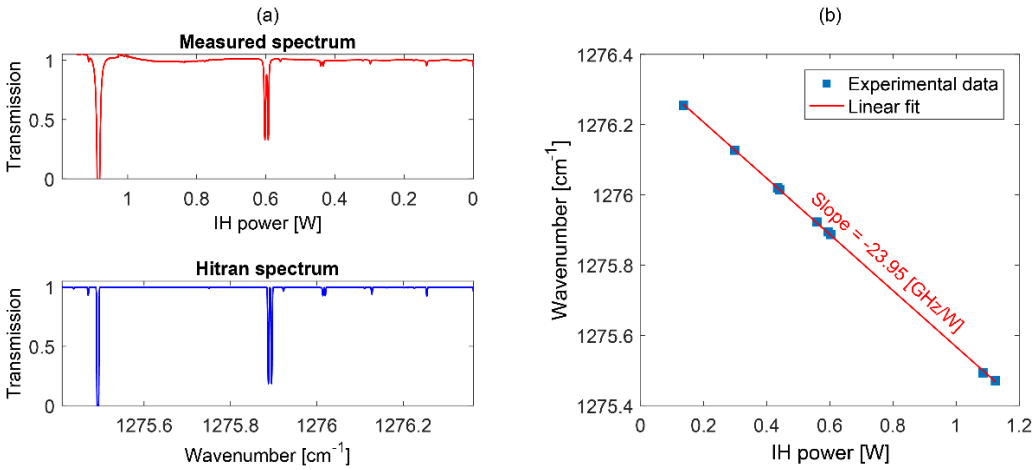

Figure 2.9: (a) Absorption spectrum of N_2O obtained by scanning the QCL integrated heater current (I_{IH}) (top spectrum obtained at active region current I_{AR} = 400 mA and sub-mount temperature T = 25 °C) and corresponding N_2O absorption spectrum from HITRAN database[30] (bottom spectrum). (b) Static tuning curve as a function of the IH power (blue markers: experimental data; solid red line: linear fit). The experimental points were extracted from the measured spectrum as the center of the different N_2O absorption lines and were compared to the corresponding wavenumbers from the HITRAN database.

In contrast to the AR current and sub-mount temperature, the QCL frequency does not tune linearly but quadratically with the IH current. The quadratic behavior shows that the effect of the IH on the QCL frequency is purely thermal via Joule's dissipation. This also leads to a linear response of the QCL frequency with the electrical power dissipated in the IH section (obtained as the product of the IH voltage and current, i.e., $P_{IH} = V_{IH} \cdot I_{IH}$) as displayed in Figure 2.9(b). The resulting static tuning coefficient is -23.95 GHz/W. This is lower than the tuning coefficient for the power dissipated in the QCL active region (-40.47 GHz/W) due to the fact that the heat dissipation in the IH occurs at a relatively larger distance from the active region. As a result, some of the heat from the IH is dissipated in the surrounding structure before reaching the active region. A thermal resistance R_{th} associated to the heating of the QCL active region arising from the electrical power P dissipated in the IH was determined from the ratio of the power and temperature tuning coefficients of the IH

as R_{th} = $(\Delta\nu/\Delta P)/(\Delta\nu/\Delta T)$, leading to a value of 14.3 W/K. A similar thermal resistance calculated for the QCL current gave a smaller value of 8.5 W/K. The combined tuning coefficients of the QCL along with the respective thermal resistances are shown in Figure 2.10.

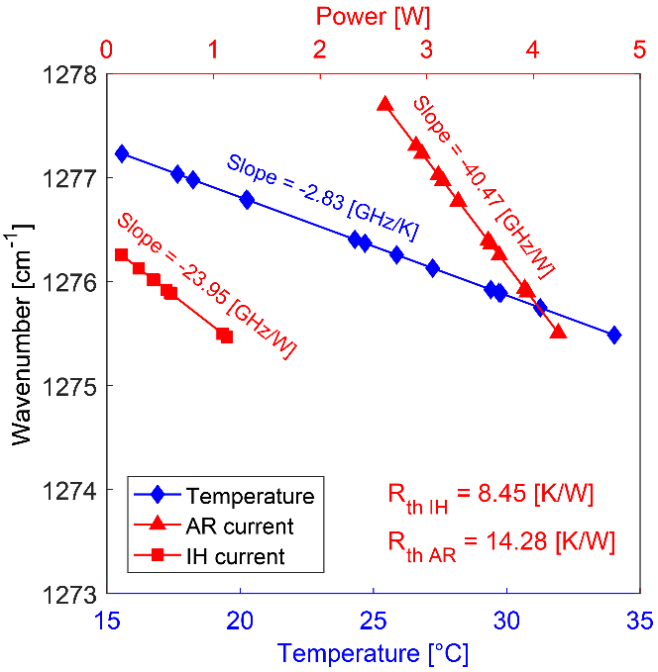

Figure 2.10: Combined static tuning coefficients of the QCL measured as a function of sub-mount temperature, QCL active region current, and IH current (markers: experimental points; lines: linear fits). The thermal resistance (R_{th}) resulting in the heating of the QCL active region for QCL current and IH current is 14.28 K/W and 8.45 K/W, respectively.

2.2.3 Impact of the IH on the QCL frequency noise

Finally, the potential impact of the IH on the frequency noise of the QCL was assessed by measuring the frequency noise power spectral density (FN-PSD) for different currents in the integrated heater. The laser frequency was tuned to the flank of a strong N_2O absorption line, which acts as a frequency discriminator to convert the laser frequency fluctuations into intensity fluctuations which are detected by a Mercury-Cadmium-Telluride (MCT) photodetector with a conversion coefficient of

~17 V/GHz (see Figure 2.11). The detector produces an output voltage that is proportional to the incident intensity at its sensing area.

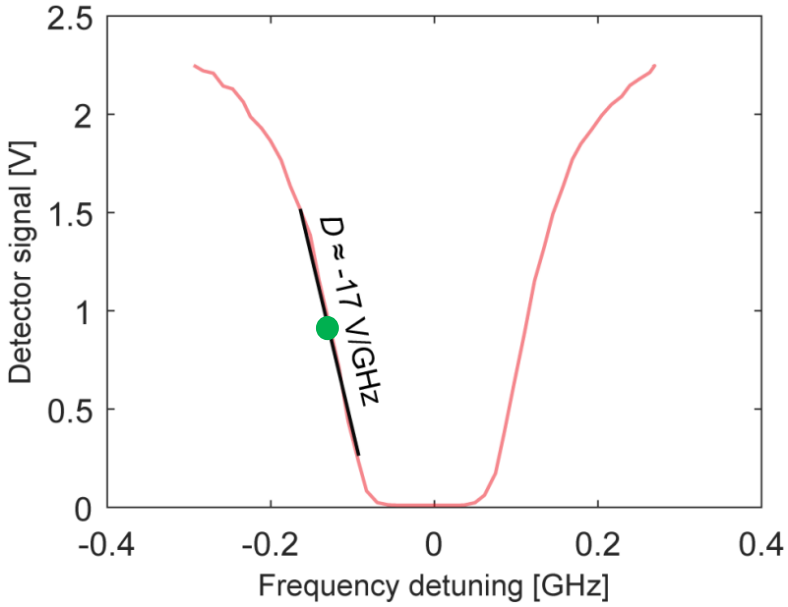

Figure 2.11: N_2O absorption line used as a frequency discriminator to measure the frequency noise of the QCL. The absorption spectrum was measured by tuning the QCL current and recording the photodetector voltage. The current axis was converted into a frequency axis using the measured current tuning coefficient of the QCL of -0.55 GHz/mA. The operating point of the QCL is shown by the green dot and the linear operation range by the black line with a slope *D*.

Initially, a DC bias current of ~360 mA was applied to the QCL and the sub-mount temperature was kept at 25 °C. As the current in the IH was increased, the frequency of the QCL decreased, and to compensate for this change, both the AR current and the sub-mount temperature were slightly changed to keep the laser on the same N_2O transition. The measured FN-PSD of the laser is shown in Figure 2.12. From this result, it is evident that the incorporated IH in the QCL does not induce any additional noise to the laser frequency.

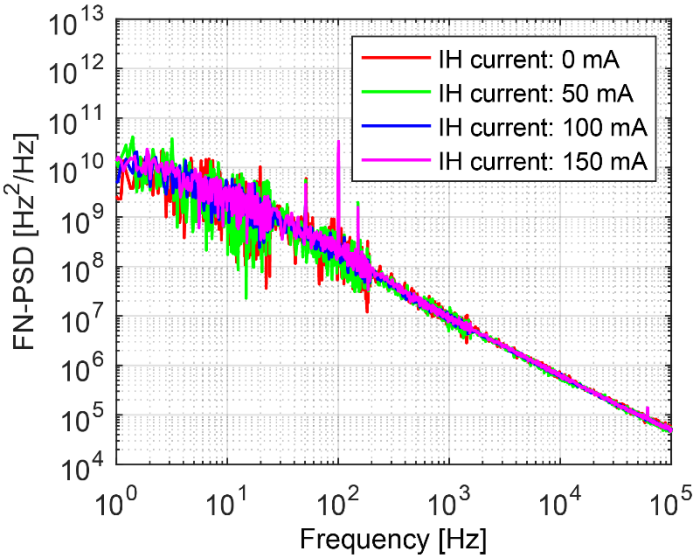

Figure 2.12: Frequency-noise power spectral density (FN-PSD) of the QCL measured at different IH currents.

2.3 Investigation of IH as a new actuator for frequency noise reduction in QCLs

2.3.1 Introduction

Frequency-stabilized and hence, narrow-linewidth QCLs are required in many applications. The intrinsic or Schawlow-Townes linewidth of DFB-QCLs is as low as a few hundred hertz that results from the laser white frequency noise[11]. However, temperature fluctuations in the laser active region arising from the electrical flicker noise in the semiconductor gain structure[31,32] and the technical noise due to laser current driver[33] lead to a broadening of the emission linewidth up to the megahertz level, for integration times ranging from milliseconds to hundreds of milliseconds.

Several schemes have been demonstrated to reduce the frequency noise that includes locking the QCL to a high finesse optical cavity[34,35], side-of-fringe locking to an absorption feature of a gas[36] (N_2O, CO, CO_2, etc.) as well as phase locking a QCL to a cavity-stabilized frequency comb[37,38]. Usually, a frequency or phase-sensitive element is used to sense the frequency or phase fluctuations, respectively, of the laser to generate an error signal that is then fed back to the QCL current driver.

In 2013, Tombez *et al.* reported a different approach for frequency noise reduction in QCLs that does not require any optical reference by utilizing the correlation observed between the voltage fluctuations across the QCL terminals and the corresponding frequency fluctuations[39]. Voltage noise was identified as a major source for electrical power fluctuations dissipated in the laser semiconductor structure, which results in fluctuations of the laser internal temperature and hence in frequency noise[31]. In a proof-of-principle demonstration, an intensity-modulated near-infrared (NIR) diode laser at 1550 nm was illuminating the top surface of a QCL chip (through a window made in the LLH) for fast

control of its internal temperature[39]. Using the QCL voltage noise as an error signal for the feedback signal applied to the NIR laser, a significant reduction of the QCL frequency noise by one order of magnitude was achieved. Driving the QCL at constant electrical power instead of constant current by processing the voltage noise in a field-programmable gate array (FPGA), also resulted in a reduction of the QCL frequency noise[40].

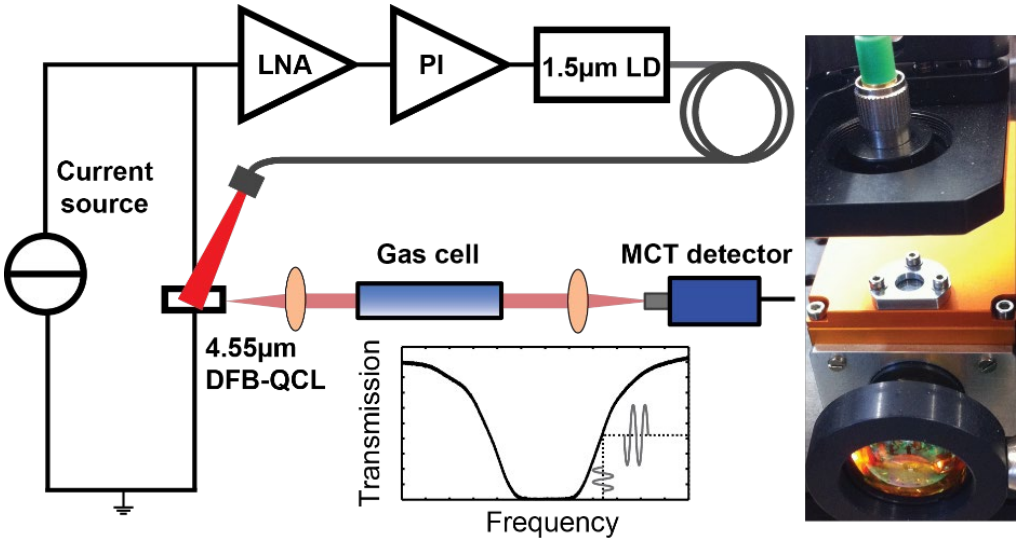

Figure 2.13: Experimental set-up used at UniNE-LTF for frequency noise reduction in a 4.55-µm QCL utilizing only the voltage noise information. The voltage noise measured across the QCL was amplified by a low-noise voltage amplifier (LNA), processed by a proportional-integral (PI) controller and fed back to the 1550-nm fiber-coupled NIR laser illuminating the top of the QCL chip. At the same time, the optical frequency of the QCL was analyzed using an absorption line of CO acting as a frequency-to-intensity converter. The figure is taken from [39].

At the time of implementation of this method, it was considered that the NIR laser used to illuminate the top surface of the QCL was acting on the QCL temperature through the absorbed incident light in its structure, leading to the possibility to reduce its voltage noise. A simple spectroscopic setup was used to characterize the frequency noise of the free-running and stabilized QCL. The output signal from a photodetector was recorded with an FFT spectrum analyzer to measure the noise spectrum and with a scope to observe the temporal fluctuations. At the

same time, the voltage across the QCL terminals was also measured in the same way. Figure 2.14 shows the voltage and frequency fluctuations recorded on the scope when the loop was open and closed. The figure clearly shows the reduction of the voltage noise and associated frequency noise for the closed loop that occurs after 2 ms. Another important aspect that must be noticed is the strong correlation between these two parameters with a correlation factor (ρ) of 0.9 calculated by Tombez.

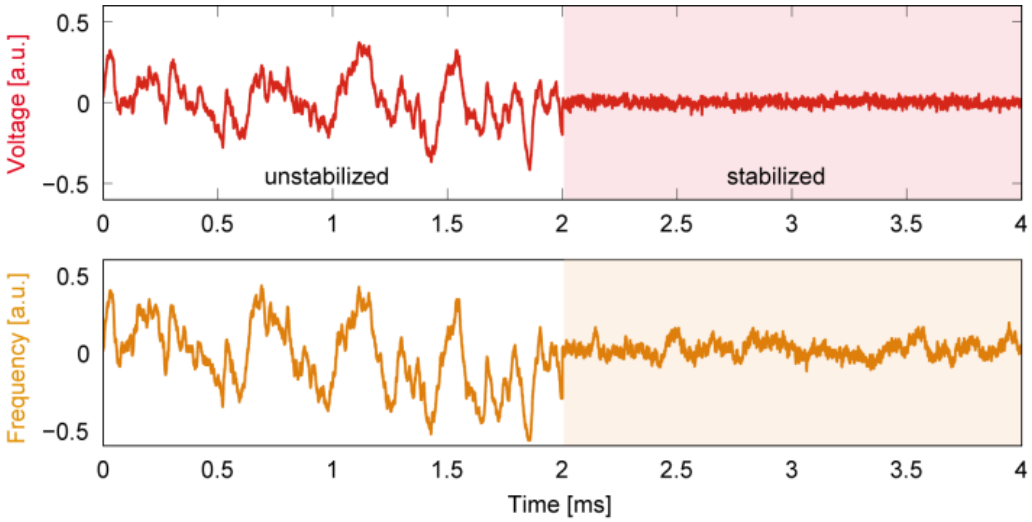

Figure 2.14: Simultaneous recordings of the voltage (upper frame) and optical frequency (lower frame) fluctuations in a 4.55-µm QCL. Before locking (t < 2 ms), a clear correlation between voltage and frequency fluctuations is observed. When locked (t > 2 ms), the loop efficiently reduces the voltage fluctuations by acting on the QCL internal temperature, and a reduction of the QCL frequency noise is also observed. The figure is taken from[39].

The frequency noise power spectral density of the free-running and stabilized QCL is shown in Figure 2.15. A reduction by a factor 10 is observed in the FN-PSD of the stabilized QCL within the locking bandwidth of the feedback loop, which is ~300 kHz as observed from the servo bump.

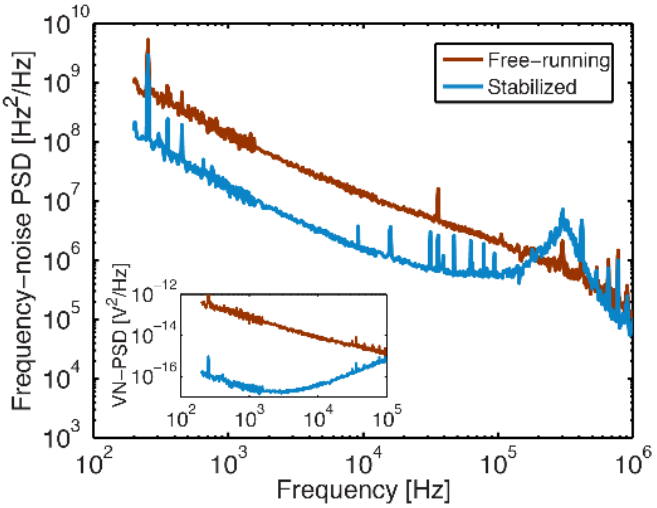

Figure 2.15: Frequency noise PSD of the free-running and stabilized QCL. Closing the feedback loop resulted in a reduction of the frequency noise PSD by a factor of 10. The servo bump observed around 300 kHz indicates the locking bandwidth. The figure is taken from [39].

At the time of the experiment, the origin of the frequency noise reduction obtained by shining the NIR light on the QCL top surface was attributed to a thermal effect (changing the temperature of a QCL changes its emission frequency). If this was the case, a QCL equipped with an IH must show a frequency noise reduction if the feedback signal is applied to the IH instead of an external laser. In the next section, the investigation of an IH as a new actuator for frequency noise reduction in QCLs and encountered problems are discussed.

2.3.2 Results of first attempts of frequency noise reduction using feedback to the IH current

The 7.8-µm DFB-QCL equipped with an IH that was presented in Section 2.2.2 was used in a similar experimental setup as implemented by Tombez as shown in Figure 2.16. The voltage between the QCL terminals was amplified by a 40-dB AC-coupled amplifier and used as an error signal for the control loop.

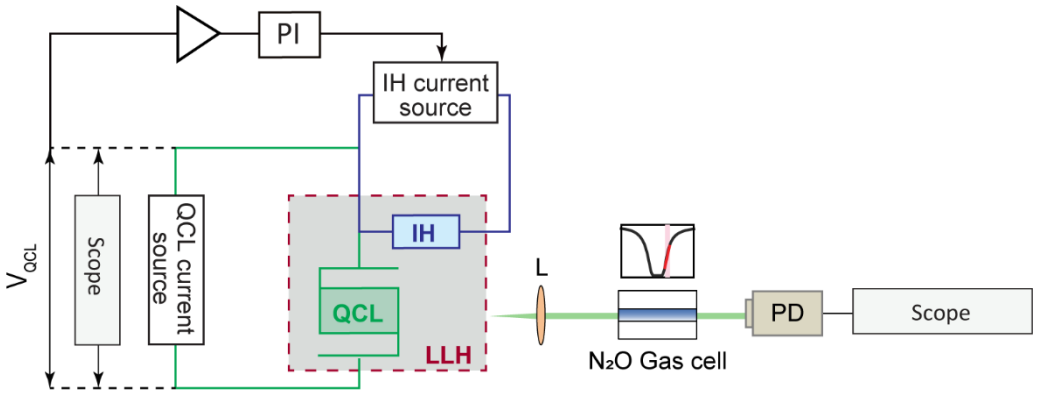

Figure 2.16: Experimental setup implemented for the tentative reduction of the QCL frequency noise using the IH. The voltage noise across QCL was sensed and amplified as an error signal while the feedback was applied to the current source of the IH. The frequency fluctuations were also simultaneously recorded by tuning the QCL frequency to the linear range of an N_2O line and observing the detector voltage on an oscilloscope.

A correlation factor of ~0.8 was observed between the voltage and frequency fluctuations of the QCL [see Figure 2.17(b)]. It is comparable to the case of the 4.5-µm QCL used by Tombez, which verifies the strong correlation between the two quantities.

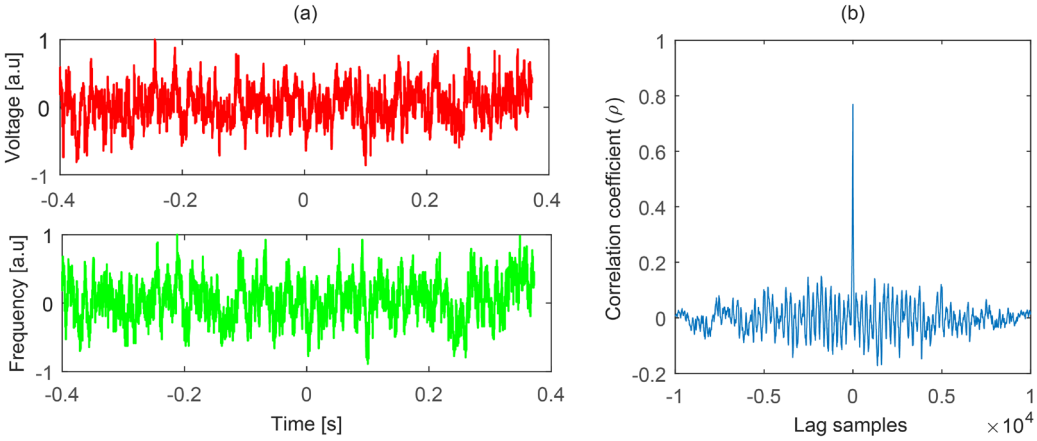

Figure 2.17: (a) Time traces for the voltage (upper frame) and optical frequency fluctuations (lower frame) in a 7.8-µm DFB-QCL. A clear correlation between voltage and frequency fluctuations is observed. (b) Correlation coefficient (ρ) computed from the time samples of the voltage and frequency fluctuations.

The feedback signal from the PI servo-controller was applied to the current source of the IH. The control loop was effectively able to reduce the voltage fluctuations across the QCL [see Figure 2.18(a)], but no reduction of the associated frequency noise of the QCL was observed [see Figure 2.18(b)], as compared to the previous implementation of the method with an external NIR illuminating laser. Even more, the frequency fluctuations of the QCL were increased for the closed control loop [see Figure 2.18(b)].

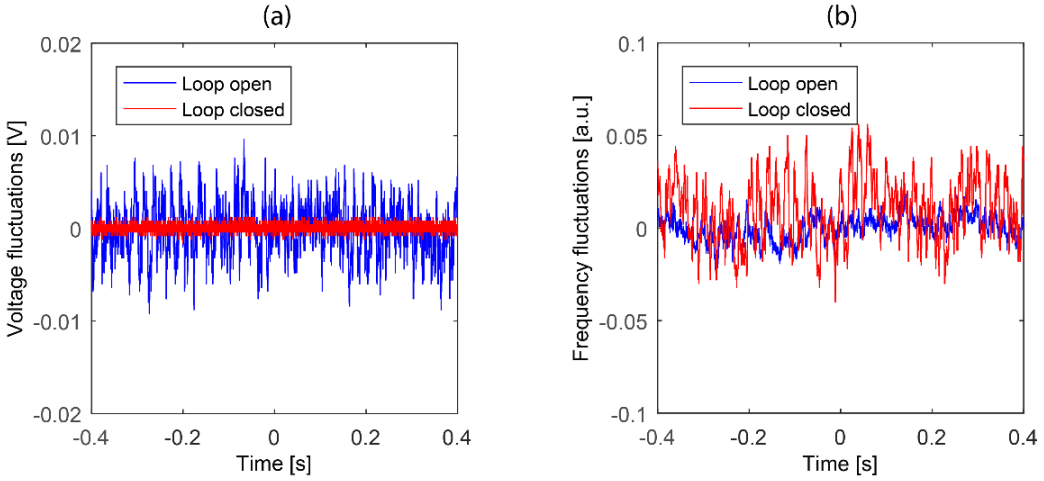

Figure 2.18: Attempt to reduce the QCL optical frequency fluctuations by stabilizing the voltage across its terminals through a feedback signal applied to the IH current source. (a) QCL voltage fluctuations recorded with the loop open (blue) and closed (red). (b) Corresponding frequency fluctuations of the QCL as measured on the side of an N_2O absorption line with the stabilization loop open (blue) and closed (red).

These results compelled to verify the previous noise reduction method using an external illumination laser. Different QCLs were used: the DFB-QCL at 4.5 μm as was used in the initial demonstration of the method[39], a DFB-QCL at 7.8 μm, and the same IH-QCL at 7.8 μm as used in the results of Figure 2.18. Frequency noise reduction was observed in all cases when the QCL voltage was stabilized. The FN-PSD of the IH-QCL is shown in Figure 2.19 as an example of the validation of the method applied by Tombez.

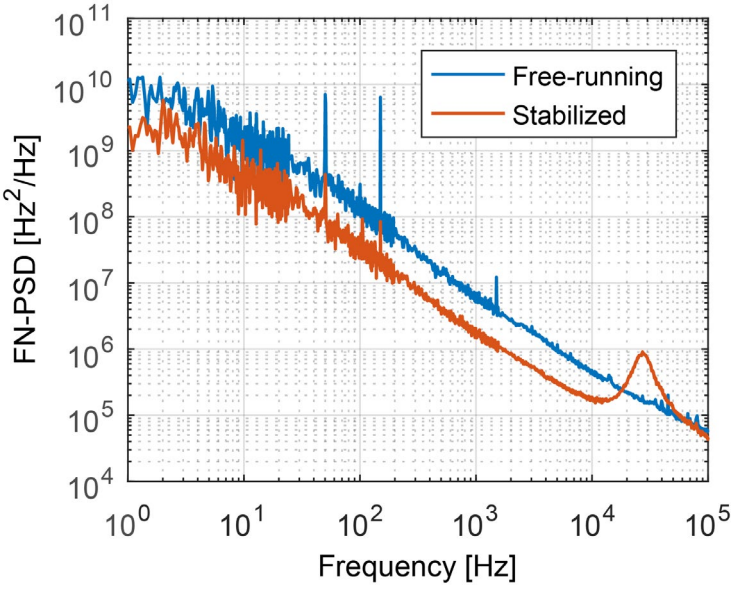

Figure 2.19: Frequency noise power spectral density (FN-PSD) of the free-running and stabilized DFB-QCL equipped with an IH by implementing the method demonstrated by Tombez (Figure 2.13). A reduction by a factor of 5 is seen in the FN-PSD of the stabilized QCL, and the locking bandwidth achieved in this case is ~30 kHz.

2.3.3 Static effect of the IH current on the QCL voltage

To identify the reason for not being able to reduce the frequency noise using feedback to the IH current, different experiments were performed. In the first step, the effect of the IH current on the QCL voltage was investigated. Generally, changing the temperature of a QCL heat-sink through its TEC decreases its voltage, which was verified in the used IH-QCL as shown in Figure 2.20(a). A slope of around -10 mV/K was observed as displayed in Figure 2.20(b), which is in good agreement with the value previously measured by Tombez[39]. The IH current is expected to produce a thermal effect in the active region by Joule's dissipation. Hence, the QCL voltage dependence on the IH current should be of the same sign as for a temperature change via its TEC. A first measurement performed with the IH-QCL mounted in the LLH showed surprisingly the opposite temperature dependence [see Figure 2.20(b)].

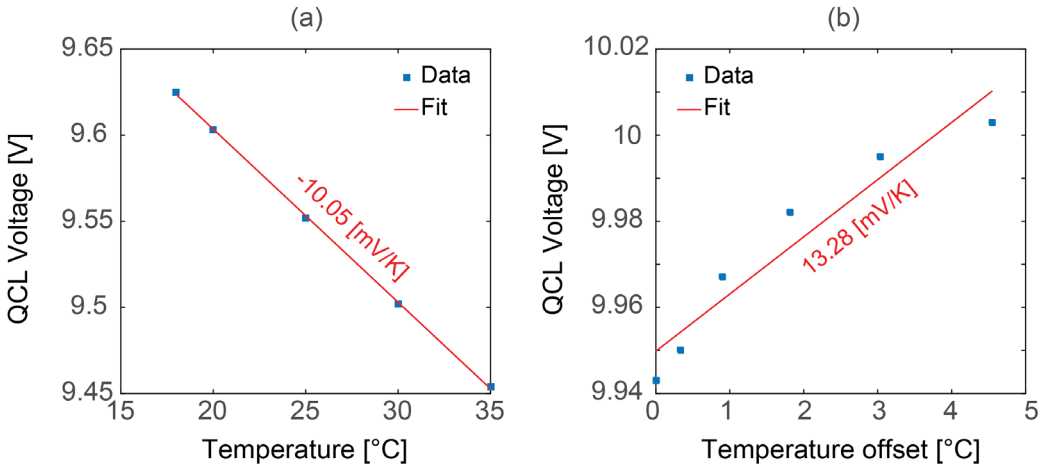

Figure 2.20: (a) Dependence of the QCL voltage as a function of temperature (varied via the TEC). (b) Dependence of the QCL voltage observed as a function of the temperature offset induced by the IH in a first measurement. The electrical power dissipated in the IH was converted into an equivalent temperature change by taking into account the temperature and IH current tuning coefficients of the laser determined in Section 2.2.2.

A parasitic resistance (R_p) occurring in the common electrical path between the two current sources used to independently drive the QCL active region and the IH (see Figure 2.21) was identified for this behavior. A relatively long common physical path between the two driving circuits existed in the initial laser housing electrical scheme, resulting in a significant parasitic resistance (evaluated to around 750 mΩ). This resistance contributes to the measured voltage across the QCL terminals. Therefore, the measured voltage did not correspond to the exact voltage between the QCL terminals and was slightly offset from this value. The IH section of the QCL can be operated in anode ground (AG) or cathode ground (CG) configuration. Depending on the polarity of the IH current source, the offset voltage resulting from the parasitic resistance can have either the same sign or the opposite sign as of the QCL voltage drop.

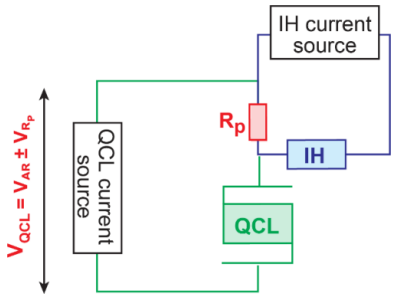

Figure 2.21: Electrical connection scheme for driving the QCL active region and the IH with independent current sources. The QCL voltage measured between the driver terminals includes a parasitic resistance R_p in the common electrical path.

In a next step, the common path between the two driving circuits was shortened by connecting the driving circuits as close as possible from the corresponding pins to the laser chip. This resulted in a reduced parasitic resistance of around 100 mΩ, assessed from the different slopes of the QCL voltage measured as a function of the IH current obtained for the two polarities (cathode ground: CG and anode ground: AG).

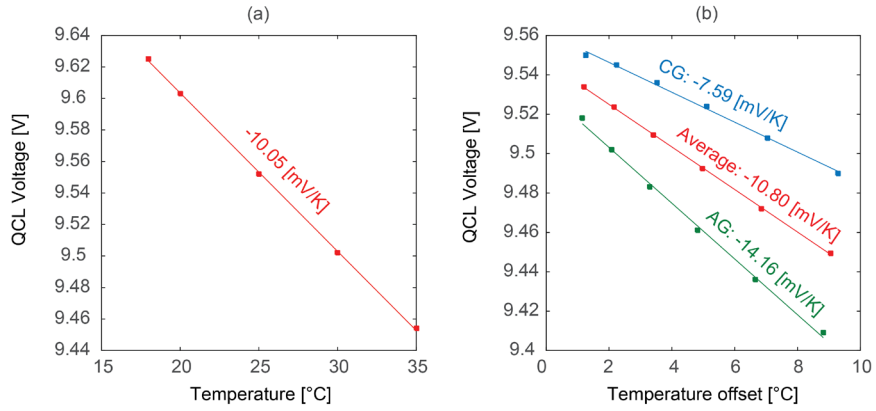

Figure 2.22: QCL voltage dependence as a function of the temperature varied via the TEC (a) and with the temperature offset induced by the IH current (b). The IH is operated in two polarities of its current (designated as cathode ground, CG, and anode ground, AG) while the QCL is operated in the cathode ground configuration. The power dissipated in the IH was converted into an equivalent temperature change using the IH thermal resistance (discussed in Section 2.2.2). The parasitic resistance $R_p \approx 100$ mΩ was retrieved from the difference between the two slopes (blue and green lines), whereas the average slope (red line) gives a similar temperature coefficient (~10 mV/K) as obtained with the TEC.

Both polarities, in this case, led to a negative dependence of the measured QCL voltage as a function of temperature, as expected, with an average slope of -10 mV/K obtained when converting the power dissipated in the IH into an equivalent temperature change using the IH thermal resistance.

2.3.4 Dynamic response of the QCL voltage for IH current modulation

The transfer function of the voltage across the QCL was measured in amplitude and phase while modulating the current in the IH section. A sine modulation was applied to the IH current driver and the resulting modulation of the QCL voltage was measured using a lock-in amplifier. Measurements were performed at two different average currents (200 mA and 400 mA, respectively) applied to the IH for the two current polarities. The corresponding transfer functions are displayed in Figure 2.23.

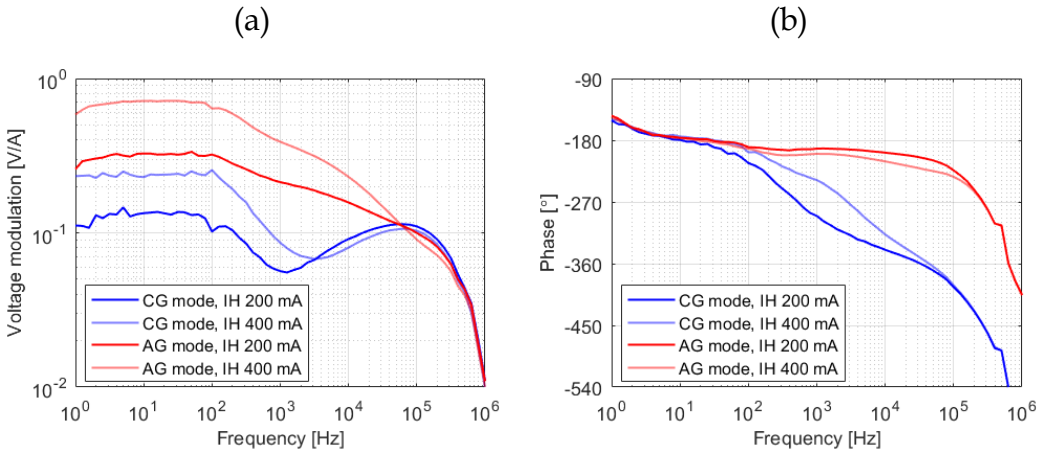

Figure 2.23: QCL voltage transfer functions in amplitude (a) and phase (b) for a sine modulation of the IH current. Measurements were performed for two polarities (red: anode ground, AG; blue: cathode ground, CG) and for two different average currents in the IH section (light color: 200 mA; dark color: 400 mA).

The measured transfer functions show a significant phase difference between the two polarities above 100-Hz modulation frequencies. In the cathode ground configuration, i.e., when the currents from both drivers

flowing through the parasitic resistance are in the same direction, a significant phase shift occurs. It can be detrimental in a stabilization loop that aims at reducing the voltage noise. Therefore, the IH driver must be used in the anode ground configuration to be applied in such a feedback loop. This is demonstrated in Figure 2.24, which shows that the QCL voltage stabilization loop works when the IH is driven in the anode ground mode (i.e., the current in the IH section is in the opposite direction than the current in the QCL active region), but not for the other mode. However, the stabilization of the QCL voltage, shown in Figure 2.25(a), did not result in a reduction of the QCL frequency noise, but in a strong degradation as shown in Figure 2.25(b).

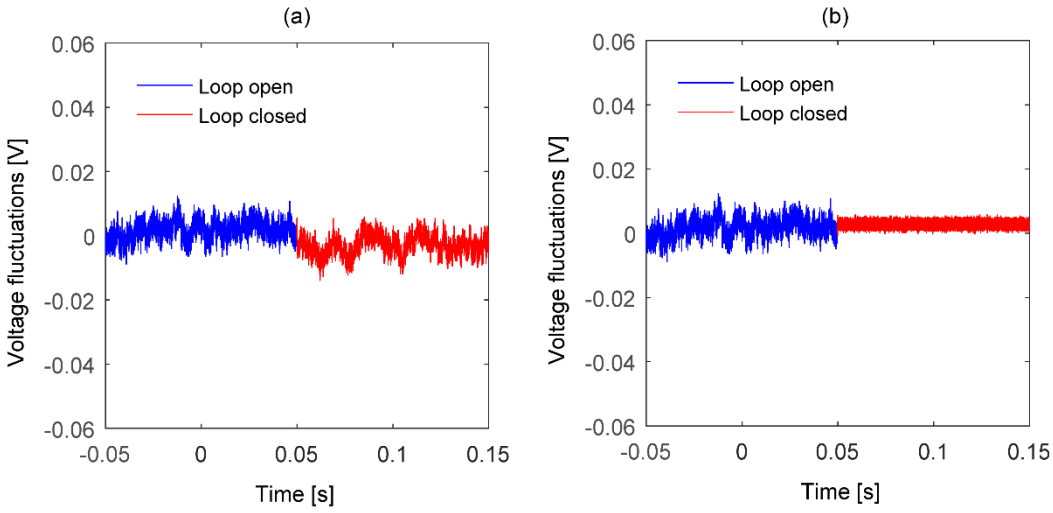

Figure 2.24: Attempt to reduce the voltage noise of the QCL by applying feedback to the IH current for the two possible polarities of the IH current [(a): cathode ground, (b): anode ground]. The plots show the voltage noise measured across the QCL terminals (including the parasitic resistance) with the loop open (first half of the plots) and closed (second half of the plots). The voltage noise reduction works only with the IH operated in the anode ground configuration [case (b)].

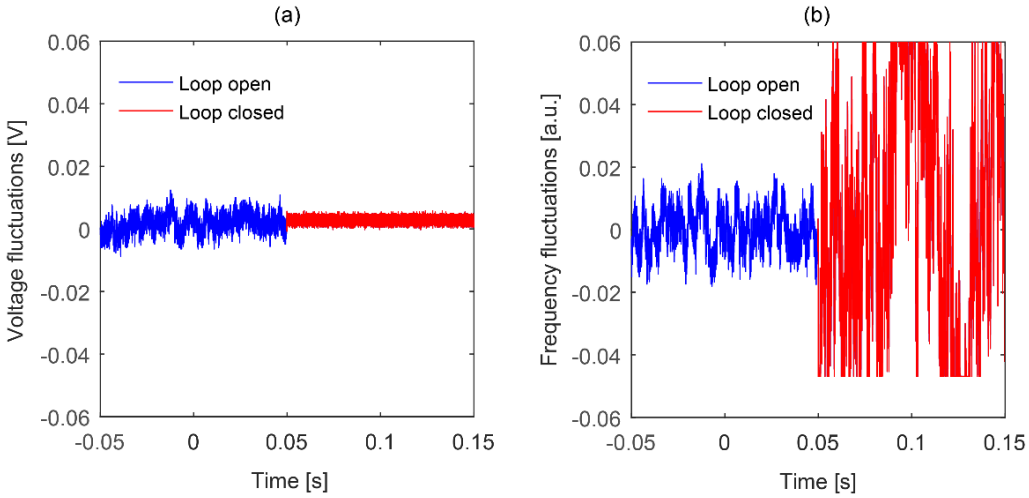

Figure 2.25: Stabilization of the QCL voltage by feedback to the IH current operated in anode ground configuration (a) and associated degradation of the laser frequency noise (b).

2.3.5 Final assessment

The dependence of the QCL frequency shift as a function of the IH power and illuminating NIR laser power used in the previous configuration was investigated. For this purpose, the QCL frequency was tuned in the linear range of a strong N_2O absorption line and the corresponding detector voltage was recorded. This voltage was converted back into frequency detuning with the discriminator of the absorption line. The laser frequency decreased with the increase in electrical power dissipated in the IH as shown in Figure 2.26(a), which is a well-known behavior resulting from a thermal effect (redshift with increasing temperature). However, the same measurement made with the NIR optical power illuminating the top of the QCL showed the opposite effect on the laser frequency (blue shift as a function of the illumination power), as depicted in Figure 2.26(b). At the same time, the internal laser temperature is believed to increase as a consequence of the partial absorption of the incident light in the QCL structure. This indicates that the observed tuning mechanism was not induced by a thermal effect, but more likely by a modification of the refractive index of the QCL resulting

from infrared light absorbed in the uncovered semiconductor material in the 50-µm wide gaps located between the top gold-coated contact sections of the laser chip.

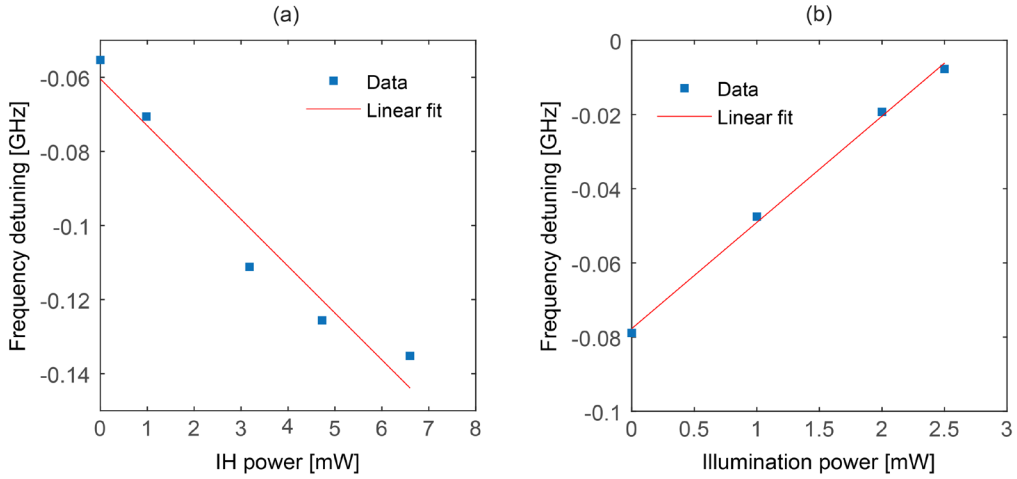

Figure 2.26: Dependence of the QCL optical frequency as a function of the electrical power dissipated in the IH section (a) and of the optical power of the NIR illuminating laser (b).

This indicates that the initial assessment of the frequency noise reduction by the optical control of a QCL by a near-infrared illumination laser presented by Tombez *et al*[39]. was incorrect. The physical effect leading to the observed change of the QCL optical frequency was not thermal but resulted from a refractive index change caused by a change in the carrier charge density. Therefore, it has the correct blue shift dependence that is required so that the applied QCL voltage stabilization loop has a simultaneous positive effect on the QCL frequency. This is not the case with the IH: the "correction" signal applied to the optical frequency has the wrong sign; therefore, the frequency fluctuations are enhanced instead of being reduced. Therefore, the IH cannot be used in a stabilization loop to reduce the frequency fluctuations of a QCL using the QCL voltage noise as an error signal.

2.4 Interest of an IH in a QCL for modulation

The modulation of the laser wavelength via its injection current is a key technique applied in wavelength modulation spectroscopy (WMS) or photoacoustic spectroscopy for trace gas sensing[13,14]. WMS is a widely employed technique to produce derivative-like signals of an absorption feature of a gas that is used for laser frequency stabilization to the center of a transition or to determine the gas concentration. The basic principle consists of dithering the laser wavelength with a sinusoidal signal and slowly scanning the laser through an absorption line (Figure 2.27). This wavelength modulation results in a modulation of the optical power that is transmitted through the gaseous sample. This intensity modulation contains components at various harmonics of the modulation frequency, and a lock-in detection scheme can be applied to measure the component at a desired harmonic. This technique generates demodulated signals that are derivative-like in nature: for instance, the signal at the n^{th} harmonic of the modulation frequency approximates the n^{th} derivative of the absorption line (Figure 2.27). For this reason, this technique is also known as derivative spectroscopy in the literature.

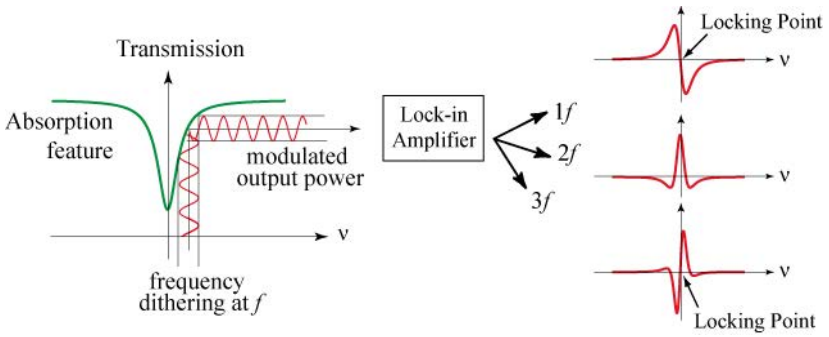

Figure 2.27: Basic principle of wavelength modulation spectroscopy. The laser frequency is modulated at frequency f and lock-in detection is performed to extract the different harmonic signals. The laser is commonly stabilized to the zero-crossing point of the odd harmonic signals ($1f$ and $3f$) at line center, indicated as "Locking Point" in the harmonic spectra on the right side of the figure. The figure is taken from[41].

Derivative spectroscopy is a convenient way to generate an error signal for laser frequency stabilization, as the zero crossings of the odd derivatives (1*f* and 3*f*) occur at the center of the absorption line. These derivative signals are in such a way that the output signal is proportional to the laser frequency detuning from the center of an absorption line. However, direct current modulation of the laser results in the optical power modulation at the same time, which is known as residual amplitude modulation (RAM). This RAM can be detrimental in some applications, for example when the first harmonic signal (1*f*) is used as an error signal for a feedback loop in the stabilization of a laser to the center of a transition, as it induces an offset in the laser locking point.

The IH incorporated in a QCL offers a new way to modulate the wavelength of the QCL at a relatively high speed as compared to the sub-mount temperature modulation[29]. A potential benefit of modulating the QCL wavelength via the IH current is the reduced associated RAM as compared to a modulation of the QCL injection current. Furthermore, a combined modulation of the QCL and IH currents can be considered with appropriate amplitudes and phases in order to generate a pure frequency modulation (FM) by cancelling the associated RAM. In a similar way, a pure amplitude modulation (AM) can be generated. In Section 2.5, this application of an IH in a QCL is reported, and the use of the IH as a new actuator to generate pure FM and AM is presented. This work is a reprint of an article published in Optics Express[42].

2.5 Electrically-driven pure amplitude and frequency modulation in a quantum cascade laser

Atif Shehzad[1], Pierre Brochard[1], Renaud Matthey[1], Stephane Blaser[2], Tobias Gresch[2], Richard Maulini[2], Antoine Muller[2], Thomas Südmeyer[1], and Stéphane Schilt[1]

[1]Laboratoire Temps-Fréquence, Université de Neuchâtel, Av. de Bellevaux 51, CH-2000 Neuchâtel, Switzerland

[2]Alpes Lasers SA, Av. des Pâquiers 1, CH-2072 Saint-Blaise, Switzerland

We present pure amplitude modulation (AM) and frequency modulation (FM) achieved electrically in a quantum cascade laser (QCL) equipped with an integrated resistive heater (IH). The QCL output power scales linearly with the current applied to the active region (AR), but decreases with the IH current, while the emission frequency decreases with both currents. Hence, a simultaneous modulation applied to the current of the AR and IH sections with a proper relative amplitude and phase can suppress the AM, resulting in a pure FM, or vice-versa. The adequate modulation parameters depend on the applied modulation frequency. Therefore, they were first determined from the individual measurements of the AM and FM transfer functions obtained for a modulation applied to the current of the AR or IH section, respectively. By optimizing the parameters of the two modulations, we demonstrate a reduction of the spurious AM or FM by almost two orders of magnitude at characteristic frequencies of 1 and 10 kHz compared to the use of the AR current only.

2.5.1 Introduction

A wide range of applications make use of modulated laser sources, notably in optical communications and sensing. Combining a modulation

scheme with a demodulation (e.g., lock-in detection) generally leads to a strong improvement in the detection sensitivity. Different types of modulation schemes can be applied, depending on the involved sensor and the parameter to be measured. The most common relate to modulation of the optical power (amplitude modulation – AM), of the optical frequency (frequency modulation – FM) or of the optical phase (phase modulation – PM). For instance, wavelength and frequency modulation spectroscopy (WMS/FMS) methods are widely used to detect small absorption features in trace gas laser spectroscopy sensing. They consist in modulating the wavelength/frequency of a laser and detecting the harmonic signals of an atomic or molecular transition obtained when the laser frequency is additionally scanned through the transition. It leads to the generation of derivative-like signals of the probed absorption profile in WMS [1,2] or to the possibility to access both the absorption and dispersion of a gaseous sample in FMS [3]. Odd-harmonic WMS signals like 1*f* or 3*f* are also commonly used to stabilize a laser onto a molecular or atomic transition [4]. The well-known Pound-Drever-Hall method [5] widely applied to narrow down the linewidth of a laser by frequency stabilization to a high-finesse optical cavity is one of the most important applications of FMS [6,7]. In a different area of gas sensing, light modulated at audio frequencies (in amplitude or wavelength) and absorbed in a gaseous sample can excite acoustic waves, which are exploited for sensitive trace gas monitoring in various photoacoustic spectroscopy (PAS) methods [8,9].

Semiconductor lasers are the most commonly used laser source in trace gas sensing applications owing to their unique properties like single-mode emission, wavelength tunability and fast modulation capabilities. They can easily be directly modulated via their injection current and up to high frequencies in the GHz range. However, both their emission frequency and output power vary with the injection current. Therefore, modulating the injection current results in combined AM-FM, with a phase shift between the two modulations that depends on the applied

modulation frequency [10]. The residual amplitude modulation (RAM) is generally an undesired effect that distorts the harmonic signals in WMS. It leads to an asymmetry in the second-harmonic (2*f*) signal often used in trace gas monitoring [11] or to an offset in the first-harmonic (1*f*) signal that can be detrimental in laser frequency stabilization experiments by inducing a frequency shift of the locking point from the center of the transition. Therefore, the use of a pure FM would be beneficial to these applications. On the other hand, a pure AM is sometimes also desired, for instance in PAS sensing of broadband or non-structured absorption spectra [12].

Quantum cascade lasers (QCLs) are the most widespread laser source for high-resolution molecular spectroscopy and trace-gas sensing in the mid-infrared fingerprint spectral region. Similar to near-infrared laser diodes, a modulation applied to their injection current results in combined AM and FM. Different approaches have been studied in the last years to generate a pure FM (or pure AM in some cases) from a QCL. A first approach for pure FM was realized optically by simultaneously illuminating the front facet of a QCL by two continuous-wave near-infrared laser sources of different wavelengths (1.55 μm and 850 nm), corresponding to photon energies smaller and higher, respectively, than the edge of the electrons energy sub-band [13]. Both incident laser beams produced a blue shift of the QCL wavelength as a result of the induced change of the carrier density, whereas they yielded AM of opposite sign. AM was thus efficiently suppressed by proper adjustment of the incident modulated powers, leading to pure FM.

Another method to produce pure FM or AM was demonstrated in a quartz-enhanced PAS sensor using a special QCL structure made of three independent sections [14]. The master oscillator (i.e., the lasing section), the gain section (amplifier) and the phase section were controlled by distinct electrical currents. The phase section enabled controlling the reflectivity of the front facet of the QCL by adjusting the reflection phase,

thus strongly affecting the emitted optical power. A combination of currents selectively applied to these three sections allowed obtaining laser wavelength tuning without changes of the optical power or power modulation without emission wavelength shifts. Pure FM was achieved by simultaneously modulating the currents of the master oscillator and phase sections, whereas pure AM was obtained by modulating only the phase section.

In this article, we present a different approach to generate electrically either pure FM or pure AM in a QCL. It makes use of a new feature that has been recently introduced in QCLs in the form of an integrated heater (IH) located in the vicinity of the active region (AR) in a distributed feedback (DFB) QCL [15]. This resistive heater enables controlling the internal temperature of the AR by Joule's dissipation via an electrical current, which is much faster than standard temperature control with a thermo-electrical cooler [16]. Changing the temperature of a QCL modifies both its frequency and its output power. Therefore, the IH simultaneously acts on these two quantities. The IH current affects the QCL optical frequency in the same way as the AR current (i.e., the optical frequency decreases with increasing current), as both current tunings result from a thermal effect. However, the optical power of the QCL decreases with increasing IH current (as the laser threshold current increases with temperature), whereas it increases with the AR current. Therefore, a modulation applied to the AR and IH currents has a different effect on the laser AM and FM. Combining a simultaneous modulation of the two currents with an appropriate relative amplitude and phase can enable suppressing either the AM (thus producing pure FM) or the FM (thus generating pure AM). We demonstrate these two situations in a QCL emitting at 7.8 μm, and show a reduction of the parasitic modulation by almost two orders of magnitude compared to the usual case where only the AR current is modulated. This high reduction of the parasitic modulation is demonstrated at two characteristic frequencies of 1 and 10 kHz. Our results incorporate a study of the dynamic response of the

output power and emission frequency of the QCL for the two applied modulation signals and show how their relative amplitude and phase must be adjusted as a function of the considered modulation frequency.

2.5.2 Experimental setup and methods

The laser used in this work is a DFB-QCL emitting at 7.8 μm and equipped with an IH with an internal resistance of ~5.6 Ω located a few micrometers from the AR. It is of the same type as initially reported by Bismuto *et al*. [15] and later on extensively characterized by Gürel *et al*. in terms of tuning speed and modulation transfer functions [16]. The QCL soldered on a copper sub-mount was placed in a standard laser laboratory housing (LLH) from Alpes Lasers and temperature-stabilized near 25°C by a thermo-electrical cooler. The static tuning curves and output power of the QCL measured at this temperature as a function of the AR and IH currents are shown in Figure 1. The static tuning coefficients are typically -0.55 GHz/mA as a function of the AR current and -23.95 GHz/W as a function of the electrical power dissipated in the IH. The tuning curves were determined from the position of several N_2O absorption lines measured in a low-pressure (2 mbar) gas cell in correspondence to their reference values from the HITRAN spectroscopic database [17]. The output power was measured using a thermal powermeter placed in front of the laser housing after an external collimating lens. As a result of the high divergence of the light beam at the output of the QCL and the limited numerical aperture of the lens, only part of the total emitted power was detected in this case. This had no impact on the measurement reported here as the purpose was only to observe the relative variation of the optical power as a function of the current in the AR or IH, respectively. The result shows that the optical power increases with the current in the AR (up to the roll-over current). On the contrary, it decreases with the IH current, which induces a heating of the laser AR that leads to an increase of the threshold current and an associated power reduction at constant AR current. At the same time, the frequency of the emitted light decreases

with both currents due to their predominant thermal effect. This dependence is fairly linear with respect to the AR current, but has a higher quadratic component for the IH current as the electrical power dissipated in the IH scales with the squared current.

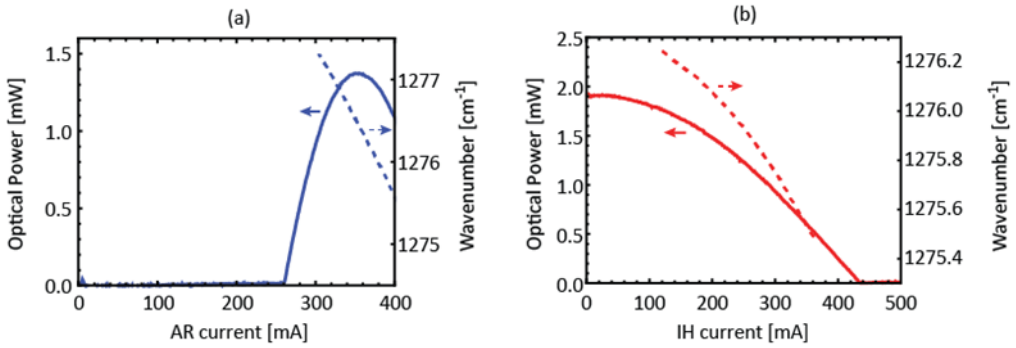

Figure 2.28: Output power (solid lines, left axis) and emission wavenumber (dashed lines, right axis) of the QCL measured as a function of the AR current I_{AR} (a) and of the IH current I_{IH} (b). The QCL heat-sink temperature was 25 °C in all cases. In (a), I_{IH} = 250 mA; in (b), I_{AR} = 320 mA.

The QCL AR and IH were driven by two distinct home-made low-noise current sources. The output beam of the laser was split into two paths by a beamsplitter plate with a nominal splitting ratio of 50/50 (however, it was closer to 60% reflection and 40% transmission at our wavelength and for the considered laser polarization). A photodiode (PD-1 in Figure 2.29) measured the AM in the first path. A low-pressure (2 mbar) 10-cm long N_2O gas cell was used in the second path to measure the FM of the laser. The QCL frequency was tuned to the flank of a strong N_2O absorption line at 1277 cm^{-1} used as frequency discriminator to convert FM into intensity modulation, which was detected by a second photodiode (PD-2, see Figure 2.29). A typical discriminator slope $D \approx$ -7.9 V/GHz was measured for a total contrast of the N_2O absorption line of ~1.2 V (see Figure 2.29). Owing to the steep slope of the absorption line, the measured signal of PD-2 was dominated by the laser FM and the direct contribution of the laser AM was negligible. The AM and FM transfer functions were measured by applying a sine modulation to the current driver of the IH or AR and by demodulating the signal of both

detectors using a lock-in amplifier (Zurich Instruments HF2LI). The drivers have a typical modulation bandwidth in the range of 1 MHz and a modulation coefficient of 2 mA/V.

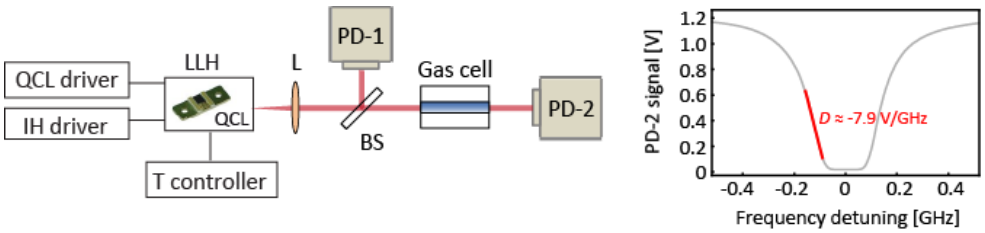

Figure 2.29: Schematic of the experimental setup used to characterize the AM and FM properties of the IH-QCL. Photodiode PD-1 directly measures the AM of the laser, while photodiode PD-2 measures the FM by means of an optical frequency discriminator made of a molecular absorption line in a spectroscopic setup. LLH: laser laboratory housing; L: collimating lens; BS: beamsplitter plate. Right: transmission profile of the P9 absorption line in the ν_3 vibrational band of N_2O at 1277.2 cm^{-1} used as frequency discriminator with a measured slope $D \approx -7.9$ V/GHz (red line).

2.5.3 Experimental results

2.5.3.1 Modulation transfer functions

The transfer functions measured for a modulation of the current applied to the AR or IH around their average values of IAR = 320 mA and IIH = 250 mA, respectively, are displayed in Figure 2.30. The FM transfer functions (dashed lines) are very comparable to those previously reported for a similar IH-QCL [16]. They are characterized by different time constants that result from the heat extraction in different areas of the laser. The FM bandwidth is larger for a modulation of the current in the AR, as the heat is directly produced in the gain medium. The AM transfer function is also significantly different for a modulation of the IH or AR current. The AM response is almost constant up to a modulation frequency close to 1 MHz for the AR current, which seems to be limited by the bandwidth of the driver. For a modulation of the IH current, the response drops much faster, resulting from the fact that the power

variations induced by the IH current arise from a thermal effect that is limited in bandwidth.

Hence, the ratio H_{IH}/H_{AR} of the amplitude of the transfer functions obtained for a modulation of the IH and AR currents (either for FM or AM) has a strong frequency dependence as displayed in Figure 2.31. The relative phase shift $\varphi_{IH\text{-}AR} = \varphi_{IH} - \varphi_{AR}$ is also frequency dependent, where φ_{IH} and φ_{AR} are the phase of the individual transfer functions displayed in Figure 2.30. The modulation of the two currents leads to a similar phase (at low modulation frequencies) of the FM transfer functions, but to an opposite phase for AM.

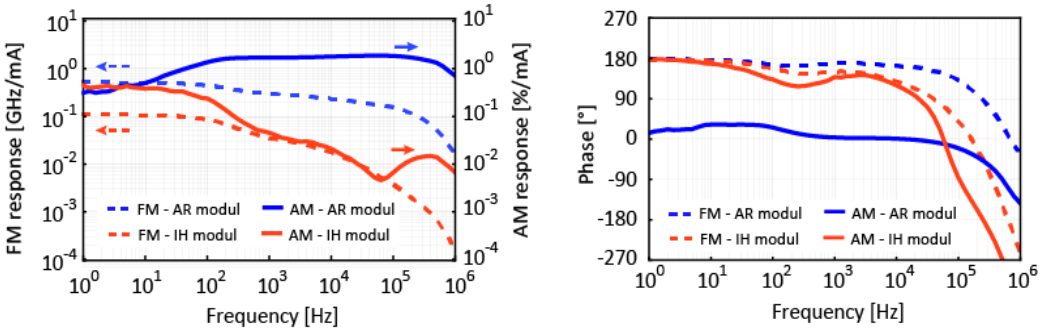

Figure 2.30: Amplitude (left) and phase (right) of the AM (solid lines) and FM (dashed lines) transfer functions measured for a modulation of the current of the AR (blue) and IH (red) around their average values of I_{AR} = 320 mA and I_{IH} = 250 mA.

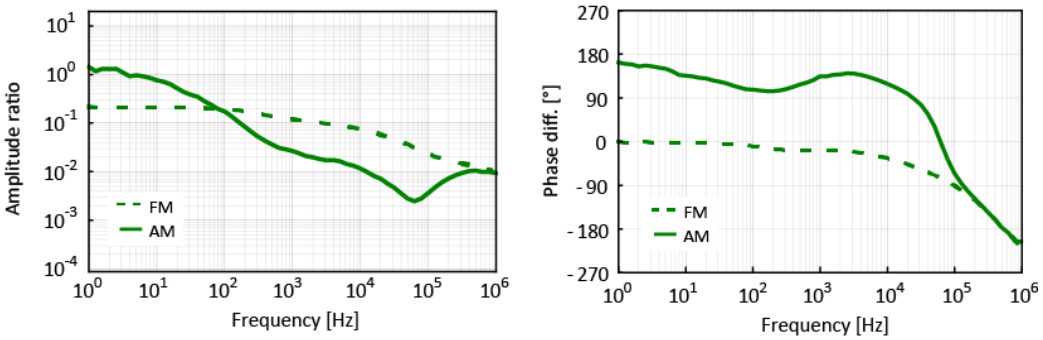

Figure 2.31: Amplitude ratio H_{IH}/H_{AR} (left) and phase shift $\varphi_{IH\text{-}AR}$ (right) between the transfer functions obtained for a modulation of the IH and AR currents in the case of AM (solid line) and FM (dashed line) at an operation point of the laser characterized by I_{AR} = 320 mA and I_{IH} = 250 mA.

Therefore, applying a simultaneous modulation to the AR and IH currents with a suitable relative amplitude and phase shift can result in a compensation of the two AM (resp. FM) contributions, leading to the possibility to produce pure FM (resp. AM).

2.5.3.2 Pure AM

The generation of a pure AM signal is illustrated in Figure 2.32 in the particular case of modulation frequencies of 1 kHz and 10 kHz chosen for the proof-of-concept demonstration of the dual modulation method. However, similar results can be achieved at other modulation frequencies following the same principle. The temporal traces of the individual AM and FM signals produced when modulating either the AR current (blue lines) or the IH current (red lines) alone are displayed together with their combination (green lines) resulting into a pure AM. The applied AM is relatively small here (<1%). It was limited in this example by the measurement of the FM signal produced by the AR or IH current modulation using the N_2O frequency discriminator. The linear range of the N_2O absorption line in which the FM can be measured without distortion is restricted to less than ~60 MHz (see Figure 2.29), corresponding to a change of the AR current smaller than 0.1 mA at low modulation frequency. The modulation signals applied to the AR and IH induce an FM depth in this range as shown in Figure 2.32.

The value of the amplitude ratio $\Delta I_{AR} / \Delta I_{IH}$ and phase shift $\phi_{IH\text{-}AR}$ between the two modulation signals to be applied for efficient FM reduction depends on the operating points (average current) of the AR and IH sections. Both parameters furthermore depend on frequency as previously shown by the frequency dependence of the relative phase shift $\varphi_{IH\text{-}AR}$ observed in Figure 4. Therefore, these parameters must be precisely determined at the considered operation point of the laser and for the modulation frequency of interest. The phase difference $\phi_{IH\text{-}AR} = \phi_{IH} - \phi_{AR}$

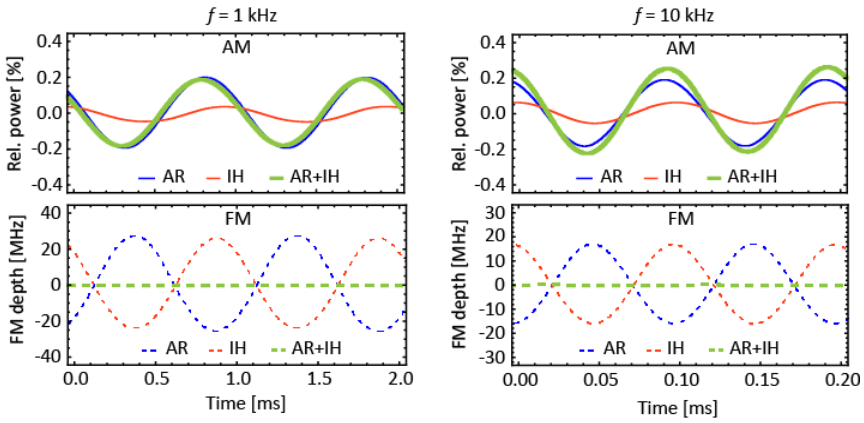

Figure 2.32: Examples of single-channel AM (top) and FM (bottom) signals resulting from a modulation of the AR current (blue curves) or of the IH current (red curves); combined AM (solid green curves) and FM (dashed green curves) modulation signals obtained for maximum FM suppression (pure AM). The left and right graphs correspond to a modulation frequency of 1 kHz and 10 kHz, respectively. The amplitude of the applied modulation signals is 50 mV to the AR driver in all cases (resulting in ΔI_{AR} = 0.1 mA), 415 mV at 1 kHz and 680 mV at 10 kHz to the IH driver (corresponding to 0.83 mA and 1.36 mA, respectively).

between the two control signals $I_{IH}(t) = \Delta I_{IH} \sin(2\pi ft + \phi_{IH})$ and $I_{AR}(t) = \Delta I_{AR} \sin(2\pi ft + \phi_{AR})$ at frequency f applied to the current drivers must be adjusted such that the total phase between the two induced modulation signals is equal to 180° for the modulation to be suppressed, in this case FM: $\phi_{IH\text{-}AR}^{FM} + \varphi_{IH\text{-}AR}^{FM} = 180°$. This total phase is the combination of the phase shift $\phi_{IH\text{-}AR}$ between the two applied current modulation signals and the phase difference $\varphi_{IH\text{-}AR}$ resulting from the laser response. Then, the relative amplitude $\Delta I_{AR}/\Delta I_{IH}$ of the two modulation signals must be adjusted to compensate for the different response of the laser to these modulations, which is characterized by the amplitude ratio H_{IH}/H_{AR} of the transfer functions displayed in Figure 2.31, i.e., ($\Delta I_{AR}/\Delta I_{IH} = H_{IH}/H_{AR}$).

At a modulation frequency of 1 kHz, the relative FM induced by the IH and AR currents is characterized by $H_{IH}^{FM}/H_{AR}^{FM} = 0.118$ and $\varphi_{IH\text{-}AR}^{FM} = -18.3°$. Pure AM is therefore expected to be achieved by applying two modulation signals such that $\Delta I_{AR}/\Delta I_{IH}$ = 0.118 and $\phi_{IH\text{-}AR} = 198.3°$.

These parameters become $\Delta I_{AR}/\Delta I_{IH}$ = 0.074 and $\phi_{IH\text{-}AR}$ = 215° at 10 kHz. The resulting FM signal has been recorded as a function of the relative ratio and phase shift between the two modulations to assess the sensitivity of their adjustment for a proper FM suppression. A fixed modulation signal of 200 mV at 1 kHz or 145 mV at 10 kHz was applied to the current driver controlling the laser AR, corresponding to a current modulation amplitude of 0.4 mA (1 kHz) or 0.29 mA (10 kHz) in the AR. These values are higher than the upper limit mentioned in the beginning of Section 2.5.3.2 for a correct measurement of the FM signal. However, it does not affect the results reported here as we are interested in the small total FM signal resulting from the combined modulation of the AR and IH currents and not in the stronger individual FM signals that may be distorted at this modulation amplitude.

A signal generator (HP 3314A) was used to modulate the IH driver. The generator was phase-locked to the modulation signal applied to the AR and delivered an output signal with a varying phase and amplitude to modulate the IH driver. The phase of the applied signal was scanned over a range of more than 60° with a step of 1° for a series of different amplitudes and the resulting FM signal (from photodiode PD-2) was measured by the lock-in amplifier. The second channel of the lock-in amplifier was used to precisely measure the phase of the applied modulation signal in comparison to the AR modulation, i.e., the phase difference $\phi_{IH\text{-}AR}$. The different sets of experimental data were processed together to calculate the density plots displayed in Figure 2.33, which show the reduction of the FM signal from the case where a modulation is applied to the AR only. The highest FM suppression is achieved for ΔI_{IH} = 3.4 mA (i.e., $\Delta I_{AR}/\Delta I_{IH} \approx 0.117$) and $\phi_{IH\text{-}AR} \approx 199°$ at f = 1 kHz, and ΔI_{IH} = 4 mA ($\Delta I_{AR}/\Delta I_{IH} \approx 0.072$) and $\phi_{IH\text{-}AR} \approx 214°$ at f = 10 kHz, in good agreement with the values extracted from the amplitude ratio and phase difference of the transfer functions displayed in Figure 2.31 ($H_{IH}^{AM}/H_{AR}^{AM} = 0.118$ and $\varphi_{IH\text{-}AR}^{AM} = -18.3°$ at f = 1 kHz, $H_{IH}^{AM}/H_{AR}^{AM} = 0.074$ and

$\varphi_{\text{IH-AR}}^{\text{AM}} = -34.2°$ at f = 10 kHz). A reduction of the FM by more than two orders of magnitude is demonstrated at both modulation frequencies of 1 kHz (>24 dB) and 10 kHz (>22 dB) when using the combined modulation with optimized parameters in comparison to the traditional modulation applied to the QCL current only. These values may be slightly underestimated as the maximum FM depth obtained for a modulation of the AR current only and used in the normalization of the recorded data to determine the FM attenuation is larger than the linear range of the N_2O frequency discriminator. Therefore, the determined normalization FM signal is slightly lower than in reality (we estimated the resulting signal reduction to be around 40%), which should lead to an effective FM attenuation that is still enhanced by around 2 dB from the aforementioned values.

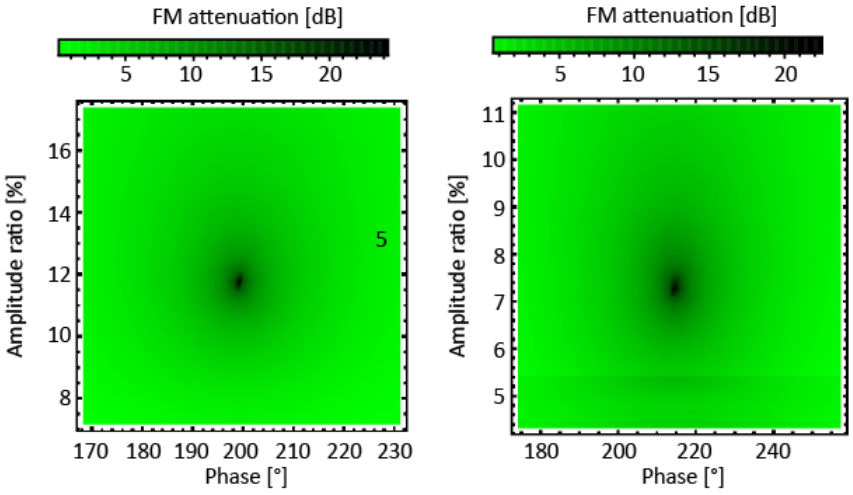

Figure 2.33: Density plot showing the reduction of the residual FM signal as a function of the amplitude ratio and phase shift between the modulation signals applied to the IH and AR currents, in comparison to the FM signal arising when only the AR current is modulated. The left and right graphs correspond to a modulation frequency of 1 kHz and 10 kHz, respectively. A modulation signal with an amplitude of 200 mV was applied to the AR driver at f = 1 kHz, and 145 mV at f = 10 kHz (resulting in ΔI_{AR} = 0.4 mA and ΔI_{AR} = 0.29 mA, respectively).

2.5.3.3 Pure FM

For pure FM, the same setup and procedure were used. The amplitude ratio and phase shift between the two modulations were adjusted in order to minimize the residual AM signal. Figure 2.34 displays the corresponding temporal traces of the individual AM and FM signals obtained when modulating either the AR current (blue lines) or the IH current (red lines) alone at 1 kHz or 10 kHz, together with their combination (green lines) resulting into a pure FM. The modulation signals applied to the AR and IH were kept small enough to ensure that the total induced FM could be correctly measured using the N_2O frequency discriminator. Therefore, the FM depth produced in these examples is smaller than 100 MHz. However, larger amplitudes can be obtained in principle while keeping an efficient suppression of the parasitic AM by increasing the amplitude of the two modulation signals by the same factor to keep their ratio constant.

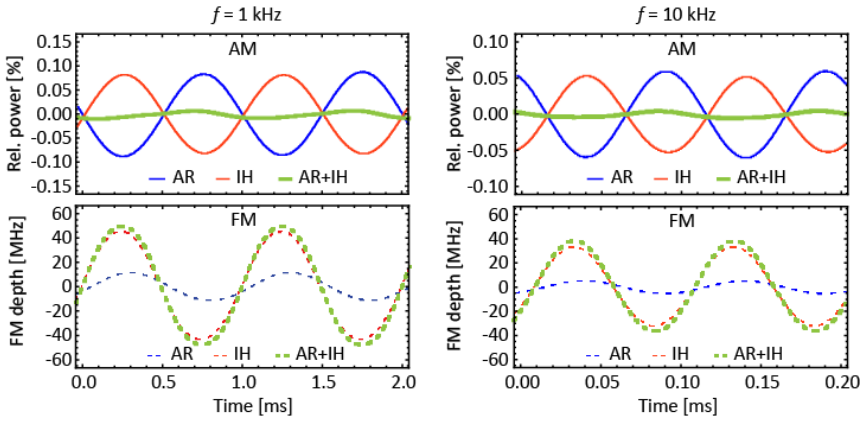

Figure 2.34: Examples of single-channel AM (top) and FM (bottom) signals resulting from a modulation of the AR current (blue curves) or of the IH current (red curves); combined AM (solid green curves) and FM (dashed green curves) modulation signals obtained for maximum AM suppression (pure FM). The left and right graphs correspond to a modulation frequency of 1 kHz and 10 kHz, respectively. The amplitude of the applied modulation signals is 22 mV (at 1 kHz) or 15 mV (10 kHz) to the AR driver (resulting in ΔI_{AR} = 0.044 mA or 0.03 mA, respectively) and 810 mV at 1 kHz and 1.2 V at 10 kHz to the IH driver (corresponding to 1.62 mA and 2.4 mA, respectively).

The residual AM signal was measured as a function of the amplitude ratio and phase shift between the two applied modulations at the two characteristic frequencies of 1 and 10 kHz. A fixed modulation signal of 160 mV (at f = 1 kHz) or 80 mV (at f = 10 kHz) was applied to the current driver controlling the laser AR, corresponding to a current modulation amplitude of 0.32 mA (1 kHz) or 0.16 mA (10 kHz) in the AR. The signal applied to the IH was scanned in amplitude and phase as previously described for the pure AM case. The individual FM signals induced by the modulation of the AR and IH currents are slightly larger than previously stated to stay in the linear range of the N_2O frequency discriminator, but it does not impact the measurement as the purpose here is to measure the residual AM signal that is not affected by this limitation.

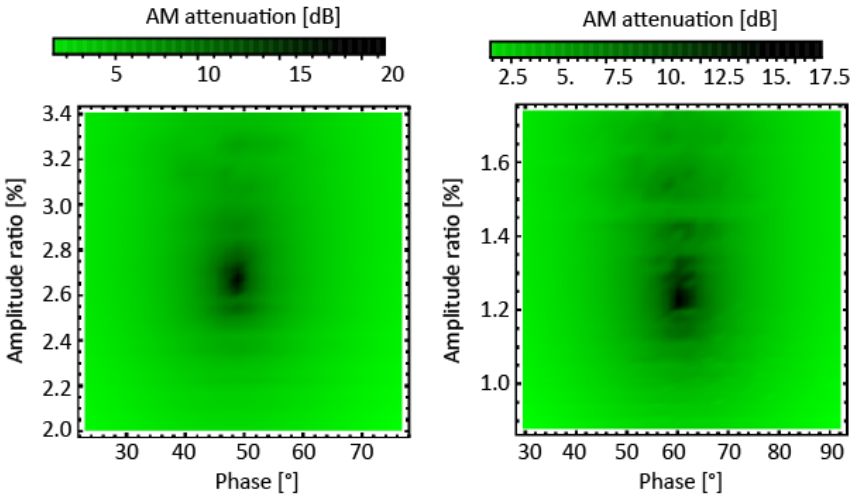

Figure 2.35: Density plot showing the reduction of the residual AM signal as a function of the amplitude ratio and phase shift between the modulation signals applied to the IH and AR currents, in comparison to the AM signal arising when only the AR current is modulated. The left and right graphs correspond to a modulation frequency of 1 kHz and 10 kHz, respectively. A modulation signal with an amplitude of 160 mV was applied to the AR driver at f = 1 kHz and 80 mV at f = 10 kHz (resulting in ΔI_{AR} = 0.32 mA and ΔI_{AR} = 0.16 mA, respectively).

The optimal AM suppression is achieved for $\Delta I_{AR}/\Delta I_{IH} \approx 0.027$ and $\phi_{IH\text{-}AR} \approx 48°$ at a modulation frequency of 1 kHz and $\Delta I_{AR}/\Delta I_{IH} \approx 0.012$ and $\phi_{IH\text{-}AR} \approx 60°$ at 10 kHz. These values are in excellent agreement with the

parameters assessed from the relative AM transfer function displayed in Figure 4 ($H_{\mathrm{IH}}^{\mathrm{AM}}/H_{\mathrm{AR}}^{\mathrm{AM}} = 0.027$ and $\varphi_{\mathrm{IH\text{-}AR}}^{\mathrm{AM}} = 134.7°$ at f = 1 kHz; $H_{\mathrm{IH}}^{\mathrm{AM}}/H_{\mathrm{AR}}^{\mathrm{AM}} = 0.012$ and $\varphi_{\mathrm{IH\text{-}AR}}^{\mathrm{AM}} = 118.9°$ at f = 10 kHz). Here also, a reduction of the AM by almost two orders of magnitude is demonstrated at both modulation frequencies of 1 kHz (>21 dB) and 10 kHz (>18 dB) with the combined modulation in comparison to the traditional modulation applied to the QCL current only.

2.5.4 Conclusions

We have demonstrated an all-electrical method to produce either pure FM or AM in a QCL by applying modulation signals of proper amplitude and phase to two different actuators. The QCL injection current and the current in an IH enable the temperature of the laser active region to be controlled with a relatively high speed. A detailed analysis of the residual modulation has been performed at two characteristic frequencies of 1 and 10 kHz, showing a reduction of the AM by almost two orders of magnitude and of the FM by more than 20 dB in comparison to the traditional modulation applied to the QCL current only. Similar results can be obtained at other modulation frequencies by a proper adjustment of the relative amplitude and phase of the two applied modulation signals. We have shown how these parameters can be obtained with a good accuracy from the measured transfer functions.

The proposed approach is attractive for enhanced performance in sensing methods in which the spurious residual modulation constitutes a parasitic effect that impacts the performance. This is for instance the case for spectroscopic trace gas sensing in which pure FM is generally desired.

Funding

We acknowledge financial support from the Swiss National Science Foundation (SNSF) under the contract No 200020_166104, by the Swiss

Confederation Program Nano-Tera.ch, scientifically evaluated by the SNSF, and by the European Space Agency (ESA) under the contract 4000117741/16/NL.

References

[1] J. M. Supplee, E. A. Whittaker, and W. Lenth, "Theoretical description of frequency modulation and wavelength modulation spectroscopy," Appl. Opt. 33(27), 6294–6302 (1994).

[2] S. Schilt, L. Thévenaz, and P. Robert, "Wavelength Modulation Spectroscopy: Combined Frequency and Intensity Laser Modulation," Appl. Opt. 42(33), 6728–6738 (2003).

[3] G. C. Bjorklund, "Frequency-modulation spectroscopy: a new method for measuring weak absorptions and dispersions," Opt. Lett. 5(1), 15–17 (1980).

[4] R. Matthey, S. Schilt, D. Werner, C. Affolderbach, L. Thévenaz, and G. Mileti, "Diode laser frequency stabilisation for water-vapour differential absorption sensing," Appl. Phys. B 85(2–3), 477–485 (2006).

[5] R. W. P. Drever, J. L. Hall, F. V. Kowalski, J. Hough, G. M. Ford, A. J. Munley, and H. Ward, "Laser phase and frequency stabilization using an optical resonator," Appl. Phys. B 31(2), 97–105 (1983).

[6] E. D. Black, "An introduction to Pound–Drever–Hall laser frequency stabilization," Am. J. Phys. 69(1), 79 (2001).

[7] R. W. Fox, C. W. Oates, and L. W. Hollberg, "Stabilizing diode lasers to high-finesse cavities," in Experimental Methods in the Physical Sciences, R. D. van Zee and J. P. Looney, eds., Cavity-Enhanced Spectroscopies (Academic Press, 2003), Vol. 40, pp. 1–46.

[8] M. W. Sigrist, "Trace gas monitoring by laser photoacoustic spectroscopy and related techniques," Rev. Sci. Instrum. 74(1), 486–490 (2003).

[9] A. A. Kosterev, Y. A. Bakhirkin, R. F. Curl, and F. K. Tittel, "Quartz-enhanced photoacoustic spectroscopy," Opt. Lett. 27(21), 1902–1904 (2002).

[10] S. Schilt and L. Thévenaz, "Experimental method based on wavelength-modulation spectroscopy for the characterization of semiconductor lasers under direct modulation," Appl. Opt. 43(22), 4446–4453 (2004).

[11] S. Schilt, L. Thévenaz, and P. Robert, "Wavelength Modulation Spectroscopy: Combined Frequency and Intensity Laser Modulation," Appl. Opt. 42(33), 6728–6738 (2003).

[12] S. Schilt, A. A. Kosterev, and F. K. Tittel, "Performance evaluation of a near infrared QEPAS based ethylene sensor," Appl. Phys. B 95(4), 813–824 (2009).

[13] C. Peng, H. Zhou, L. Zhu, T. Chen, Q. Liu, D. Wang, J. Li, Q. Peng, G. Chen, and Z. Li, "Purified frequency modulation of a quantum cascade laser with an all-optical approach," Opt. Lett. 42(21), 4506–4509 (2017).

[14] P. Patimisco, A. Sampaolo, Y. Bidaux, A. Bismuto, M. Scott, J. Jiang, A. Muller, J. Faist, F. K. Tittel, and V. Spagnolo, "Purely wavelength and amplitude-modulated quartz-enhanced photoacoustic spectroscopy," Opt. Express 24(23), 25943–25954 (2016).

[15] A. Bismuto, Y. Bidaux, C. Tardy, R. Terazzi, T. Gresch, J. Wolf, S. Blaser, A. Muller, and J. Faist, "Extended tuning of mid-ir quantum cascade lasers using integrated resistive heaters," Opt. Express 23(23), 29715–29722 (2015).

[16] K. Gürel, S. Schilt, A. Bismuto, Y. Bidaux, C. Tardy, S. Blaser, T. Gresch, and T. Südmeyer, "Frequency Tuning and Modulation of a

Quantum Cascade Laser with an Integrated Resistive Heater," Photonics 3(3), 47 (2016).

[17] L. S. Rothman, I. E. Gordon, Y. Babikov, A. Barbe, D. Chris Benner, P. F. Bernath, M. Birk, L. Bizzocchi, V. Boudon, L. R. Brown, A. Campargue, K. Chance, E. A. Cohen, L. H. Coudert, V. M. Devi, B. J. Drouin, A. Fayt, J.-M. Flaud, R. R. Gamache, J. J. Harrison, J.-M. Hartmann, C. Hill, J. T. Hodges, D. Jacquemart, A. Jolly, J. Lamouroux, R. J. Le Roy, G. Li, D. A. Long, O. M. Lyulin, C. J. Mackie, S. T. Massie, S. Mikhailenko, H. S. P. Müller, O. V. Naumenko, A. V. Nikitin, J. Orphal, V. Perevalov, A. Perrin, E. R. Polovtseva, C. Richard, M. A. H. Smith, E. Starikova, K. Sung, S. Tashkun, J. Tennyson, G. C. Toon, V. G. Tyuterev, and G. Wagner, "The HITRAN2012 molecular spectroscopic database," J. Quant. Spectrosc. Radiat. Transf. 1304–50 (2013).

Chapter 3

QCL frequency noise reduction using an optical delay line

3.1 Introduction

High-resolution spectroscopy applications in the MIR require narrow-linewidth lasers. MIR QCLs are attractive laser sources for such applications owing to their unique properties such as their high output power, room temperature operation, spectral tunability, and high spectral purity. However, the spectral linewidth of these lasers that is typically in the megahertz range in free-running DFB QCLs is insufficient for some advanced applications and methods to reduce this linewidth are required.

In the past, several methods have been studied and implemented to reduce the frequency noise and, hence, narrow the linewidth of a QCL. Some approaches based on active stabilization that did not require an optical reference have already been discussed in Chapter 2[39,40]. However, these techniques resulted in a fair frequency noise reduction. A few works reported the direct stabilization of a QCL to a MIR optical cavity. Facsi *et*

al. reported the linewidth reduction of a DFB-QCL using a V-shaped optical cavity[35]. The QCL was phase-locked to the optical feedback from the high-finesse cavity. The linewidth of the QCL was reduced from 3.2 MHz in free-running mode to 4 kHz at 1-ms integration time for the locked case. Similarly, Taubman *et al*. presented a few Hz linewidth of the beat signal between two cavity-stabilized QCLs[34]. To compensate for environmental effects on the optical cavities (drifts, low-frequency fluctuations, etc.), one of the cavities was locked to the other with a low-bandwidth (6 kHz) servo loop. Therefore, the reported performance represents the relative linewidth of the beat signal between the two QCLs and not their absolute linewidth as the cavities were locked to each other. The schemes that involve optical cavities for QCL linewidth reduction are fairly complex and costly, as the high-finesse cavities are much less common in the MIR than in the NIR. Moreover, optical cavities are sensitive to environmental noise and perturbations, which makes them not so convenient for field-based applications. Ultra-stable and low-frequency noise QCLs have been achieved in the MIR by phase-locking a QCL to a cavity-stabilized NIR laser using a frequency comb. These schemes involve frequency combs, optical cavities, and non-linear processes that lead to fairly bulky and complex experimental setups.

In this chapter, an alternative method to reduce the frequency noise in a QCL is demonstrated, based on an optical delay line in contrast to the ultra-stable optical cavities that are widely used in the NIR spectral region. An optical delay-line is a very promising approach to achieve a high degree of performance over complexity and cost, resulting in a simple compact system. This method has been previously used in the NIR spectral region[16,43] by delaying the beam of a laser using long optical fibers. The same technique is applied for the first time to a MIR QCL by using a short, meter-scale free-space delay line resulting in a significant reduction of the QCL frequency noise.

Section 3.2 presents a general overview of the stabilization scheme based on a delay line, whereas Section 3.3 reports on its implementation to a QCL in the MIR spectral region and constitutes a reprint of an article published in Optics Letters[44].

3.2 Optical delay line

An optical delay line can be created by using an imbalanced interferometer, such as the Michelson interferometer (MI) or Mach-Zehnder interferometer (MZI) with a long pathlength difference between the two arms. The delay line can be created either with optical fibers or in free space. The schematic of an optical delay line in the MZI configuration using optical fiber is shown in Figure 3.1.

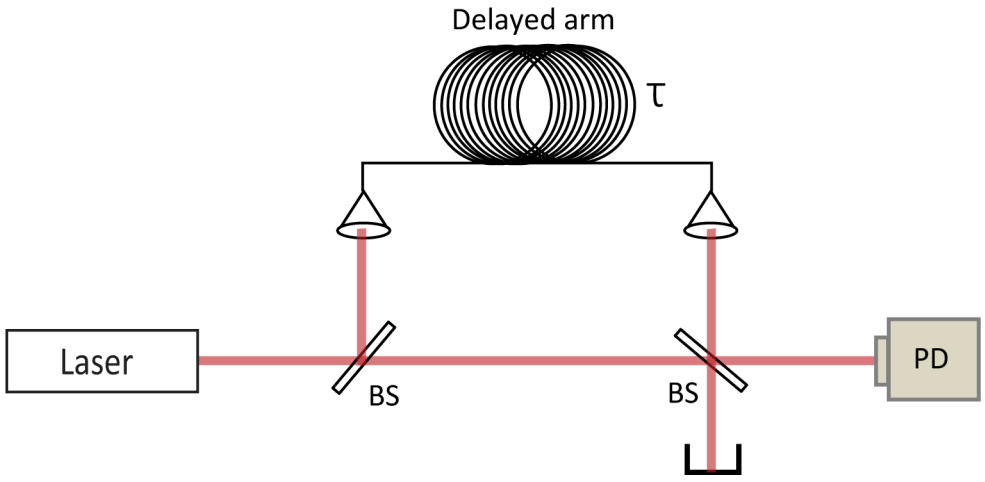

Figure 3.1. Schematic of a Mach-Zehnder interferometer with a long optical delay.

The laser frequency fluctuations are detected by comparing the emitted frequency to a delayed copy of itself at the output of the interferometer. The interferometer converts the laser frequency fluctuations into voltage fluctuations with the following transfer function $T_F(f)$ [45,46].

$$T_F(f) = V_{pk}\left(1 - e^{-i2\pi f\tau}\right) / \, if \quad [\mathrm{V/Hz}] \tag{1}$$

where $V_{pk}$is the amplitude of the interference fringes and τ is the time delay between the two beam paths. The magnitude of the frequency transfer function plotted for two different time delays (τ = 10 µs and 5 µs) is displayed in Figure 3.2.

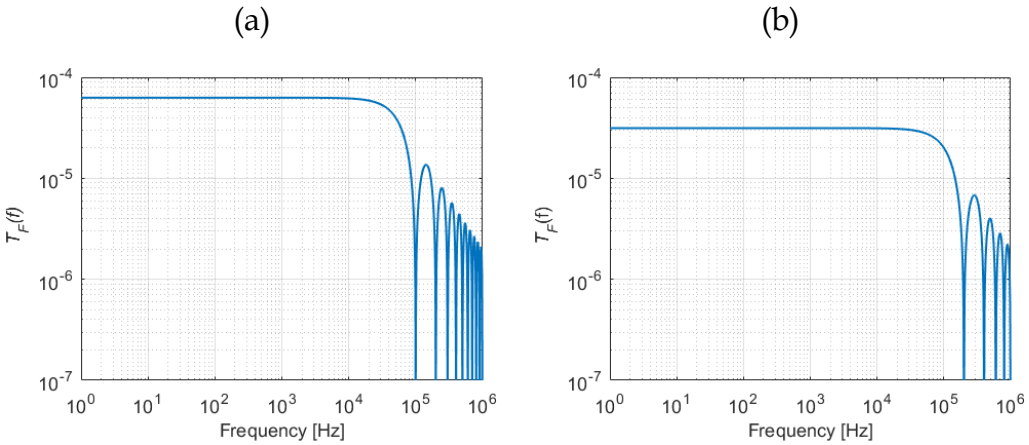

Figure 3.2: Example of a simulated amplitude of transfer function $T_F(f)$ of an optical delay line with (a) $\tau = 10$ µs and (b) $\tau = 5$ µs. For simplicity, the coefficient V_{pk} is considered as 1 V in the simulation.

There are three important frequency regions in the transfer function plots. At low frequencies $f \ll \tau^{-1}$ the frequency transfer function can be approximated as $T_F(f) \approx 2\pi\tau V_{pk}$ that is represented by a flat response in Figure 3.2. This also implies that the optical delay-line acts as a frequency discriminator with a factor of $2\pi\tau V_{pk}$, which is proportional to the pathlength difference (Figure 3.2) and does not depend on the carrier frequency of the signal. The transfer function has a series of zeros at $f = n/\tau$ with integer $n \geq 1$. This can be explained if one considers that the signal is modulated by a sine function at a carrier frequency f_{mod}. For a time delay equal to a multiple of $1/f_{mod}$, the photodetector sees no frequency difference between the signals travelling by the two arms. And for frequencies above the first null point, i.e., $f > \tau^{-1}$, the response is that of a low-pass filter with an envelope of $1/f$ resulting from the multiple poles occurring in the transfer function.

As the light propagates in two different arms of the interferometer, it is subjected to different environmental noises such as temperature, pressure, mechanical and acoustical vibrations, etc., which are detected in the output signal of the interferometer in addition to the laser frequency noise. Some other extra noise sources generally occur in the

photodetection process at the interferometer output, such as flicker ($1/f$) noise originating from the electronics or from other conversion processes (shot noise, laser intensity noise, etc.) occurring in the photodetector itself, resulting in a reduction of the final system performance. One possibility to mitigate these limitations is to use a longer time delay between the two arms of the interferometer to increase the conversion factor of the laser frequency fluctuations with respect to the extra noise, which is independent of the time delay. However, increasing the time delay results in a decrease of the first frequency null point of the transfer function and reduces the achievable locking bandwidth of the servo loop (see Figure 3.2). Consequently, a trade-off must be found between the frequency discrimination factor of the interferometer and the position of the first frequency null point, i.e., the loop bandwidth. The impact of the laser intensity noise can be reduced by using a balanced detection scheme[46] or with the use of a self-heterodyne detection[16] as compared to the self-homodyne detection[46]. In the self-heterodyne configuration, the laser frequency in one of the interferometer arms is shifted (typically by a few MHz) using a modulator (e.g., an acousto-optic modulator (AOM)), and the heterodyne signal at the shifting frequency is detected in the photodetector output signal, which is much less affected by $1/f$ noise than the low-frequency (around 0 Hz) signal of the self-homodyne method.

The optical delay line method can be applied in principle at any wavelength, but it was mainly implemented in the NIR spectral region because of the long delays (km-scale pathlength difference) that can be obtained by the use of optical fibers. So far, this method has not been implemented in the MIR spectral region because long delays are difficult to achieve due to costly and low-performance fibers. Besides this, AOMs in the MIR are costly and poorly available. In Section 3.3, the application of this approach to a MIR QCL is presented for the first time. A strong reduction of the QCL linewidth from the megahertz range (in free-running) to <10 kHz (at 1-s integration time) is achieved using a

pathlength difference of only 1 m between the two arms of an imbalanced free-space MZI in the self-homodyne configuration.

3.3 10-kHz-linewidth mid-infrared quantum cascade laser by stabilization to an optical delay line

Atif Shehzad[1], Pierre Brochard[1], Renaud Matthey[1], Thomas Südmeyer[1], and Stéphane Schilt[1]

[1]Laboratoire Temps-Fréquence, Institut de Physique, Université de Neuchâtel, CH-2000 Neuchâtel, Switzerland.

We present a mid-infrared quantum cascade laser (QCL) with a sub-10-kHz full width at half maximum linewidth (at 1-s integration time) achieved by stabilization to a free-space optical delay line. The linear range in the center of a fringe detected at the output of an imbalanced Mach-Zehnder interferometer implemented with a short free-space pathlength difference of only 1 m is used as frequency discriminator to detect the frequency fluctuations of the QCL. Feedback is applied to the QCL current to lock the laser frequency to the delay line. The application of this method in the mid-infrared is reported for the first time. By implementing it in a simple self-homodyne configuration, we have been able to reduce the frequency noise power spectral density of the QCL by almost 40 dB below 10-kHz Fourier frequency, leading to a linewidth reduction by a factor of almost 60 compared to the free-running laser. The present limits of the setup are assessed and discussed.

Distributed-feedback (DFB) quantum cascade lasers (QCLs) offer a unique combination of high output power, single-mode emission, and continuous spectral tunability that make them the most widely used type of continuous-wave laser sources in the mid-infrared (MIR) molecular fingerprint spectral region for gas-phase spectroscopy and trace gas sensing applications. The intrinsic or Schawlow-Townes linewidth [1] of DFB-QCLs that results from the laser white frequency noise can be as low as a few hundred hertz [2]. However, excess electrical flicker noise in the

semiconductor structure that induces internal temperature fluctuations of the laser active region [3,4], as well as technical noise that may arise from the current driver [5] lead to a broadening of the observed QCL emission linewidth (full width at half maximum - FWHM) to the megahertz level, typically, for integration times of milliseconds to hundreds of millisecond [2,3,6–8]. This is most often sufficient for gas sensing and many molecular spectroscopy applications, but more advanced applications that aim at controlling molecular degrees of freedom, for example, to test fundamental symmetries, or to measure fundamental constants and their possible time variation [9], require QCLs with a lower frequency noise and, thus, a narrower linewidth.

Different fairly simple approaches have been implemented to reduce the frequency noise of QCLs, e.g., by using the voltage noise detected between the QCL terminals as an error signal in a stabilization loop [10,11], but these methods resulted in a modest reduction of the frequency noise power spectral density (FN-PSD) by typically one order of magnitude. More sophisticated setups involved stabilization to a reference optical cavity. However, high-finesse cavities are much less developed in the MIR than in the near infrared (NIR) range where lasers stabilized down to the sub-hertz level are routinely used [12–15] today in optical clocks or for ultra-low noise microwave generation. Therefore, only few works of direct laser stabilization to a MIR high-finesse cavity have been reported. M.S. Taubman and co-workers measured a heterodyne beat note with a linewidth of a few hertz only between two cavity-stabilized QCLs at 8.5 µm [16], but the measurement did not constitute an absolute assessment of the linewidth of these lasers as the two cavities were locked to each other with a bandwidth of 6 kHz. Fasci et al. reported a 1-ms linewidth of less than 4 kHz for a 8.6-µm QCL locked to a high-finesse V-shaped cavity by optical feedback [17]. However, the most stable and low-frequency noise lasers in this spectral region have been achieved by phase-locking a QCL to a cavity-stabilized NIR laser through a nonlinear process using a frequency comb, leading to fairly complex setups [9,18].

An alternative method to an optical cavity enabling a significant reduction of the frequency noise of a laser was demonstrated in the NIR with the use of a much simpler setup based on an optical delay line [19–21]. The interference fringes occurring in an imbalanced Michelson or Mach-Zehnder interferometer act as a frequency discriminator that converts frequency fluctuations of the laser into intensity fluctuations, which are detected by a photodiode at the interferometer output. In the interferometer, part of the light is delayed in one path by propagating through a time delay before being recombined with the other part of the light that propagates through a much shorter path. The magnitude of the discrimination factor (in V/Hz) is approximately given by $2\pi\tau V_{\mathrm{pk}}$, where τ is the imbalanced interferometer time delay and V_{pk} is the amplitude of the error signal [19]. The most standard configuration makes use of a frequency-shifter acousto-optic modulator (AOM) in one arm to produce a self-heterodyne beat signal at the interferometer output. This beat signal is demodulated at the shifting frequency to stabilize the laser emission frequency to the delay line, by applying a feedback signal either directly to the laser driver, or to another AOM, resulting in a high feedback locking bandwidth. Thus, high laser noise reduction can be achieved, and a resulting linewidth at the sub-hertz level has been demonstrated in the NIR using a 500 m fiber length in a Michelson interferometer [21].

As the resulting frequency discrimination factor scales linearly with the pathlength difference between the two interferometer arms, long delay lines lead to a high discriminator factor and, thus, to a high frequency noise sensitivity. In the NIR, long delays of hundreds of meters to a few kilometers are easily achievable using low-loss single-mode optical fibers. Hence, very low FN-PSD was demonstrated for a 1.5-µm laser stabilized to a kilometer-scale fiber delay, comparable to the residual noise achieved by stabilization to an ultra-low expansion (ULE) high-finesse optical cavity in a large range of Fourier frequencies [20]. Only at low offset frequencies (typically below 100 Hz), the laser stabilized to the delay line was affected by higher frequency noise and drift resulting from

acoustic/mechanical noise and thermal drift of the interferometer, as compared to a ULE cavity that is usually better protected against such disturbances by being mounted in a more advanced protective enclosure.

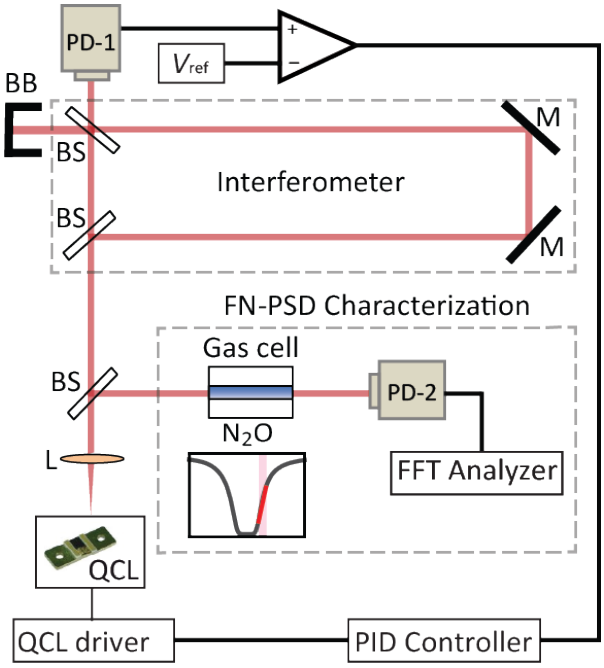

Figure 3.3: Experimental setup for QCL frequency noise reduction using a delay line; L, lens; BS, beam splitter; M, mirror; PD, photodetector; BB, beam blocker, PID, proportional-integral-derivative servo controller; FFT, fast Fourier transform. The linear range of a N_2O transition in a gas cell (red part of the absorption line) is used to measure the frequency noise of the laser with a frequency-to-voltage conversion factor of 27.9 V/GHz.

In this Letter, we demonstrate a significant frequency noise reduction achieved for the first time, to the best of our knowledge, for a MIR QCL by stabilization to an optical delay line. However, AOMs are much less common in the MIR range than in the NIR and, furthermore, require a high radio-frequency power resulting in an elevated power dissipation and the need for a water cooling that can induce excess noise in the interferometer. Therefore, a self-heterodyne configuration as used with NIR lasers is not convenient at MIR wavelengths. Hence, our first proof-of-principle demonstration reported here is based on a simpler self-homodyne scheme that does not need an AOM. Consequently, this scheme is much more sensitive to $1/f$ flicker noise arising from laser

intensity noise and detector noise that may limit the achieved frequency noise of the stabilized laser. Furthermore, the poor availability of low-loss single-mode optical fibers in the MIR prevents the use of a fibered delay line. Hence, we restricted the experimental setup to a short free-space pathlength difference of around 1 m acting as frequency-to-amplitude noise converter in this first proof-of-principle demonstration.

With this scheme, we nevertheless achieved a QCL FN-PSD reduction by almost 40 dB over a large range of Fourier frequencies and a narrowing of the corresponding linewidth below 10 kHz at 1-s integration time, as compared to almost 500 kHz for the free-running laser. A scheme of the experimental setup is shown in Figure 3.3. A DFB-QCL emitting at ~7.8 µm (from Alpes Lasers, Switzerland) and driven by a homemade low-noise current source is coupled to a Mach-Zehnder interferometer with a pathlength difference of ~90 cm. The laser is operated at a temperature of 20°C and an average current of ~435 mA located approximately in the middle of its operation range at this temperature. At this operation point, its current-tuning coefficient was assessed to be -0.29 GHz/mA. This value was spectroscopically obtained from the position of several N_2O absorption lines observed in a large current scan through a low-pressure gas cell and their comparison to the HITRAN database [22]. A second-order fit of the QCL frequency versus current was performed to extract the tuning coefficient at the operating point. The beat signal at the output of the interferometer is detected with a Mercury-Cadmium-Telluride (MCT) photodiode (Vigo Systems, model PVMI-4TE-8) and is compared to a stable reference voltage V_{ref} to generate an error signal for the laser frequency stabilization. The interference fringes observed when scanning the QCL frequency (via a current scan) are displayed in Figure 3.4. A high contrast of the interference of about 90% is achieved here with an optimized alignment of the interferometer, which is important to get a high discrimination factor that lowers the noise floor of the setup, as discussed later. The measured slope D_{fringe} = 7.9 V/GHz in the center of a fringe is in good agreement with the calculated value

$2\pi\tau V_{pk}$ = 8.3 V/GHz assessed from the applied pathlength difference of ~88 cm and the observed fringe amplitude of 0.45 V. The reference voltage is adjusted so that the zero-crossing point of the resulting error signal lies in the middle of a fringe, in the linear range. A proportional-integral-derivative (PID) servo-controller (Vescent D2-125) amplifies the error signal and produces a feedback signal that is applied to the current driver of the QCL. A feedback bandwidth larger than 100 kHz is typically needed to achieve a substantial reduction of the QCL frequency noise and linewidth according to the crossing point of the FN-PSD of the free-running laser with the β-separation line [23]. The impact of acoustic and mechanical noise on the interferometer was reduced by enclosing the whole experimental setup in a closed wooden box whose walls are covered by a foam layer. Some foam was additionally placed underneath the optical breadboard of the interferometer.

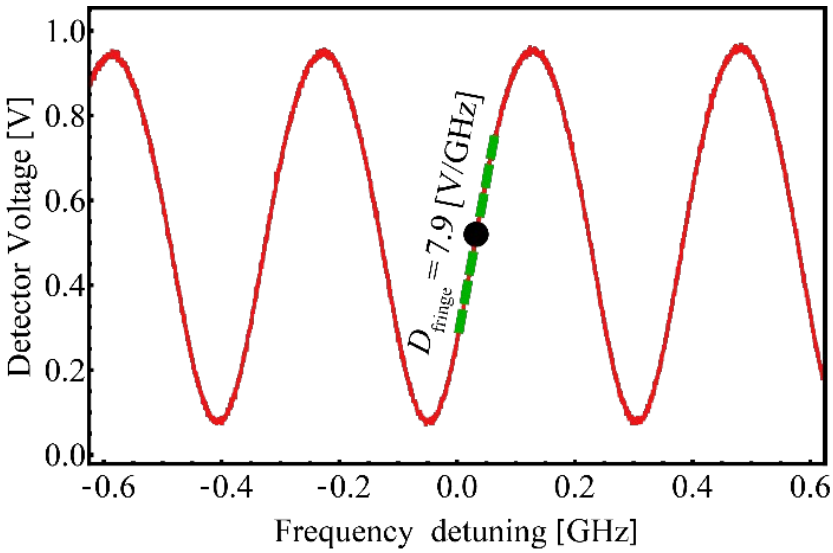

Figure 3.4: Interference fringes detected at the output of the interferometer when scanning the QCL current. The locking point indicated by a black dot is located in the linear range of a fringe with a slope D_{fringe}. The frequency axis of the graph was obtained using the measured tuning coefficient of the QCL of -0.29 GHz/mA.

Before the interferometer, a beam splitter directs part of the laser output beam through a 10-cm-long sealed gas cell filled with a low-pressure (2 mbar) of pure N_2O that is followed by a photodiode. This

setup is used to independently characterize the frequency noise of the laser (absolute out-of-loop measurement). The laser is tuned to the flank of a strong N_2O absorption line at 1276.4 cm^{-1}, which acts as a frequency discriminator with a typical conversion coefficient D_{gas} = 27.9 V/GHz measured in the setup (see Figure 3.3). The voltage noise of the detector signal is measured with a fast Fourier transform (FFT) analyzer (Rhode-Schwarz FSWP-26) and is converted into laser frequency noise using the measured frequency discriminator, both for the free-running and locked laser. The frequency noise of the free-running QCL was also assessed from the error signal using the slope of the fringe (D_{fringe}) around the locking point displayed in Figure 3.4 for cross-check. The two distinct measurements of the FN-PSD of the free-running QCL displayed in Figure 3.5 are in good agreement, which proves their proper scaling with the discriminators slopes D_{gas} or D_{fringe}, respectively.

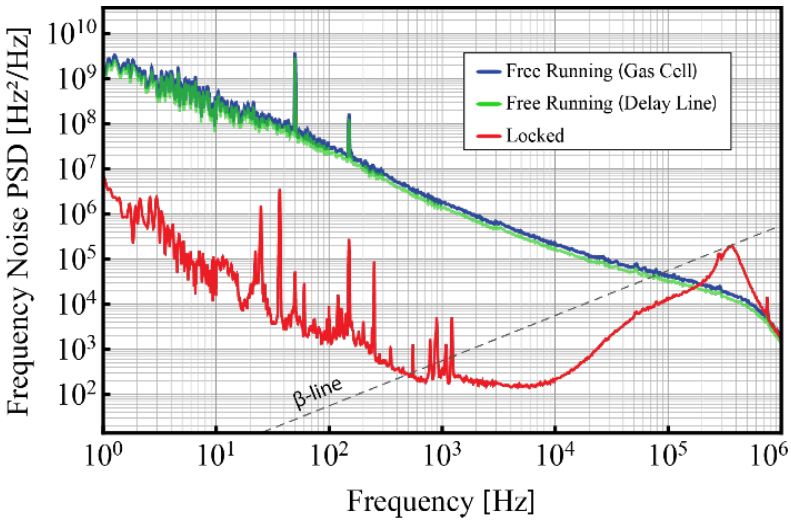

Figure 3.5: Frequency noise PSD of the QCL in free-running (blue and green curves measured in two different ways) and locked (red) modes. The servo bump of the locked laser indicates a locking bandwidth of ~400 kHz. The grey dashed line corresponds to the β-separation line used to calculate the corresponding laser linewidth [23].

The results of the stabilization to the delay line show a significant noise reduction (by almost 40 dB) at Fourier frequencies lower than 10 kHz. A locking bandwidth slightly lower than 400 kHz is assessed from the servo bump in the FN-PSD. However, the locked laser is affected by a

fairly large $1/f$ noise at low frequencies. This is a consequence of the self-homodyne scheme implemented here, as the beat signal detected around DC is sensitive to $1/f$ noise originating from different sources such as laser intensity noise and detector noise. The narrow noise peaks occurring at frequencies of 50 Hz and odd harmonics in the spectrum of the locked laser are of electronic origin, while the series of broader noise features below 1 kHz result from acoustic and mechanical noise in the interferometer, which is transferred to the laser by the feedback.

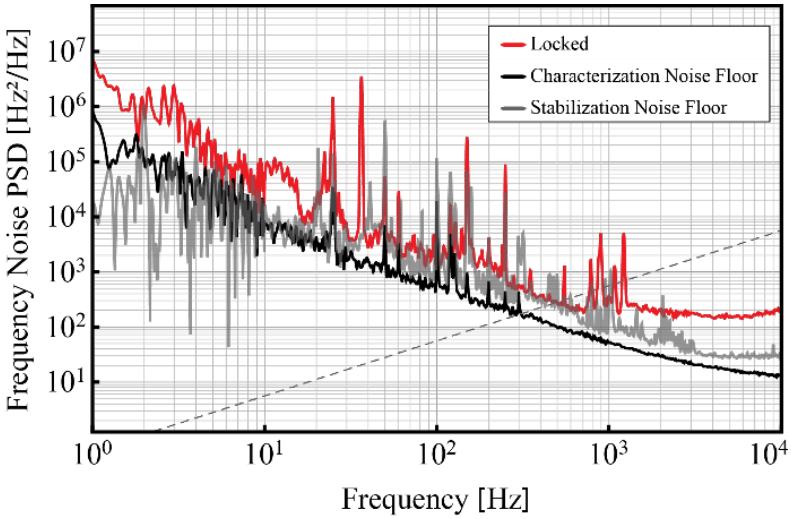

Figure 3.6: Comparison of the frequency noise PSD of the locked laser with the noise floors originating from the characterization and stabilization parts of the experimental setup.

In order to identify the present limitation in the setup, different noise floors have been measured (see Figure 3.6). The noise floor of the characterization setup (frequency discriminator from the gas cell and associated detector) was assessed by recording the combination of the voltage noise of the detector (PD-2) and of the laser intensity noise without the reference gas cell. The measured voltage noise floor was converted it into an equivalent frequency noise floor by scaling with the measured frequency discriminator slope D_{gas}. One notices that the spectroscopic frequency noise characterization setup used here does not constitute a limitation at the presently achieved noise level of the QCL. Hence, this simple spectroscopic setup is suitable to characterize the frequency noise

of a laser with a linewidth around or closely below 10 kHz (provided that its intensity noise is not too large). However, there is only little margin between the measured FN-PSD of the locked QCL and the noise floor of the characterization setup, so that a steeper frequency discriminator (e.g., obtained from a sub-Doppler transition) would be needed to characterize the noise of a narrower linewidth laser, e.g., at the level of a few kilohertz or below.

The achieved frequency noise of the stabilized QCL matches the system noise floor obtained when blocking one beam in the interferometer, which sets the limit corresponding to the detector noise and laser intensity noise. The measured noise was converted into an equivalent FN-PSD by scaling with the interferometer frequency discrimination factor $D_{\text{fringe}} = 7.9$ V/GHz (see Figure 3.4). The associated $1/f$ noise currently limits the achieved frequency noise of the locked QCL at Fourier frequencies in the range of around 20 Hz to 1 kHz. At lower frequencies, the drift of the interferometer is likely responsible for the observed laser frequency noise that is no longer limited by the detector or intensity noise.

The laser linewidth estimated from the measured FN-PSD using the β-separation line approximation [23] is 7.8 kHz at 1-s integration time, which is 60 times narrower than the linewidth of the free-running laser (Figure 3.7). This reduction factor is even larger than 100 at shorter integration times of 10 ms and below. The achieved linewidth narrowing is much higher than with other simple approaches previously reported for frequency noise reduction in QCLs [10,11], while being obtained with a fairly simple setup consisting only of a few standard optical components (two gold-coated mirrors and two polarization-independent beam splitters in the interferometer). This simple arrangement does not involve any vacuum chamber, temperature stabilization of the setup or active anti-vibration platform.

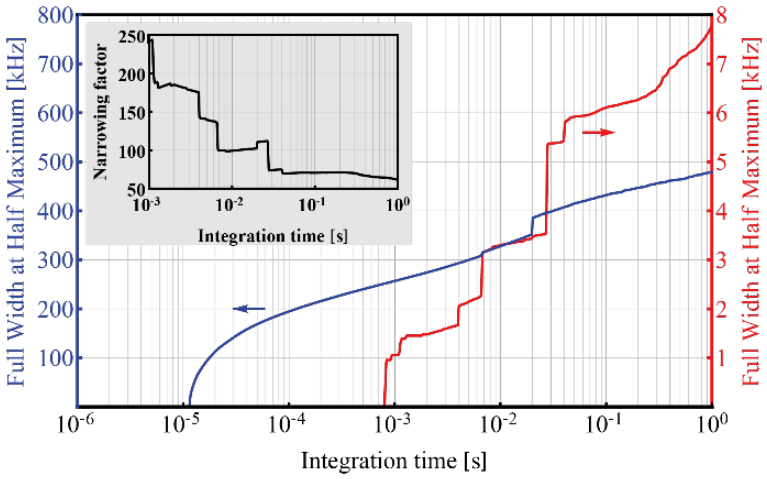

Figure 3.7: Full width at half maximum (FWHM) linewidth of the QCL calculated from the frequency noise spectrum based on the β-separation line approximation [23] as a function of the integration time (inverse of the lower cut-off frequency for the FN-PSD integration) in free-running regime (blue) and for the QCL stabilized to the delay line (red). Inset: linewidth narrowing factor as a function of the integration time.

In conclusion, we have reported, to the best of our knowledge, the first proof-of-principle demonstration of QCL frequency noise reduction using a free-space delay line. The achieved results are presently limited by the implemented self-homodyne scheme and by the fact that a fairly short imbalance pathlength (less than 1 m) is used in this experiment. The next steps to improve the stabilization will consist on one hand in increasing the pathlength difference to enhance the sensitivity to the laser frequency noise and decrease the stabilization noise floor, which can be achieved for instance with the use of a multipass cell to keep the setup compact. On the other hand, we will implement an absolute lock of the delay line to a molecular transition to combine the linewidth reduction brought by the stabilization to the delay line with the absolute frequency stability of the molecular reference.

Funding

Swiss National Science Foundation (SNSF) (200020_178864), European Space Agency (ESA).

References

[1] A. L. Schawlow and C. H. Townes, Phys. Rev. 112, 1940 (1958).

[2] S. Bartalini, S. Borri, P. Cancio, A. Castrillo, I. Galli, G. Giusfredi, D. Mazzotti, L. Gianfrani, and P. De Natale, Phys. Rev. Lett. 104, 083904 (2010).

[3] L. Tombez, S. Schilt, J. Di Francesco, P. Thomann, and D. Hofstetter, Opt. Express 20, 6851 (2012).

[4] S. Schilt, L. Tombez, C. Tardy, A. Bismuto, S. Blaser, R. Maulini, R. Terazzi, M. Rochat, and T. Südmeyer, Appl. Phys. B 119, 189 (2015).

[5] L. Tombez, S. Schilt, J. Francesco, T. Führer, B. Rein, T. Walther, G. Domenico, D. Hofstetter, and P. Thomann, Appl. Phys. B 109, 407 (2012).

[6] L. Tombez, J. Di Francesco, S. Schilt, G. Di Domenico, J. Faist, P. Thomann, and D. Hofstetter, Opt. Lett. 36, 3109 (2011).

[7] S. Bartalini, S. Borri, I. Galli, G. Giusfredi, D. Mazzotti, T. Edamura, N. Akikusa, M. Yamanishi, and P. De Natale, Opt. Express 19, 17996 (2011).

[8] S. Schilt, L. Tombez, G. D. Domenico, and D. Hofstetter, in The Wonder of Nanotechnology: Quantum Optoelectronic Devices and Applications (SPIE, 2013).

[9] B. Argence, B. Chanteau, O. Lopez, D. Nicolodi, M. Abgrall, C. Chardonnet, C. Daussy, B. Darquié, Y. Le Coq, and A. Amy-Klein, Nat. Photonics 9, 456 (2015).

[10] L. Tombez, S. Schilt, D. Hofstetter, and T. Südmeyer, Opt. Lett. 38, 5079 (2013).

[11] I. Sergachev, R. Maulini, A. Bismuto, S. Blaser, T. Gresch, Y. Bidaux, A. Müller, S. Schilt, and T. Südmeyer, Opt. Lett. 39, 6411 (2014).

[12] J. Alnis, A. Matveev, N. Kolachevsky, Th. Udem, and T. W. Hänsch, Phys. Rev. A 77, 053809 (2008).

[13] K. Numata, A. Kemery, and J. Camp, Phys. Rev. Lett. 93, 250602 (2004).

[14] T. Kessler, C. Hagemann, C. Grebing, T. Legero, U. Sterr, F. Riehle, M. J. Martin, L. Chen, and J. Ye, Nat. Photonics 6, 687 (2012).

[15] D. G. Matei, T. Legero, S. Häfner, C. Grebing, R. Weyrich, W. Zhang, L. Sonderhouse, J. M. Robinson, J. Ye, F. Riehle, and U. Sterr, Phys. Rev. Lett. 118, 263202 (2017).

[16] M. S. Taubman, T. L. Myers, B. D. Cannon, R. M. Williams, F. Capasso, C. Gmachl, D. L. Sivco, and A. Y. Cho, Opt. Lett. 27, 2164 (2002).

[17] E. Fasci, N. Coluccelli, M. Cassinerio, A. Gambetta, L. Hilico, L. Gianfrani, P. Laporta, A. Castrillo, and G. Galzerano, Opt. Lett. 39, 4946 (2014).

[18] M. G. Hansen, E. Magoulakis, Q.-F. Chen, I. Ernsting, and S. Schiller, Opt. Lett. 40, 2289 (2015).

[19] B. S. Sheard, M. B. Gray, and D. E. McClelland, Appl. Opt. 45, 8491 (2006).

[20] F. Kéfélian, H. Jiang, P. Lemonde, and G. Santarelli, Opt. Lett. 34, 914 (2009).

[21] J. Dong, Y. Hu, J. Huang, M. Ye, Q. Qu, T. Li, and L. Liu, Appl. Opt. 54, 1152 (2015).

[22] L. S. Rothman et al., J. Quant. Spectrosc. Radiat. Transf. 130, 4 (2013).

[23] G. Di Domenico, S. Schilt, and P. Thomann, Appl. Opt. 49, 4801 (2010)

Chapter 4

Noise investigation in a QCL frequency comb

4.1 Optical frequency combs

An optical frequency comb is a laser source that emits a spectrum made of optical modes that are equidistant in frequency. The optical spectrum of a frequency comb can be expressed as a series of delta functions given by the comb equation[47]: $\nu_N = N \cdot f_{\mathrm{FSR}} + f_0$, where f_{FSR} is the mode spacing (i.e., the spacing between two consecutive comb teeth), f_0 is the offset frequency that shifts the entire comb spectrum from the origin, and N is an integer number that corresponds to the mode number. The full spectrum of a frequency comb is determined by only two radio-frequencies: the mode spacing f_{FSR} and the offset frequency f_0.

The first optical frequency combs were demonstrated from mode-locked lasers (MLLs) by T.W. Hänsch[48] and J.L Hall[49] and led to the 2005 Nobel Prize in Physics[50,51]. The optical modes of an MLL are locked to each other using different techniques[52] and have a definite phase relation.

As a result, the laser emits light pulses with an extremely short duration (in the order of tens to hundreds of femtoseconds). These pulses are separated in time by the laser cavity round-trip time while in the frequency domain the spectrum of such a pulse train is also a series of sharp spectral lines separated in frequency by the inverse of the cavity round-trip time as shown in Figure 4.1. In MLLs, the offset frequency, also known as the carrier-envelope offset frequency (f_{CEO}), is related to the pulse-to-pulse phase shift between the maximum of the pulse and its envelope. It arises because of the difference between group and phase velocities inside a dispersive gain medium.

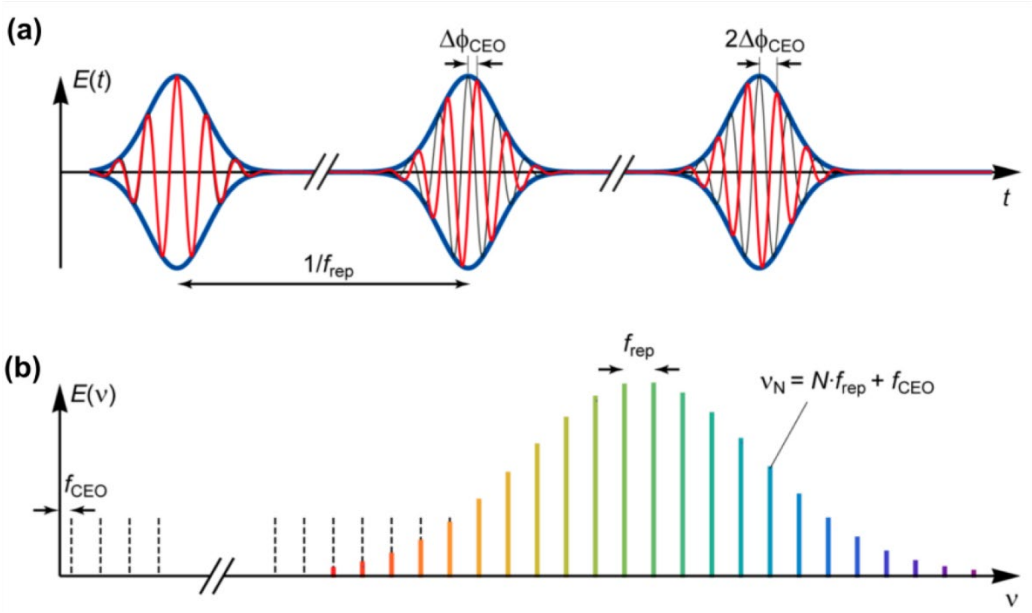

Figure 4.1: (a) Pulse train with evolving carrier-envelope phase in the time domain and (b) frequency-domain representation of a frequency comb with the optical modes extrapolated to the origin to present the carrier envelope-offset frequency (f_{CEO}). Figure taken from[53].

The mode spacing f_{rep} or repetition rate of combs based on mode-locked lasers can be easily detected and thus, characterized, by sending the laser light directly onto a fast photodetector with a sufficient bandwidth, such detectors being straightforwardly available in the NIR spectral region. However, the detection of f_{CEO} is much more challenging

and was a major contribution to the 2005 Nobel Prize in Physics. The traditional method to detect f_{CEO} is based on non-linear interferometry (*f*-to-2*f* interferometry), in which the longer wavelength part of an octave-spanning comb spectrum is frequency-doubled and heterodyned with the shorter wavelength comb spectrum[21]. Most generally, MLLs do not inherently emit a spectrum that spans over a full octave. Only some specially-designed and optimized Ti:sapphire mode-locked lasers emit an optical spectrum that covers a full frequency octave[54]. In all other MLLs, the emitted optical spectrum needs to be externally broadened, which is usually done using a highly non-linear fiber or photonic crystal fiber (PCF). The external broadening to an octave-spanning spectrum also requires pulses with a low repetition rate and short duration (high peak power). As a rule of thumb, the lower the repetition rate and pulse duration, the broader the generated supercontinuum (SC) spectrum at constant average optical power. To achieve an optical spectrum that is broadened coherently to a full octave becomes quite challenging, especially for combs with repetition rates higher than 1 GHz.

4.2 Dual comb spectroscopy

Dual comb spectroscopy (DCS) also known as multi-heterodyne spectroscopy is an unprecedented technique to acquire simultaneously broadband and high-resolution spectra with microseconds acquisition time. This technique is distinguished by a high signal-to-noise ratio (SNR), a small footprint, is free from moving parts, and is field-deployable as compared to traditional Fourier transform spectroscopy. This method was first proposed by S. Schiller in 2002[55].

In this technique, two frequency combs with slightly different repetition rates are interfered onto a photodetector resulting in an RF comb that can be recorded with a single photodetector having a sufficient bandwidth. The RF comb is the result of the beating between successive pairs of teeth of the two combs. In spectroscopic applications, at least one

of the combs probes the sample while the other acts as a local oscillator as shown in Figure 4.2. In DCS, both amplitude and phase (important in noisy environments) information of the sample can be recorded.

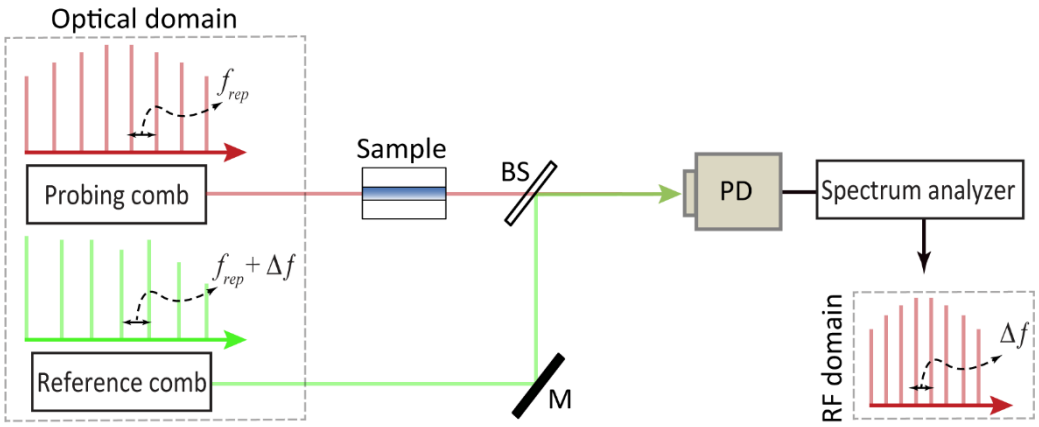

Figure 4.2: Principle of dual comb spectroscopy. Two laser frequency combs with slightly different repetition rates are used. One of the combs (probing) is passed through a sample and superimposed with the reference comb. Resulting beat notes create a frequency comb in the radio frequency domain. BS; beamsplitter, M; mirror, PD; photodetector.

Performing spectroscopy with frequency comb sources has the advantage that a single light source can probe multiple species simultaneously. In the next section, frequency comb sources in the MIR spectral region are discussed.

4.3 MIR frequency comb sources

In the MIR, mode-locked lasers are scarce; one prominent example being Cr^{2+}:ZnSe and Cr^{2+}:ZnS lasers[55,56] that emit at 2.4 microns with >300 cm^{-1} wide spectral bandwidth and have been used in dual-comb spectroscopy applications[57]. Beyond 3 μm mode-locked lasers are absent and other techniques are utilized to generate frequency combs. A few of them are briefly discussed here.

One of the approaches to generate MIR frequency combs is based on the difference frequency generation (DFG) process[58]. In DFG, a photon

with a frequency that is the difference of the two other photons is produced by nonlinear effects [Figure 4.3(a)]. In a typical DFG setup, light from a NIR frequency comb is split into two separate arms, the light in one of the arms is broadened in a nonlinear fiber and filtered to select either the short- or long-wavelength component. The two components are then separately amplified and recombined in a nonlinear crystal to produce MIR light. A DFG process can generate a MIR frequency comb over a wide wavelength range, depending on the pump source, spectral broadening scheme, and the type of nonlinear crystal. For instance, using periodically-poled lithium niobite (PPLN) as a nonlinear medium, this technique has demonstrated the generation of a spectral range of ~ 500 cm^{-1} with tens of nanowatt power per comb tooth in the 3.2 μm to 4.8-μm wavelength range by utilizing two pulse trains derived from a two-branch mode-locked erbium-doped fiber laser source[59]. One branch was centered at 1058 nm while the other branch was tunable from 1.05 to 1.4 μm. Other non-linear media, for instance, gallium selenide (GaSe) can be used to produce MIR combs covering a larger spectral range. For example, a MIR comb with a spectral bandwidth of ~2400 cm^{-1} tunable in the range of 3 to 10 μm and with an average power per comb mode of 50 nW has been demonstrated using 1.4 to 1.9-W average power of an Yb:fiber frequency comb centered at 1055 nm and 20 mW of pump power[60] from the Raman soliton generated from the same comb. The spectral tuning of the MIR comb was achieved by tuning the Raman soliton wavelength in the range of 1.15 to 1.65 μm. The MIR sources produced by using the DFG process have been used in several spectroscopic applications[61–64]. One of the major problems in this approach is the limited efficiency arising from the spatial and temporal walk-off of the interacting pulses in the nonlinear crystal resulting in a limited interaction length[65].

The low conversion efficiency problem can be solved with the use of an optical parametric oscillator (OPO). In an OPO, a photon with a high frequency ω_p is converted into two photons of lower frequency employing

second-order non-linear interaction [Figure 4.3(b)]. Among the converted photons, the one with higher frequency (ω_s) is known as "signal", while the other with the lower frequency (ω_i) as "idler" due to historical reasons. As the energy is conserved in an OPO, it can be mathematically written as $\omega_p = \omega_s + \omega_i$. OPO system consists of an optical resonator, a non-linear crystal, and a pump beam. The interaction of pump, signal, and idler inside the nonlinear crystal leads to the amplification of the signal or idler or both whileattenuating the pump beam. An OPO system with PPLN as a non-linear crystal synchronously-pumped by a 10-W femtosecond Yb:fiber laser resulted in the generation of a MIR comb with 30-µW power per comb mode[66]. The comb tunability, from 2.8 to 4.8 µm, was solely achieved by using different poling periods of the non-linear crystal.

(a)

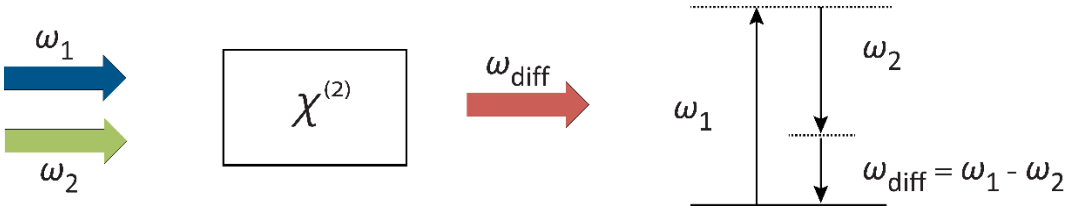

(b)

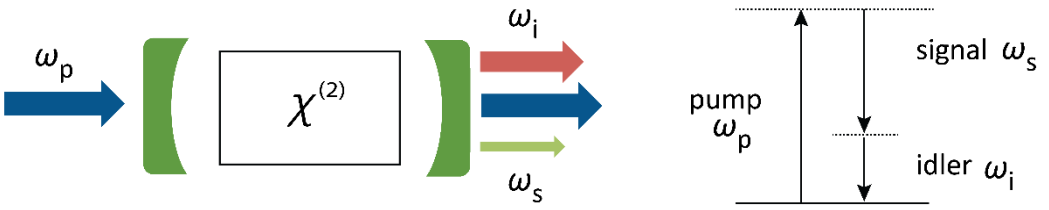

Figure 4.3: Illustration of different processes for generating MIR frequency comb through: (a) Difference frequency generation; (b) Optical parametric oscillation.

In the next section, a new type of comb technology that inherently produces a comb in the MIR is discussed.

4.4 QCL combs

In some particular conditions, MIR broadband QCL sources can emit a comb spectrum. QCL combs have attractive applications in MIR spectroscopy and especially in DCS because of their compact size. Unlike frequency combs based on passively mode-locked lasers in the NIR, their operation relies on a four-wave mixing (FWM) process in the semiconductor gain medium. The modes generated by the FWM process inside the QCL gain medium injection-lock the dispersed Fabry-Perot cavity modes of the resonator and force them to be equidistant, resulting in a frequency comb in the spectral domain that fulfills the frequency comb equation[18] (Figure 4.4). However, in contrast to frequency combs from MLLs, the laser does not emit short pulses, but only light with slight amplitude modulation. QCL frequency combs were first demonstrated by Andreas Hugi, during his Ph.D. thesis at ETH Zurich, Switzerland[17].

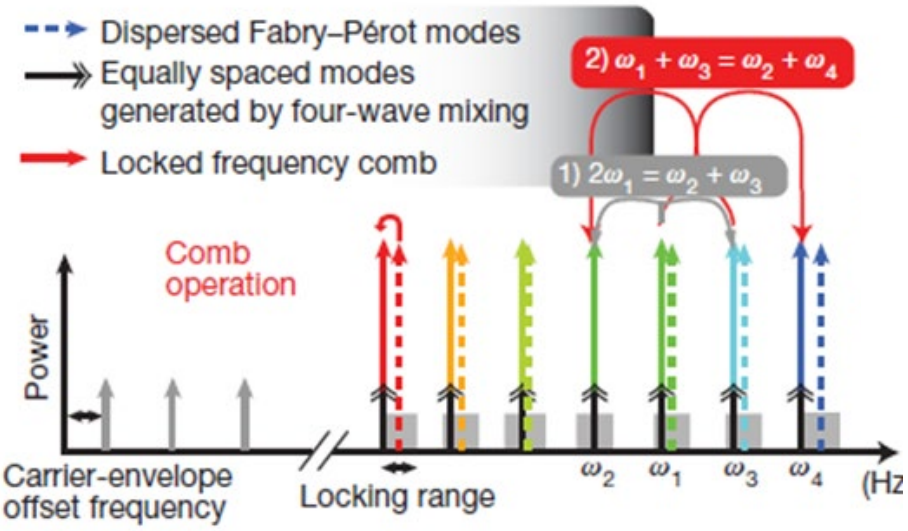

Figure 4.4: Depiction of the four-wave mixing process in the semiconductor gain medium of a QCL comb that results in the locking of the modes together under certain conditions. The figure is taken from[17].

The first demonstration of DCS using QCL combs has been performed by Villares *et al.* that paved a new way to directly perform

spectroscopy in the MIR[18]. In this first demonstration, both QCL combs were free-running, meaning that their mode spacing and offset frequency were not locked to an RF reference. In general, the complexity increases in moving from free-running combs to fully-referenced combs, but at the same time performance in terms of spectral resolution, frequency accuracy, and SNR in DCS (through increased coherent averaging times) also increases[67]. No full stabilization of a QCL frequency comb has been achieved so far because the detection of the offset frequency using standard *f*-to-2*f* interferometry has not been possible for two reasons. Firstly, the spectral width of QCL combs has been limited to ~110 cm^{-1} at 8 μm[68], which is far from an octave-spanning spectrum required in the standard method for the offset frequency detection based on nonlinear *f*-to-2*f* interferometry . Secondly, QCL combs do not generate short pulses that are required for nonlinear spectral broadening to achieve the requested octave-spanning spectrum. Nevertheless, getting some information about the frequency noise level of the offset frequency and its modulation characteristics is quite handy in order to better understand this new comb technology.

Pierre Brochard *et al*., at UniNE-LTF, presented a new method to indirectly access the offset frequency of a comb based on the transfer oscillator concept[22]. This method was previously successively applied to characterize the noise of the carrier-envelope offset frequency in different NIR mode-locked lasers for which a direct detection using the standard *f*-to-2*f* interferometry method was not possible, i.e., a vertical external-cavity surface-emitting laser (VECSEL) emitting at 1030 nm with a repetition rate frequency of 1.8 GHz[69] and an Er:Yb:glass laser oscillator (ERGO) emitting at 1.5 μm with a repetition rate of 25 GHz[70].

Implementing a similar scheme in the MIR to characterize QCL combs is quite challenging because of the two following main reasons: (i) photodetectors in the MIR generally do not have high enough detection bandwidth to optically detect the repetition rate of QCL combs, which is

usually in the range of a few GHz to tens of GHz because of the short cavity length (a few mm in QCL-combs); (ii) a narrow-linewidth auxiliary laser is required to make a beat note with one of the QCL comb modes.

As QCLs are based on intersubband transitions in quantum wells, the upper state lifetime is in the sub-picosecond range, much shorter than the cavity round trip time. Due to the short upper state lifetime, the transport dynamics in QCLs is extremely fast. For this reason, QCLs can be modulated at frequencies up to tens of GHz. Conversely, the current faithfully follows the intensity of light inside the laser cavity at its RF beat note frequency and transduced onto the QCL bias current. The beat note can be extracted electrically across the QCL using a bias-tee was first demonstrated by Villares *et al*[18]. This eliminates the requirement of high bandwidth photodetector in the MIR for the detection of the mode spacing.

To get a narrow-linewidth laser for the characterization of the QCL comb, the scheme based on a delay-line discussed in Section 3.3 was applied to reduce the linewidth of a DFB-QCL. Hence, a scheme based on the method proposed by Brochard *et al*. was implemented, for the first time in the MIR, to characterize the noise of the offset frequency of a QCL comb. Section 4.5, which is a reprint of an article published in Optics Express[71], presents the implemented method and the achieved results.

4.5 Frequency noise correlation between the offset frequency and the mode spacing in a mid-infrared quantum cascade laser frequency comb

Atif Shehzad[1], Pierre Brochard[1], Renaud Matthey[1], Filippos Kapsalidis[2], Mehran Shahmohammadi[2], Mattias Beck[2], Andreas Hugi[3], Pierre Jouy[3], Jérôme Faist[2], Thomas Südmeyer[1], Stéphane Schilt[1]

[1]Laboratoire Temps-Fréquence, Institut de Physique, Université de Neuchâtel, CH-2000 Neuchâtel, Switzerland

[2]Institute for Quantum Electronics, ETH Zurich, CH-8093 Zurich, Switzerland

[3]IRsweep SA, Laubisruetistrasse 44, CH-8712 Stäfa, Switzerland

The generation of frequency combs in the mid-infrared (MIR) spectral range by quantum cascade lasers (QCLs) has the potential for revolutionizing dual-comb multi-heterodyne spectroscopy in the molecular fingerprint region. However, in contrast to frequency combs based on passively mode-locked ultrafast lasers, their operation relies on a completely different mechanism resulting from a four-wave mixing process occurring in the semiconductor gain medium that locks the modes together. As a result, these lasers do not emit pulses and no direct self-referencing of a QCL comb spectrum has been achieved so far. Here, we present a detailed frequency noise characterization of a MIR QCL frequency comb operating at a wavelength of 8 μm with a mode spacing of ~7.4 GHz. Using a beat measurement with a narrow-linewidth single-mode QCL in combination with a dedicated electrical scheme, we measured the frequency noise properties of an optical mode of the QCL comb, and indirectly of its offset frequency for the first time, without detecting it by the standard approach of nonlinear interferometry applied to ultrafast mode-locked lasers. In addition, we

also separately measured the noise of the comb mode spacing extracted electrically from the QCL. We observed a strong anti-correlation between the frequency fluctuations of the offset frequency and mode spacing, leading to optical modes with a linewidth slightly below 1 MHz in the free-running QCL comb (at 1-s integration time), which is narrower than the individual contributions of the offset frequency and mode spacing that are at least 2 MHz each.

4.5.1 Introduction

Optical frequency combs (OFCs) generated from mode-locked lasers have been a revolution in time and frequency metrology since their first demonstration 20 years ago by providing a direct and phase-coherent link between optical and microwave frequencies[1-3]. Their emission spectrum is determined by only two radio-frequencies, the constant spacing between the optical modes and the global frequency offset of the comb spectrum. In OFCs generated from ultrafast mode-locked lasers, the mode spacing corresponds to the repetition rate frequency f_{rep} of the pulsed laser train, whereas the global offset frequency is referred to as the carrier-envelope offset (CEO) frequency f_{CEO}, which results from the pulse-to-pulse phase shift occurring between the optical carrier and the envelope of the emitted laser pulses. The repetition rate that can range up to tens of GHz is straightforwardly measured by photo-detecting the laser pulse train using a high-bandwidth photodiode. On the other hand, the standard method to detect the CEO frequency is the self-referencing scheme, which in the usual implementation requires a coherent octave-spanning spectrum and nonlinear *f*-to-2*f* interferometry [1].

A different type of frequency combs has been demonstrated in the mid-infrared (MIR) spectral region that is important for molecular spectroscopy, based on the occurrence of four-wave mixing in the semiconductor gain medium of broadband quantum cascade lasers (QCLs) [4]. These lasers produce a frequency comb in some particular conditions where all emitted modes become equidistant as a result of the

parametric four-wave mixing process. QCL combs are very attractive for dual-comb spectroscopy [5-7] in the MIR spectral range that is of particular importance for high-resolution molecular spectroscopy and trace gas sensing. As a result of the very short upper state lifetime of the gain medium, these comb sources do not generate optical pulses, but deliver a fairly constant output power [8] that is associated to a frequency-modulated (FM) spectrum. A recent model proposed by Opacak and Schwarz describes the formation of FM combs with the combined contributions of spatial hole burning, gain saturation and a minimum group velocity dispersion or Kerr nonlinearity due to gain asymmetry [9]. The FM nature of QCL combs has made the self-referencing method not possible so far and no detection of the offset frequency of a MIR QCL comb has ever been reported to the best of our knowledge, even if the full phase stabilization of a THz QCL comb to a CEO-free metrological THz comb was recently demonstrated [10]. For this purpose, the authors investigated the use of two different actuators, which are radio-frequency (RF) injection locking of the comb mode spacing by an external frequency reference signal and the QCL drive current to phase-lock one beat signal with the metrological comb to a reference oscillator. A constant width of the beat notes of around 120 kHz was observed when stabilizing the mode spacing only, while the linewidth of the beat notes increased linearly with the mode number N of the QCL comb when the phase-locked loop only was activated. An alternative approach to stabilize a QCL comb was implemented by Cappelli et al. [11] by phase-locking one mode of the QCL comb to a line of a metrological comb by feedback to the QCL current, reducing the linewidth of all modes below 23 kHz and showing a linear increase of this linewidth as a function of the distance from the locked mode. Simple relations between the QCL comb frequencies and the effective and group refractive indices were presented, showing that the QCL current acts predominantly on the offset frequency. The implemented stabilization scheme removed the common noise between the optical modes of the QCL comb that includes the combined

contribution of the offset frequency and of the mode spacing, but no information about the noise of the offset frequency of the free-running QCL comb was assessed. In the recent work of Cappelli et al. [12], the amplitude and phase of the different modes of THz and MIR QCL combs were retrieved by a Fourier-transform analysis of the multi-heterodyne spectrum obtained in a dual-comb setup with a metrological comb. The relative frequency noise between the QCL comb modes was analyzed by implementing a scheme that combines a phase-lock of the mode spacing to an external reference oscillator by feedback to the QCL current, and a noise compensation scheme to remove the common noise between all modes of the multi-heterodyne beat signal with the metrological comb. This scheme removed a large part of the frequency noise of the multi-heterodyne beat signal, but did not reduce at all the noise of the optical modes of the QCL comb.

In this work, we show the first evaluation of the frequency noise properties of the offset frequency of a free-running QCL comb. We refer here to the offset frequency that we label f_0 and not to the CEO frequency f_{CEO}, as this terminology is not well-suited to MIR QCL combs that do not emit pulses. For the same reason, we refer to the mode spacing (or free spectral range) f_{FSR} of the QCL comb spectrum instead of the repetition rate f_{rep} used for mode-locked lasers. But the significance of these two parameters in the frequency domain is the same and they completely determine the frequency of an optical line ν_N of index N according to the well-known comb equation $\nu_N = N \cdot f_{FSR} + f_0$. By analogy to frequency combs generated from mode-locked lasers where f_{CEO} is defined by convention as $f_{CEO} \leq f_{rep}/2$, we consider here the offset frequency as $f_0 \leq f_{FSR}/2$ independently of the underlying physical effect responsible for the comb generation. Hence, N represents the mode number measured from the origin of the frequency axis. Our investigation relies on a dedicated scheme that we have developed to separately characterize the frequency noise of the two characteristic frequencies defining the optical spectrum of the QCL comb, i.e., the mode spacing f_{FSR} and the offset

frequency f_0. The measurement involves an electrical scheme that circumvents the standard *f*-to-2*f* interferometry method and enables the frequency noise spectrum of f_0 to be indirectly measured, without direct detection of this signal. In addition, the mode spacing can also be detected electrically in QCL combs by extracting the intermode beat signal from the laser current [13]. Hence, we are able for the first time to separately quantify the noise contributions of the two degrees of freedom of the QCL comb to its optical spectrum. We observe a strong anti-correlation between the noise of f_{FSR} and f_0 leading to a much lower frequency noise of the optical mode, similar to our previous observations in different types of ultrafast mode-locked lasers [14-16]. From this result, we assess the position of the fixed point [17] of the QCL comb spectrum.

4.5.2 Experimental setup and noise investigation of the free-running QCL comb

The used QCL has a length of 6 mm. Its back facet is high-reflectivity-coated and the device is mounted junction-down. A comb regime was achieved at a temperature of 10°C and at a typical laser current of ~1.7 A. In these conditions, the optical spectrum centered at 1245 cm^{-1} typically extends over 50 cm^{-1} and consists of ~200 lines separated by ~7.4 GHz. This frequency can be detected electrically from the intermode beat signal extracted from the modulation of the injected current in the laser [13]. We used this signal to characterize the QCL comb mode spacing, as it is difficult to detect it optically with a good signal-to-noise due to the lack of high bandwidth detectors in the MIR.

The experimental setup shown in Figure 4.5 was implemented to beat one line of the QCL comb (with a mode number $N \approx 5{,}112$) with a low-noise single-mode reference laser in order to measure the frequency noise of one of the comb modes. The mode number N was estimated from the frequency of the reference laser assessed spectroscopically using the position of N_2O absorption lines and the measured mode spacing of the

QCL comb. The reference laser is a distributed feedback (DFB) QCL operating at 1256.7 cm^{-1}. It was temperature-controlled and driven by a home-made low-noise laser driver. The DFB-QCL was stabilized to a Mach-Zehnder interferometer to reduce its frequency noise and narrow its linewidth so that the measured heterodyne beat reflects the noise properties of the QCL comb with a negligible noise contribution of the reference laser. The stabilization was realized with a short free-space imbalanced path of about 1 m in a similar way as in our recent demonstration of this approach [18], leading to a linewidth in the 10-kHz range (at 1-s integration time), which is much narrower than the linewidth of the QCL comb presented later.

In addition, this setup enabled us to indirectly assess the frequency noise of the offset frequency f_0 of the QCL comb without directly detecting it by the traditional method of f to $2f$ interferometry, but based on an approach that we previously developed and validated using a self-referenced Er:fiber frequency comb [19]. This method was also successfully applied later to perform a detailed investigation of the noise properties of the CEO frequency in a mode-locked semiconductor laser [15] and in a 25-GHz repetition rate diode-pumped solid-state mode-locked laser [16]. It is applied here to a MIR comb to investigate the offset frequency noise in a QCL comb.

Basically, the method consists of suppressing the contribution of the mode spacing f_{FSR} in the frequency noise of an optical line $\nu_N = (N \cdot f_{FSR} + f_0)$ of the QCL comb, measured from the heterodyne beat $f_b = (\nu_N - \nu_{cw})$ with the narrow-linewidth QCL of frequency ν_{cw}. The suppression of the noise of the mode spacing was achieved using an electrical scheme (see Figure 4.5) and not optically as with f-to-$2f$ interferometry. For this purpose, the beat signal needs to be frequency-divided by the large integer number N and mixed with the mode spacing f_{FSR} separately extracted from the QCL current with the use of a bias-tee (Marki Microwave BTN2-0018) in order to generate the output signal $f_{out} = f_{FSR} - f_b/N = (\nu_{cw} - f_0)/N$. The noise of

this signal is dominated by the contribution of f_0 if the auxiliary laser ν_{cw} has a much lower noise, which is the case here. In order to perform the frequency division by the large number N, the heterodyne beat signal detected at a frequency of ~200 MHz (within the 1-GHz bandwidth of the used photodetector) was first up-converted to ~15 GHz by mixing it with the signal from a synthesizer in a triple-balanced mixer (Marki Microwave T3H-18LS). In this process, the noise contribution from the synthesizer is negligible in comparison to the frequency noise of the beat signal.

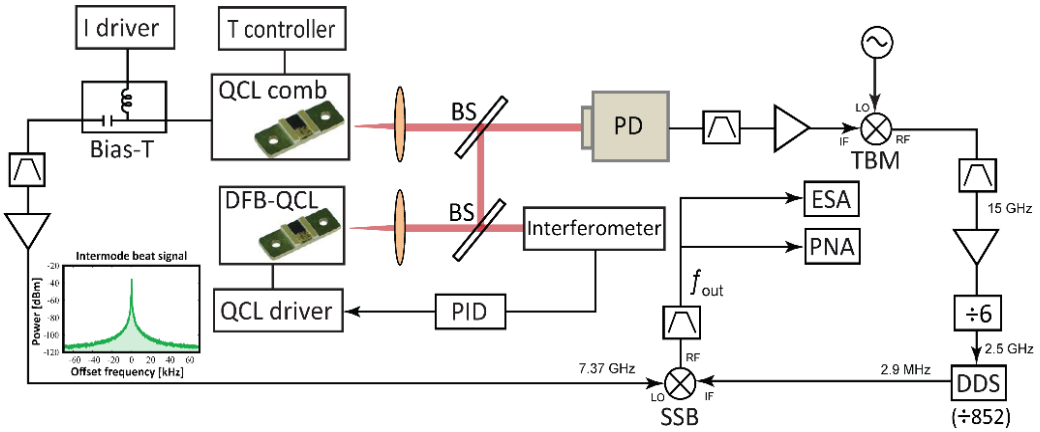

Figure 4.5: Scheme of the experimental setup implemented to measure the frequency noise of the unknown free-running offset f_0 of the QCL comb. The frequency noise of f_0 is indirectly measured by separately detecting the mode spacing f_{FSR} by RF extraction (lower branch of the scheme) and the heterodyne beat between one optical line of the QCL comb and a narrow-linewidth DFB-QCL at 1256.7 cm^{-1}. The beat signal is filtered, up-converted and frequency-divided by a large number N = 5,112 using a frequency pre-scaler (÷6) and a direct digital synthesizer (DDS, upper branch of the scheme). The two signals are then combined (mixed) to remove the noise contribution of f_{FSR}, such that the resulting signal f_{out} is representative of the noise of f_0 only. BS: beamsplitter; PD: photodetector: PID: proportional-integral-derivative servo controller; TBM: triple-balanced mixer; SSB: single sideband mixer; DDS: direct digital synthesizer; ESA: electrical spectrum analyzer; PNA: phase noise analyzer. A representative intermode beat note electrically extracted from the QCL comb with a bias-T is shown on the lower left part of the figure, after amplification. The signal is centered at 7.37 GHz.

The up-converted beat signal was then frequency-divided by a factor of 6 in a frequency pre-scaler (RF Bay FPS-6-15), whereas the subsequent division by a factor of 852 was realized by a direct digital synthesizer (DDS, Analog Devices AD9915). The resulting divided signal at ~2.9 MHz was further mixed in a single sideband (SSB) mixer (Marki Microwave SSB-0618LXW-1, lower sideband) with the ~7.37-GHz mode spacing electrically extracted from the QCL, then filtered and amplified. The resulting output signal f_{out} was analyzed with a phase noise analyzer (Rohde-Schwarz FSWP-26). As a result of the implemented scheme, the frequency noise originating from f_0 is the dominant noise contribution in the analyzed signal, which could be measured even if f_0 itself remained unknown.

The frequency noise power spectral density (FN-PSD) measured for an optical mode ν_N of the free-running QCL comb (from the beat signal f_b with the narrow-linewidth QCL) is displayed in Figure 4.6. It is compared to the mathematically up-scaled frequency noise spectra separately measured for the mode spacing of the QCL comb and indirectly assessed for f_0 using our experimental scheme. A similar noise spectrum (in both shape and magnitude) is observed for the indirect f_0 signal and for the up-scaled mode spacing $N \cdot f_{FSR}$, whereas the noise of the optical line is significantly lower. The corresponding linewidth (full width at half-maximum) calculated from the measured frequency noise PSD using the β-separation line concept [20] is slightly below 1 MHz (at 1-s integration time) for the optical line, whereas it amounts to 2 MHz and 2.5 MHz, respectively, for the individual noise contributions of f_0 and $N \cdot f_{FSR}$ if one disregards the influence of the technical noise peaks at 50 Hz and harmonics. As the FN-PSD of f_0 and f_{FSR} is limited by the measurement noise floor at high Fourier frequencies, the $1/f$ trend of these spectra was extrapolated down to the β-separation line for the linewidth estimations.

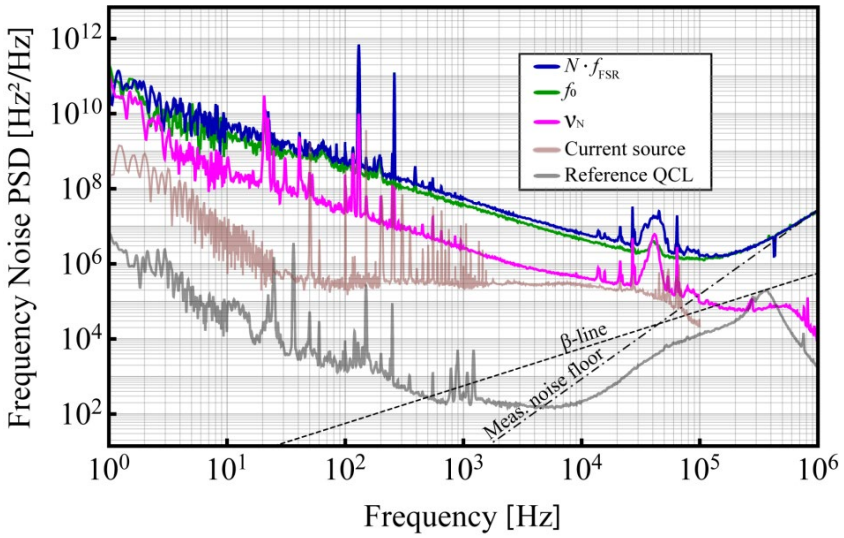

Figure 4.6: Frequency noise power spectral density (FN-PSD) separately measured for an optical mode ν_N (pink), for the mode spacing up-scaled to the optical frequency ($N \cdot f_{FSR}$, blue) and indirectly assessed for the offset signal f_0 (green). The typical frequency noise spectrum of the reference DFB-QCL locked to the delay line and used to characterize the QCL comb is also displayed (grey, from[44]), as well as the contribution of the current noise of the QCL driver to the comb frequency noise (light brown, obtained by recording the current noise on a resistive load and converting it into an equivalent frequency noise using the measured transfer function discussed in Section 4.5.2.1, here for the optical line ν_N). The measurement noise floor at high frequency is indicated by the dash-dotted line and the β-separation line[72] used to estimate the linewidths by the dashed line.

The narrower linewidth of the optical line indicates that the fluctuations of f_{FSR} and f_0 are anti-correlated and partially compensate each other in the optical line. This behavior implies the existence of a fixed point [17,21] in the vicinity of the optical carrier in the spectrum of the QCL comb according to the elastic tape model of frequency combs introduced for mode-locked lasers [22,23]. This fixed point is calculated from the ratio of the FN-PSD of the offset frequency (S_{f_0}) and of the mode spacing ($S_{f_{FSR}}$) as $N_{fix} = \sqrt{S_{f_0} / S_{f_{FSR}}} \approx 4{,}300$, leading to a fixed frequency of ~1056 cm^{-1} located outside of the comb spectrum. This fixed point results from the dominant noise source in our QCL comb, which is believed to

arise from the voltage noise between the QCL terminals as previously observed in single-mode QCLs [24,25][18,52], which induces fluctuations of the internal temperature of the gain medium and, thus, produces frequency noise in all comb modes.

The degree of correlation between the frequency fluctuations $N \cdot \Delta f_{FSR}$ of the up-scaled mode spacing $N \cdot f_{FSR}$ and Δf_0 of the offset signal f_0 was assessed from the measured FN-PSDs by calculating the sum $\Gamma_\Delta = \gamma_{\Delta f_0\, N\cdot\Delta f_{FSR}} + \gamma_{N\cdot\Delta f_{FSR}\, \Delta f_0}$ of the complex coherences $\gamma_{\Delta f_0\, N\cdot\Delta f_{FSR}}$ and $\gamma_{N\cdot\Delta f_{FSR}\, \Delta f_0}$ between the frequency variations Δf_0 and $N \cdot \Delta f_{FSR}$ in the free-running QCL comb following the approach presented by Dolgovskiy and co-workers [14]. The complex coherence between two quantities x and y is defined in the general case as $\gamma_{xy} = S_{xy} \Big/ \sqrt{S_x \cdot S_y}$, where S_x represents the FN-PSD of the parameter x and S_{xy} is the cross-spectrum of the parameters x and y. Using the comb equation, the sum of the complex coherences can be obtained from the measured FN-PSDs as (see Ref. [14] for more explanations):

$$\Gamma_\Delta = \frac{S_{f_b} - S_{f_0} - S_{N\cdot f_{FSR}}}{\sqrt{S_{f_0} - S_{N\cdot f_{FSR}}}} \tag{1}$$

The calculated value of Γ_Δ displayed in Figure 4.7 is close to -2 in the entire considered spectral range, which demonstrates the strong anti-correlation of the frequency noise of $N \cdot f_{FSR}$ and f_0. The value of Γ_Δ close to zero observed at a frequency of ~20 Hz results from a noise peak present in the FN-PSDs in Figure 4.6. This peak is believed to be of technical origin in the experimental setup, we do not believe that it originates from the QCL itself. It is visible in the FN-PSD of ν_N, f_0 and f_{FSR}. As it does not arise from the QCL, this noise is uncorrelated between f_0 and f_{FSR}. This is why the sum of the complex coherence reaches a value close to zero at this frequency. This uncorrelation leads to a noise peak in the FN-PSD of ν_N that is as strong as in the FN-PSD of f_{FSR} in Figure 4.6, whereas the FN-PSD of ν_N is much weaker than that of f_{FSR} at other frequencies where a high

correlation occurs. The strong noise anti-correlation, combined with the similar amplitude of the FN-PSD measured for $N \cdot f_{FSR}$ and indirectly for f_0, explains the lower frequency noise observed for the optical mode of the QCL comb compared to the individual noise contributions of $N \cdot f_{FSR}$ and f_0. This behavior is very similar to the case of comb spectra generated from ultrafast mode-locked lasers of various types that have been reported previously, such as an Er-fiber [14], a semiconductor mode-locked laser with a repetition rate in the GHz range [15], or a diode-pumped solid-state mode-locked laser (DPSSL) with 25-GHz repetition rate [16], even if the comb formation mechanism is completely different.

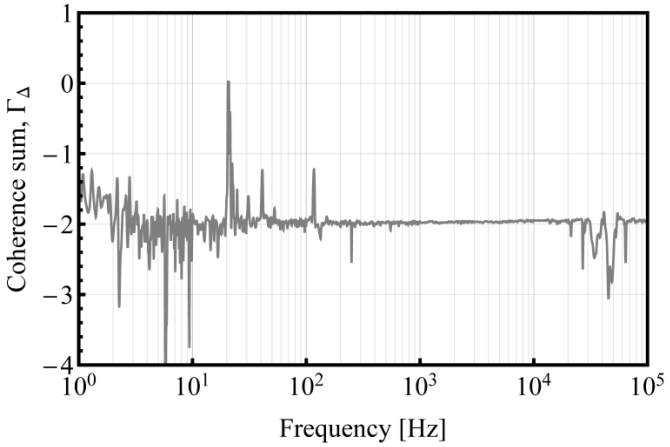

Figure 4.7: Frequency dependence of the sum of the complex coherences Γ_Δ between the frequency variations of f_0 and f_{FSR} in the free-running QCL comb. The plot is restricted to 100 kHz, as the noise spectra of f_0 and $N \cdot f_{FSR}$ are limited by the experimental noise floor at higher frequencies.

4.5.2.1 QCL comb transfer functions for current modulation

Frequency combs emitted from ultrafast mode-locked lasers typically make use of two different actuators to separately stabilize their two degrees of freedom, i.e., the repetition rate and the CEO frequency, even if these actuators may not be independent and a cross influence generally occurs between their effect on f_{rep} and f_{CEO} [14]. The cavity length, controlled for instance with a piezo-electric transducer (PZT), is generally used to stabilize the repetition rate, whereas the pump power mainly acts

on the CEO frequency. The situation is different for QCL combs that do not have an equivalent knob to the PZT used in ultrafast mode-locked lasers as they are monolithically-integrated, electrically-driven light sources. Different actuators are available to control their emission spectrum, which are the laser current and temperature, but they are strongly correlated. Furthermore, temperature control is fairly slow and does not appear practicable for proper frequency stabilization. Both comb parameters are expected to be affected by the laser average (or DC) current. However, a distinct way to control and lock the mode spacing in QCL combs is by injecting a radio-frequency (RF) current in the QCL at a frequency close to the native mode spacing, which can injection-lock this parameter [26] via the coupled dynamics of the optical field and carrier density in the QCL semiconductor medium [13].

Using the same setup as before to indirectly characterize the offset frequency of the QCL comb, we have separately investigated the effect of a modulation of the laser driving current (baseband component) onto the two comb parameters f_{FSR} and f_0, as well as onto an optical line ν_N, by measuring their modulation transfer functions. For this purpose, we modulated the QCL current with a sine waveform with a small amplitude ΔI, ranging between 20 μA and 3 mA depending on the considered measurement, and demodulated the corresponding signals (optical beat, electrically-extracted mode spacing or indirect offset signal obtained using the scheme of Figure 4.5) using a frequency discriminator [27] and a lock-in amplifier.

The measured transfer functions are displayed in Figure 4.8. They present the same behavior, both in amplitude and in phase, with a flat amplitude response up to ~10 kHz. This limited bandwidth results from the fact that the frequency of the QCL comb modes varies with the laser current mainly due to a thermal effect, as for single-mode QCLs [28]. Even if the QCL current can be modulated much faster (the used current driver has a bandwidth larger than 100 kHz, measured on a resistive load), as

well as the output optical power, the effect on the emitted optical frequencies is limited by the thermal dynamics of the QCL. The effect of the QCL drive current was determined to be around 2,550 times larger on the offset frequency ($\Delta f_0/\Delta I \approx 125$ MHz/mA) than on the mode spacing ($\Delta f_{FSR}/\Delta I \approx 49$ kHz/mA), but the respective contribution of the two parameters to the modulation of the optical line ν_N is of the same order of magnitude. Hence, the fixed point for current modulation corresponds to $N_{fix} = (\partial f_0/\partial I)/(\partial f_{FSR}/\partial I) \approx 2{,}550$. A phase shift of 180° is observed between the transfer functions of f_{FSR} and f_0, which indicates that a change of the QCL current produces an opposite effect on these two parameters.

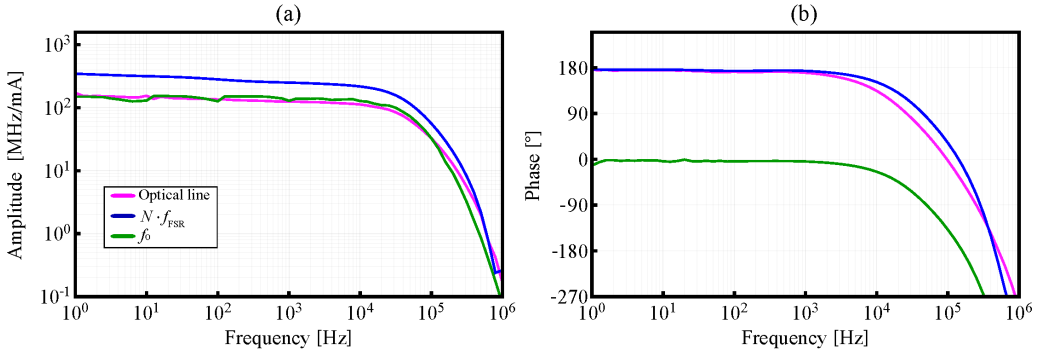

Figure 4.8: Transfer function in amplitude (a) and phase (b) of $N \cdot f_{FSR}$ (blue), f_0 (green) and ν_N (optical line, pink) measured for a modulation of the QCL current applied through its driver.

4.5.2.2 Impact of the stabilization of the mode spacing on an optical line

The QCL current can be used to phase-lock the mode spacing to an external RF reference (synthesizer) as schematized in Figure 4.9(a). With an achieved loop bandwidth in the range of 30 40 kHz that is limited by the QCL comb transfer function displayed in Figure 4.8, the phase noise of the mode spacing is strongly reduced and reaches the noise of the reference oscillator at low Fourier frequencies as illustrated in Figure 4.9(b). The mode spacing analyzed here was electrically extracted from the QCL current and its limited signal-to-noise is the reason for the

observed noise floor of the measurement in the range of -100 to 110 dBc/Hz.

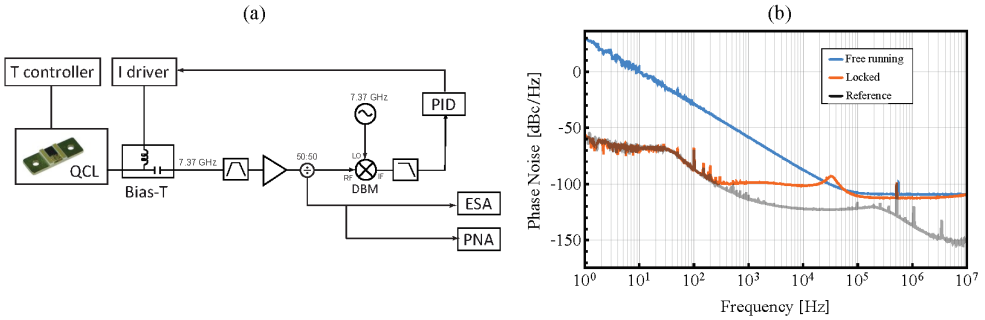

Figure 4.9: (a) Experimental scheme used to stabilize the mode spacing of the QCL comb to an external frequency reference at 7.37 GHz by feedback to the QCL current. DBM: double balanced mixer; PID: proportional-integral-derivative servo controller; ESA: electrical spectrum analyzer; PNA: phase noise analyzer. (b) Phase noise PSD of the QCL mode spacing in free-running mode (blue) and phase-locked to an external reference (red). The phase noise of the frequency reference is also displayed in grey.

The impact of the mode spacing stabilization onto an optical comb line was also assessed by analyzing the frequency noise of the heterodyne beat signal f_b between the comb line and the narrow-linewidth QCL. Results are displayed in Figure 4.10. They show that while the frequency noise of the mode spacing f_{FSR} is strongly reduced by the stabilization loop, the frequency noise of the optical line ν_N is significantly degraded by the stabilization (by about one order of magnitude). In terms of optical linewidth, it corresponds to a broadening from ~1 MHz for the free-running comb (at 1-s integration time) to 4.5 MHz when the mode spacing is locked. This results from the same reason as analyzed and discussed in details in a similar observation previously made with a 25-GHz DPSSL comb, where stabilizing the repetition rate with the use of a piezo-electric transducer also led to an increase of the frequency noise of the optical lines compared to the free-running case [16].

As explained before, the noise of f_{FSR} and f_0 partially compensates each other in the optical lines of the free-running QCL as a result of their

anti-correlation, which leads to a resulting frequency noise that is lower than the individual contributions of $N \cdot f_{FSR}$ or f_0. When f_{FSR} is stabilized to an external reference, this partial compensation disappears, and the frequency noise of the optical line mainly corresponds to the noise of f_0, as the contribution of f_{FSR} becomes negligible. Therefore, the noise of the optical line increases compared to the free-running case. The reason resides in the fact that the effect of the QCL current on the comb spectrum corresponds to a different fixed point ($N_{fix} \approx 2{,}550$) than the principal noise source that affects the free-running laser ($N_{fix} \approx 4{,}300$). Therefore, stabilizing f_{FSR} does not have an effect on f_0, which becomes totally uncorrelated from the locked f_{FSR}, so that the frequency noise of the optical comb line becomes essentially equal to the one of f_0.

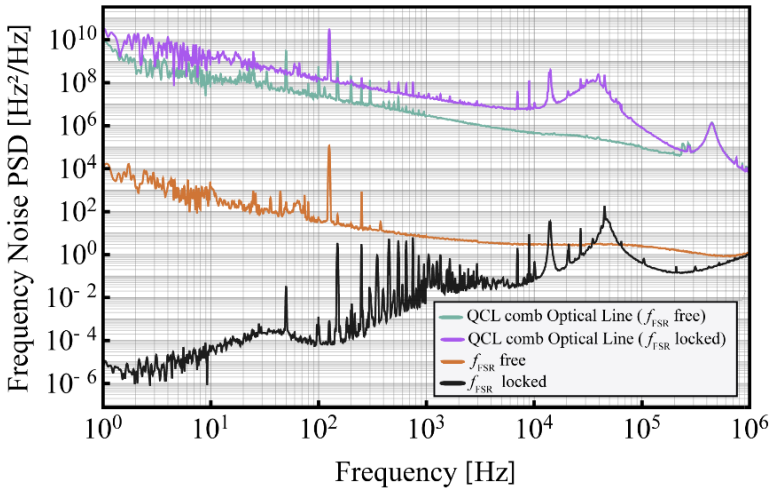

Figure 4.10: Frequency noise PSD of an optical comb line (upper traces) and of the mode spacing (lower curves) measured for the free-running QCL and when the mode spacing is phase-locked to an external RF reference. The noise bump occurring in the latter case at ~40 kHz corresponds to the servo bump of the stabilization loop.

4.5.3 Conclusion and outlook

We have reported the first noise characterization of the offset frequency in a MIR QCL comb. It was carried out using an electrical scheme that does not require the direct detection of the offset frequency

based on a nonlinear interferometry scheme, which is not applicable yet to the unpulsed emission of this type of frequency combs. By means of this scheme, we were able to measure separately the frequency noise of the two parameters of the QCL comb, the mode spacing and the offset frequency. The strong observed anti-correlation between these two signals explains the lower noise and narrower linewidth obtained for the lines of the QCL comb operating around 1245 cm^{-1}, with the presence of a fixed point estimated at 1056 cm^{-1}, as well as the degradation of the frequency noise and linewidth of the optical mode when phase-locking the mode spacing to an external RF reference.

Funding

BRIDGE CombTrace (grant 20B2-1_176584), Swiss Space Office MdP COSMICS, Swiss National Science Foundation (SNSF) (200020_178864)

Acknowledgments

We thank Alpes Lasers SA in Neuchâtel, Switzerland, for providing the DFB laser used in this study to characterize the QCL comb.

Disclosures

The authors declare no conflicts of interest.

References

[1] H. R. Telle, G. Steinmeyer, A. E. Dunlop, J. Stenger, D. H. Sutter, and U. Keller, "Carrier-envelope offset phase control: A novel concept for absolute optical frequency measurement and ultrashort pulse generation," Appl. Phys. B **69**(4), 327–332 (1999).

[2] D. J. Jones, S. A. Diddams, J. K. Ranka, A. Stentz, R. S. Windeler, J. L. Hall, and S. T. Cundiff, "Carrier-Envelope Phase Control of

Femtosecond Mode-Locked Lasers and Direct Optical Frequency Synthesis," Science **288**(5466), 635–639 (2000).

[3] A. Apolonski, A. Poppe, G. Tempea, C. Spielmann, T. Udem, R. Holzwarth, T. W. Hänsch, and F. Krausz, "Controlling the Phase Evolution of Few-Cycle Light Pulses," Phys. Rev. Lett. **85**(4), 740–743 (2000).

[4] A. Hugi, G. Villares, S. Blaser, H. C. Liu, and J. Faist, "Mid-infrared frequency comb based on a quantum cascade laser," Nature **492**(7428), 229–233 (2012).

[5] A. Schlatter, S. C. Zeller, R. Paschotta, and U. Keller, "Simultaneous measurement of the phase noise on all optical modes of a mode-locked laser," Appl. Phys. B **88**(3), 385–391 (2007).

[6] S. Schiller, "Spectrometry with frequency combs," Opt. Lett. **27**(9), 766–768 (2002).

[7] I. Coddington, N. Newbury, and W. Swann, "Dual-comb spectroscopy," Optica **3**(4), 414 (2016).

[8] M. Singleton, P. Jouy, M. Beck, and J. Faist, "Evidence of linear chirp in mid-infrared quantum cascade lasers," Optica **5**(8), 948–953 (2018).

[9] N. Opačak and B. Schwarz, "Theory of Frequency-Modulated Combs in Lasers with Spatial Hole Burning, Dispersion, and Kerr Nonlinearity," Phys. Rev. Lett. **123**(24), 243902 (2019).

[10] L. Consolino, M. Nafa, F. Cappelli, K. Garrasi, F. P. Mezzapesa, L. Li, A. G. Davies, E. H. Linfield, M. S. Vitiello, P. De Natale, and S. Bartalini, "Fully phase-stabilized quantum cascade laser frequency comb," Nat. Commun. **10**(1), 2938 (2019).

[11] F. Cappelli, G. Campo, I. Galli, G. Giusfredi, S. Bartalini, D. Mazzotti, P. Cancio, S. Borri, B. Hinkov, J. Faist, and P. De Natale,

"Frequency stability characterization of a quantum cascade laser frequency comb," Laser Photonics Rev. **10**(4), 623–630 (2016).

[12] F. Cappelli, L. Consolino, G. Campo, I. Galli, D. Mazzotti, A. Campa, M. Siciliani de Cumis, P. Cancio Pastor, R. Eramo, M. Rösch, M. Beck, G. Scalari, J. Faist, P. De Natale, and S. Bartalini, "Retrieval of phase relation and emission profile of quantum cascade laser frequency combs," Nat. Photonics **13**(8), 562–568 (2019).

[13] M. Piccardo, D. Kazakov, N. A. Rubin, P. Chevalier, Y. Wang, F. Xie, K. Lascola, A. Belyanin, and F. Capasso, "Time-dependent population inversion gratings in laser frequency combs," Optica **5**(4), 475 (2018).

[14] V. Dolgovskiy, N. Bucalovic, P. Thomann, C. Schori, G. Di Domenico, and S. Schilt, "Cross-influence between the two servo loops of a fully stabilized Er: fiber optical frequency comb," J. Opt. Soc. Am. B **29**(10), 2944–2957 (2012).

[15] P. Brochard, N. Jornod, S. Schilt, V. J. Wittwer, S. Hakobyan, D. Waldburger, S. M. Link, C. G. E. Alfieri, M. Golling, L. Devenoges, J. Morel, U. Keller, and T. Südmeyer, "First investigation of the noise and modulation properties of the carrier-envelope offset in a modelocked semiconductor laser," Opt. Lett. **41**(14), 3165–3168 (2016).

[16] P. Brochard, V. J. Wittwer, S. Bilicki, B. Resan, K. J. Weingarten, S. Schilt, and T. Südmeyer, "Frequency Noise Characterization of a 25-GHz Diode-Pumped Mode-Locked Laser With Indirect Carrier-Envelope Offset Noise Assessment," IEEE Photonics J. **10**(1), 1–10 (2018).

[17] D. R. Walker, Th. Udem, Ch. Gohle, B. Stein, and T. W. Hänsch, "Frequency dependence of the fixed point in a fluctuating frequency comb," Appl. Phys. B **89**(4), 535–538 (2007).

[18] A. Shehzad, P. Brochard, R. Matthey, S. Schilt, and T. Sudmeyer, "10-kHz-Linewidth Mid-Infrared Quantum Cascade Laser by Stabilization to an Optical Delay Line," Opt. Lett. (in press) (2019).

[19] P. Brochard, S. Schilt, V. J. Wittwer, and T. Südmeyer, "Characterizing the carrier-envelope offset in an optical frequency comb without traditional f-to-2f interferometry," Opt. Lett. **40**(23), 5522–5525 (2015).

[20] G. Di Domenico, S. Schilt, and P. Thomann, "Simple approach to the relation between laser frequency noise and laser line shape," Appl. Opt. **49**(25), 4801–4807 (2010).

[21] N. R. Newbury and W. C. Swann, "Low-noise fiber-laser frequency combs," J. Opt. Soc. Am. B **24**(8), 1756–1770 (2007).

[22] H. R. Telle, B. Lipphardt, and J. Stenger, "Kerr-lens, mode-locked lasers as transfer oscillators for optical frequency measurements," Appl. Phys. B Lasers Opt. **74**(1), 1–6 (2002).

[23] R. Paschotta, A. Schlatter, S. C. Zeller, H. R. Telle, and U. Keller, "Optical phase noise and carrier-envelope offset noise of mode-locked lasers," Appl. Phys. B **82**(2), 265–273 (2006).

[24] L. Tombez, S. Schilt, J. Di Francesco, P. Thomann, and D. Hofstetter, "Temperature dependence of the frequency noise in a mid-IR DFB quantum cascade laser from cryogenic to room temperature," Opt. Express **20**(7), 6851–6859 (2012).

[25] S. Schilt, L. Tombez, C. Tardy, A. Bismuto, S. Blaser, R. Maulini, R. Terazzi, M. Rochat, and T. Südmeyer, "An experimental study of noise in mid-infrared quantum cascade lasers of different designs," Appl. Phys. B **119**(1), 189–201 (2015).

[26] J. Hillbrand, A. M. Andrews, H. Detz, G. Strasser, and B. Schwarz, "Coherent injection locking of quantum cascade laser frequency combs," Nat. Photonics **13**(2), 101–104 (2019).

[27] S. Schilt, N. Bucalovic, L. Tombez, V. Dolgovskiy, C. Schori, G. Di Domenico, M. Zaffalon, and P. Thomann, "Frequency discriminators for the characterization of narrow-spectrum heterodyne beat signals: Application to the measurement of a sub-hertz carrier-envelope-offset beat in an optical frequency comb," Rev. Sci. Instrum. **82**(12), 123116 (2011).

[28] L. Tombez, F. Cappelli, S. Schilt, G. Di Domenico, S. Bartalini, and D.Hofstetter, "Wavelength tuning and thermal dynamics of continuous-wave mid-infrared distributed feedback quantum cascade lasers," Appl. Phys. Lett. **103**(3), 031111 (2013).

Chapter 5

Conclusion

During the course of my 4-year doctoral studies, I mainly worked with singlemode QCLs and QCL combs, and developed different methods to characterize and reduce their frequency noise. Most of the techniques that had been previously implemented in the NIR spectral region are difficult to transpose in the MIR due to the lack of optical components or to their lower performance. For instance, photodetectors in the MIR are strongly limited in bandwidth compared to their NIR counterparts. Nevertheless, I was able to implement some techniques previously demonstrated in the NIR to MIR QCLs for the first time. Hence, I gained hands-on experience with different measurement tools such as phase noise analyzer, spectrum analyzer, lock-in-amplifier, oscilloscopes, proportional-integral-derivative servo controllers, etc.

In a first part of my work, I studied the potential use of an integrated heater to reduce the frequency noise of a QCL. Through extensive experiments, I was finally able to understand why the correction signal of the voltage noise measured between the QCL terminals applied to the integrated heater could not lead to frequency noise reduction. The

generation of pure amplitude and frequency modulation in QCLs has many applications, especially in spectroscopy. With this new integrated heater actuator that was meant for fast frequency tuning, I was able to produce pure AM and FM in a QCL by applying a combined modulation of suitable amplitudes and phases to the currents in the QCL active region and integrated heater. This approach is much simpler than previously proposed methods that include shining the front facet of a QCL with NIR lasers (850 nm and 1550 nm)[73] or a specially-designed QCL having three different sections (master oscillator, gain section, and phase section) controlled by distinct currents[74,75]. The performance of the method was carefully characterized in terms of residual modulation.

The reduction of the frequency noise of a laser using an optical delay line is quite an established technology in the NIR spectral region[46] owing to the long delays that can be implemented using optical fibers. High performance comparable to the one achieved by locking to a high finesse optical cavity were demonstrated. The implementation of a long delay line to reduce the frequency noise of a QCL is much more challenging due to the lack or poor performance of fibers in this spectral range. Nevertheless, using a scheme with only 1-m of free-space delay line in a self-homodyne configuration, I was able to reduce the linewidth of a MIR QCL below 10 kHz for an integration time of 1 s.

QCL combs constitute another very attractive technology for MIR spectroscopy, as it combines some properties of single-mode QCLs with the capability to perform broadband spectroscopy with a single source. These sources are of great interest for dual-comb spectroscopy. So far, dual QCL comb spectroscopy has been performed mainly with free-running QCLs. In these combs, the standard method to detect the offset frequency based on non-linear *f*-to-2*f* interferometry has not been applicable so far, as these lasers do not emit short pulses. In the last part of this thesis, I used the concept of the transfer oscillator[9] to indirectly characterize for the first time the noise properties and modulation

response of the offset frequency in a MIR QCL comb without the need to detect it using a common *f*-to-2*f* interferometer. The achieved results will help researchers and manufacturers of QCL combs in a better understanding of this emerging comb technology.

Bibliography

1. Kosterev, A., Wysocki, G., Bakhirkin, Y., So, S., Lewicki, R., Fraser, M., Tittel, F. & Curl, R. F. Application of quantum cascade lasers to trace gas analysis. *Appl. Phys. B* **90,** 165–176 (2008).
2. Bartalini, S., Cancio, P., Giusfredi, G., Mazzotti, D., Natale, P. D., Borri, S., Galli, I., Leveque, T. & Gianfrani, L. Frequency-comb-referenced quantum-cascade laser at 4.4 μm. *Opt. Lett.* **32,** 988–990 (2007).
3. Patel, C. K. N. Continuous-Wave Laser Action on Vibrational-Rotational Transitions of CO2. *Phys. Rev.* **136,** A1187–A1193 (1964).
4. Butler, J. F., Calawa, A. R., Phelan, R. J., Harman, T. C., Strauss, A. J. & Rediker, R. H. PbTe DIODE LASER. *Appl. Phys. Lett.* **5,** 75–77 (1964).
5. Meyer, J. R., Hoffman, C. A., Bartoli, F. J. & Ram-Mohan, L. R. Type-II quantum-well lasers for the mid-wavelength infrared. *Appl. Phys. Lett.* **67,** 757–759 (1995).
6. Kim, J., Shterengas, L., Martinelli, R. & Belenky, G. High-power room-temperature continuous wave operation of 2.7 and 2.8 μm

In(Al)GaAsSb/GaSb diode lasers. *Appl. Phys. Lett.* **83,** 1926–1928 (2003).

7. Bewley, W. W., Canedy, C. L., Kim, C. S., Kim, M., Merritt, C. D., Abell, J., Vurgaftman, I. & Meyer, J. R. Continuous-wave interband cascade lasers operating above room temperature at λ = 4.7-5.6 µm. *Opt Express* **20,** 3235–3240 (2012).

8. Richter, D., Fried, A., Wert, B. P., Walega, J. G. & Tittel, F. Development of a tunable mid-IR difference frequency laser source for highly sensitive airborne trace gas detection. *Appl. Phys. B Lasers Opt.* **75,** 281–288 (2002).

9. Balakrishnan, A., Sanders, S., DeMars, S., Webjörn, J., Nam, D. W., Lang, R. J., Mehuys, D. G., Waarts, R. G. & Welch, D. F. Broadly tunable laser-diode-based mid-infrared source with up to 31 µW of power at 4.3-µm wavelength. *Opt. Lett.* **21,** 952–954 (1996).

10. Faist, J., Capasso, F., Sivco, D. L., Sirtori, C., Hutchinson, A. L. & Cho, A. Y. Quantum Cascade Laser. *Science* **264,** 553–556 (1994).

11. Bartalini, S., Borri, S., Cancio, P., Castrillo, A., Galli, I., Giusfredi, G., Mazzotti, D., Gianfrani, L. & De Natale, P. Observing the Intrinsic Linewidth of a Quantum-Cascade Laser: Beyond the Schawlow-Townes Limit. *Phys. Rev. Lett.* **104,** 083904 (2010).

12. Germann, M., Tong, X. & Willitsch, S. Observation of electric-dipole-forbidden infrared transitions in cold molecular ions. *Nat. Phys.* **10,** 820–824 (2014).

13. Supplee, J. M., Whittaker, E. A. & Lenth, W. Theoretical description of frequency modulation and wavelengthmodulation spectroscopy. *Appl. Opt.* **33,** 6294–6302 (1994).

14. Bjorklund, G. C. Frequency-modulation spectroscopy: a new method for measuring weak absorptions and dispersions. *Opt. Lett.* **5,** 15–17 (1980).

15. Bismuto, A., Bidaux, Y., Tardy, C., Terazzi, R., Gresch, T., Wolf, J., Blaser, S., Muller, A. & Faist, J. Extended tuning of mid-ir quantum cascade lasers using integrated resistive heaters. *Opt. Express* **23,** 29715–29722 (2015).

16. Kéfélian, F., Jiang, H., Lemonde, P. & Santarelli, G. Ultralow-frequency-noise stabilization of a laser by locking to an optical fiber-delay line. *Opt. Lett.* **34,** 914–916 (2009).

17. Hugi, A., Villares, G., Blaser, S., Liu, H. C. & Faist, J. Mid-infrared frequency comb based on a quantum cascade laser. *Nature* **492,** 229–233 (2012).

18. Villares, G., Hugi, A., Blaser, S. & Faist, J. Dual-comb spectroscopy based on quantum-cascade-laser frequency combs. *Nat. Commun.* **5,** 5192 (2014).

19. Jouy, P., Mangold, M., Tuzson, B., Emmenegger, L., Chang, Y.-C., Hvozdara, L., Herzig, H. P., Wägli, P., Homsy, A., de Rooij, N. F., Wirthmueller, A., Hofstetter, D., Looser, H. & Faist, J. Mid-infrared spectroscopy for gases and liquids based on quantum cascade technologies. *The Analyst* **139,** 2039–2046 (2014).

20. Zhang, G., Horvath, R., Liu, D., Geiser, M. & Farooq, A. QCL-Based Dual-Comb Spectrometer for Multi-Species Measurements at High Temperatures and High Pressures. *Sensors* **20,** 3602 (2020).

21. Telle, H. R., Steinmeyer, G., Dunlop, A. E., Stenger, J., Sutter, D. H. & Keller, U. Carrier-envelope offset phase control: A novel concept for absolute optical frequency measurement and ultrashort pulse generation. *Appl. Phys. B* **69,** 327–332 (1999).

22. Telle, H. R., Lipphardt, B. & Stenger, J. Kerr-lens, mode-locked lasers as transfer oscillators for optical frequency measurements. *Appl. Phys. B Lasers Opt.* **74,** 1–6 (2002).

23. Kazarinov, R. and Suris, R. Possible Amplification of Electromagnetic Waves in a Semiconductor with a Superlattice. *Fizikai Tekhnika Poluprovodnikov*, **5**(4), 797–800 (1971).

24. Cathabard, O., Teissier, R., Devenson, J., Moreno, J. C. & Baranov, A. N. Quantum cascade lasers emitting near 2.6 μm. *Appl. Phys. Lett.* **96,** 141110 (2010).

25. Walther, C., Fischer, M., Scalari, G., Terazzi, R., Hoyler, N. & Faist, J. Quantum cascade lasers operating from 1.2 to 1.6 THz. *Appl. Phys. Lett.* **91,** 131122 (2007).

26. Wolf, J. M., Bismuto, A., Beck, M. & Faist, J. Distributed-feedback quantum cascade laser emitting at 32 μm. *Opt. Express* **22,** 2111–2118 (2014).

27. Hofstetter, D., Faist, J., Beck, M., Müller, A. & Oesterle, U. Demonstration of high-performance 10.16 μm quantum cascade distributed feedback lasers fabricated without epitaxial regrowth. *Appl. Phys. Lett.* **75,** 665–667 (1999).

28. Tombez, L., Cappelli, F., Schilt, S., Domenico, G. D., Bartalini, S. & Hofstetter, D. Wavelength tuning and thermal dynamics of continuous-wave mid-infrared distributed feedback quantum cascade lasers. *Appl. Phys. Lett.* **103,** 031111 (2013).

29. Gürel, K., Schilt, S., Bismuto, A., Bidaux, Y., Tardy, C., Blaser, S., Gresch, T. & Südmeyer, T. Frequency Tuning and Modulation of a Quantum Cascade Laser with an Integrated Resistive Heater. *Photonics* **3,** 47 (2016).

30. Gordon, I. E., Rothman, L. S., Hill, C., Kochanov, R. V., Tan, Y., Bernath, P. F., Birk, M., Boudon, V., Campargue, A., Chance, K. V., Drouin, B. J., Flaud, J.-M., Gamache, R. R., Hodges, J. T., Jacquemart, D., Perevalov, V. I., Perrin, A., Shine, K. P., Smith, M.-A. H., Tennyson, J., Toon, G. C., Tran, H., Tyuterev, V. G., Barbe, A., Császár, A. G., Devi, V. M., Furtenbacher, T., Harrison, J. J.,

Hartmann, J.-M., Jolly, A., Johnson, T. J., Karman, T., Kleiner, I., Kyuberis, A. A., Loos, J., Lyulin, O. M., Massie, S. T., Mikhailenko, S. N., Moazzen-Ahmadi, N., Müller, H. S. P., Naumenko, O. V., Nikitin, A. V., Polyansky, O. L., Rey, M., Rotger, M., Sharpe, S. W., Sung, K., Starikova, E., Tashkun, S. A., Auwera, J. V., Wagner, G., Wilzewski, J., Wcisło, P., Yu, S. & Zak, E. J. The HITRAN2016 molecular spectroscopic database. *J. Quant. Spectrosc. Radiat. Transf.* **203,** 3–69 (2017).

31. Schilt, S., Tombez, L., Tardy, C., Bismuto, A., Blaser, S., Maulini, R., Terazzi, R., Rochat, M. & Südmeyer, T. An experimental study of noise in mid-infrared quantum cascade lasers of different designs. *Appl. Phys. B* **119,** 189–201 (2015).

32. Tombez, L., Schilt, S., Di Francesco, J., Thomann, P. & Hofstetter, D. Temperature dependence of the frequency noise in a mid-IR DFB quantum cascade laser from cryogenic to room temperature. *Opt. Express* **20,** 6851–6859 (2012).

33. Tombez, L., Schilt, S., Francesco, J., Führer, T., Rein, B., Walther, T., Domenico, G., Hofstetter, D. & Thomann, P. Linewidth of a quantum-cascade laser assessed from its frequency noise spectrum and impact of the current driver. *Appl. Phys. B* **109,** 407–414 (2012).

34. Taubman, M. S., Myers, T. L., Cannon, B. D., Williams, R. M., Capasso, F., Gmachl, C., Sivco, D. L. & Cho, A. Y. Frequency stabilization of quantum-cascade lasers by use of optical cavities. *Opt. Lett.* **27,** 2164–2166 (2002).

35. Fasci, E., Coluccelli, N., Cassinerio, M., Gambetta, A., Hilico, L., Gianfrani, L., Laporta, P., Castrillo, A. & Galzerano, G. Narrow-linewidth quantum cascade laser at 8.6 μm. *Opt. Lett.* **39,** 4946–4949 (2014).

36. Cappelli, F., Galli, I., Borri, S., Giusfredi, G., Cancio, P., Mazzotti, D., Montori, A., Akikusa, N., Yamanishi, M. & Bartalini, S.

Subkilohertz linewidth room-temperature mid-infrared quantum cascade laser using a molecular sub-Doppler reference. *Opt. Lett.* **37,** 4811–4813 (2012).

37. Hansen, M. G., Magoulakis, E., Chen, Q.-F., Ernsting, I. & Schiller, S. Quantum cascade laser-based mid-IR frequency metrology system with ultra-narrow linewidth and 1 × 10^−13-level frequency instability. *Opt. Lett.* **40,** 2289–2292 (2015).

38. Argence, B., Chanteau, B., Lopez, O., Nicolodi, D., Abgrall, M., Chardonnet, C., Daussy, C. & Darquié, B. Quantum cascade laser frequency stabilisation at the sub-Hz level. *Nat. Photonics* **9,** 456–460 (2015).

39. Tombez, L., Schilt, S., Hofstetter, D. & Südmeyer, T. Active linewidth-narrowing of a mid-infrared quantum cascade laser without optical reference. *Opt. Lett.* **38,** 5079–5082 (2013).

40. Sergachev, I., Maulini, R., Bismuto, A., Blaser, S., Gresch, T., Bidaux, Y., Müller, A., Schilt, S. & Südmeyer, T. All-electrical frequency noise reduction and linewidth narrowing in quantum cascade lasers. *Opt. Lett.* **39,** 6411–6414 (2014).

41. Schilt, S. *Mesure de traces de gaz à l'aide de lasers à semi-conducteur*, Thèse No 2525, Ecole Polytechnique Fédérale de Lausanne (EPFL), (2002).

42. Shehzad, A., Brochard, P., Matthey, R., Blaser, S., Gresch, T., Maulini, R., Muller, A., Südmeyer, T. & Schilt, S. Electrically-driven pure amplitude and frequency modulation in a quantum cascade laser. *Opt. Express* **26,** 12306–12317 (2018).

43. Dong, J., Hu, Y., Huang, J., Ye, M., Qu, Q., Li, T. & Liu, L. Subhertz linewidth laser by locking to a fiber delay line. *Appl. Opt.* **54,** 1152–1158 (2015).

44. Shehzad, A., Brochard, P., Matthey, R., Südmeyer, T. & Schilt, S. 10 kHz linewidth mid-infrared quantum cascade laser by stabilization to an optical delay line. *Opt. Lett.* **44,** 3470–3473 (2019).

45. Rubiola, E., Salik, E., Huang, S., Yu, N. & Maleki, L. Photonic-delay technique for phase-noise measurement of microwave oscillators. *J Opt Soc Am B* **22,** 987–997 (2005).

46. Sheard, B. S., Gray, M. B. & McClelland, D. E. High-bandwidth laser frequency stabilization to a fiber-optic delay line. *Appl. Opt.* **45,** 8491–8499 (2006).

47. Fortier, T. & Baumann, E. 20 years of developments in optical frequency comb technology and applications. *Commun. Phys.* **2,** 153 (2019).

48. Diddams, S. A., Jones, D. J., Ye, J., Cundiff, S. T., Hall, J. L., Ranka, J. K., Windeler, R. S., Holzwarth, R., Udem, T. & Hänsch, T. W. Direct link between microwave and optical frequencies with a 300 THz femtosecond laser comb. *Phys. Rev. Lett.* **84,** 5102–5105 (2000).

49. Holzwarth, R., Udem, Th., Hänsch, T. W., Knight, J. C., Wadsworth, W. J. & Russell, P. St. J. Optical Frequency Synthesizer for Precision Spectroscopy. *Phys. Rev. Lett.* **85,** 2264–2267 (2000).

50. Hänsch, T. W. Nobel Lecture: Passion for precision. *Rev. Mod. Phys.* **78,** 1297–1309 (2006).

51. Hall, J. L. Nobel Lecture: Defining and measuring optical frequencies. *Rev. Mod. Phys.* **78,** 1279–1295 (2006).

52. Renaudier, J., Brenot, R., Dagens, B., Lelarge, B., Rousseau, B., Legouezigou, O., Poingt, F., Pommereau, F., Accard, A., Gosset, C., Oudar, J.-, Gallion, P. & Daun, G.-. Active and passive mode-locking in buried ridge mode-locked quantum dots Fabry-Perot semiconductor lasers. in *2005 31st Eur. Conf. Opt. Commun. ECOC 2005* **3,** 571–572 (2005).

53. Schilt, S. & Südmeyer, T. Carrier-Envelope Offset Stabilized Ultrafast Diode-Pumped Solid-State Lasers. *Appl. Sci.* **5,** 787–816 (2015).

54. Ell, R., Morgner, U., Kärtner, F. X., Fujimoto, J. G., Ippen, E. P., Scheuer, V., Angelow, G., Tschudi, T., Lederer, M. J., Boiko, A. & Luther-Davies, B. Generation of 5-fs pulses and octave-spanning spectra directly from a Ti:sapphire laser. *Opt. Lett.* **26,** 373–375 (2001).

55. Schiller, S. Spectrometry with frequency combs. *Opt. Lett.* **27,** 766–768 (2002).

56. Sorokin, E., Sorokina, I. T., Mandon, J., Guelachvili, G. & Picqué, N. Sensitive multiplex spectroscopy in the molecular fingerprint 2.4 μm region with a Cr^{2+}:ZnSe femtosecond laser. *Opt. Express* **15,** 16540–16545 (2007).

57. Bernhardt, B., Sorokin, E., Jacquet, P., Thon, R., Becker, T., Sorokina, I. T., Picqué, N. & Hänsch, T. W. Mid-infrared dual-comb spectroscopy with 2.4 μm Cr2+:ZnSe femtosecond lasers. *Appl. Phys. B* **100,** 3–8 (2010).

58. Murray, R. T., Runcorn, T. H., Kelleher, E. J. R. & Taylor, J. R. Highly efficient mid-infrared difference-frequency generation using synchronously pulsed fiber lasers. *Opt. Lett.* **41,** 2446–2449 (2016).

59. Erny, C., Moutzouris, K., Biegert, J., Kühlke, D., Adler, F., Leitenstorfer, A. & Keller, U. Mid-infrared difference-frequency generation of ultrashort pulses tunable between 3.2 and 4.8 μm from a compact fiber source. *Opt. Lett.* **32,** 1138–1140 (2007).

60. Ruehl, A., Gambetta, A., Hartl, I., Fermann, M. E., Eikema, K. S. E. & Marangoni, M. Widely-tunable mid-infrared frequency comb source based on difference frequency generation. *Opt. Lett.* **37,** 2232–2234 (2012).

61. Keilmann, F., Gohle, C. & Holzwarth, R. Time-domain mid-infrared frequency-comb spectrometer. *Opt. Lett.* **29,** 1542–1544 (2004).

62. Schliesser, A., Brehm, M., Keilmann, F. & van der Weide, D. Frequency-comb infrared spectrometer for rapid, remote chemical sensing. *Opt. Express* **13,** 9029–9038 (2005).

63. Ycas, G., Giorgetta, F. R., Baumann, E., Coddington, I., Herman, D., Diddams, S. A. & Newbury, N. R. High-coherence mid-infrared dual-comb spectroscopy spanning 2.6 to 5.2 μm. *Nat. Photonics* **12,** 202–208 (2018).

64. Timmers, H., Kowligy, A., Lind, A., Cruz, F. C., Nader, N., Silfies, M., Ycas, G., Allison, T. K., Schunemann, P. G., Papp, S. B. & Diddams, S. A. Molecular fingerprinting with bright, broadband infrared frequency combs. *Optica* **5,** 727–732 (2018).

65. Smith, A. V., Armstrong, D. J. & Alford, W. J. Increased acceptance bandwidths in optical frequency conversion by use of multiple walk-off-compensating nonlinear crystals. *J. Opt. Soc. Am. B* **15,** 122–141 (1998).

66. Adler, F., Cossel, K. C., Thorpe, M. J., Hartl, I., Fermann, M. E. & Ye, J. Phase-stabilized, 1.5 W frequency comb at 2.8–4.8 μm. *Opt. Lett.* **34,** 1330–1332 (2009).

67. Coddington, I., Newbury, N. & Swann, W. Dual-comb spectroscopy. *Optica* **3,** 414–426 (2016).

68. Lu, Q., Wu, D., Slivken, S. & Razeghi, M. High efficiency quantum cascade laser frequency comb. *Sci. Rep.* **7,** 43806 (2017).

69. Brochard, P., Jornod, N., Schilt, S., Wittwer, V. J., Hakobyan, S., Waldburger, D., Link, S. M., Alfieri, C. G. E., Golling, M., Devenoges, L., Morel, J., Keller, U. & Südmeyer, T. First investigation of the noise and modulation properties of the carrier-

envelope offset in a modelocked semiconductor laser. *Opt. Lett.* **41,** 3165–3168 (2016).

70. Brochard, P., Wittwer, V. J., Bilicki, S., Resan, B., Weingarten, K. J., Schilt, S. & Südmeyer, T. Frequency Noise Characterization of a 25-GHz Diode-Pumped Mode-Locked Laser With Indirect Carrier-Envelope Offset Noise Assessment. *IEEE Photonics J.* **10,** 1–10 (2018).

71. Shehzad, A., Brochard, P., Matthey, R., Kapsalidis, F., Shahmohammadi, M., Beck, M., Hugi, A., Jouy, P., Faist, J., Südmeyer, T. & Schilt, S. Frequency noise correlation between the offset frequency and the mode spacing in a mid-infrared quantum cascade laser frequency comb. *Opt. Express* **28,** 8200–8210 (2020).

72. Di Domenico, G., Schilt, S. & Thomann, P. Simple approach to the relation between laser frequency noise and laser line shape. *Appl. Opt.* **49,** 4801–4807 (2010).

73. Peng, C., Zhou, H., Zhu, L., Chen, T., Liu, Q., Wang, D., Li, J., Peng, Q., Chen, G. & Li, Z. Purified frequency modulation of a quantum cascade laser with an all-optical approach. *Opt. Lett.* **42,** 4506–4509 (2017).

74. Bidaux, Y., Bismuto, A., Patimisco, P., Sampaolo, A., Gresch, T., Strubi, G., Blaser, S., Tittel, F. K., Spagnolo, V., Muller, A. & Faist, J. Mid infrared quantum cascade laser operating in pure amplitude modulation for background-free trace gas spectroscopy. *Opt. Express* **24,** 26464–26471 (2016).

75. Patimisco, P., Sampaolo, A., Bidaux, Y., Bismuto, A., Scott, M., Jiang, J., Muller, A., Faist, J., Tittel, F. K. & Spagnolo, V. Purely wavelength- and amplitude-modulated quartz-enhanced photoacoustic spectroscopy. *Opt. Express* **24,** 25943–25954 (2016).

Acknowledgement

I would like to thank,

Prof. Marco Marangoni and Dr. Richard Maulini for sparing their precious time and accepting the request for being the jury members of my Ph.D. thesis exam, useful discussion, and corrections in the thesis.

Thomas, for providing me a chance to work in his lab, supporting me throughout my Ph.D., and encouraging me to participate in the international conferences.

Marc, for providing quick solutions to the technical difficulties in different instruments and the QCL drivers.

Pierre, for helping me in the lab related to experimental stuff and teaching me how to use different instruments. He has a major contribution in my articles.

Valentin, for his high-end technical support in data recording, fruitful suggestions in presentations, and interfacing different instruments.

Norbert, for being a good roommate during the stay abroad for technical conferences and giving me courage for the talks.

Renaud, for his support in data analysis, interpretation, and technical details related to the projects.

Kenichi being a good friend, useful discussions about the QCLs, and letting me borrow instruments for performing experiments.

Stephane, for always being there through thin and thick, spending late nights in the lab, helping me in my experiments, in the writing process of the articles, and pushing me for presenting my research work in the technical conferences. Having an eagle eye for finding my mistakes in the draft of the articles and the thesis. I owe him a lot and I think without his support this Ph.D. would not have been possible. In these four years, I found him calm, patient, a person who really knows technical stuff and has a great deal of experience in troubleshooting technical problems during the experiments.

My parents, brothers, and sister in supporting me through this journey of four years and being there with me in all circumstances.

In the end my wife, Tooba Ahmad, and my son, Muhammad Abdullah for being patient with me and understanding me for being late at home sometimes because of the lab work.